FINAL REPORT

Development of Emission Factors for Dust Generated by Unique Military Activities

SERDP Project RC-1400

September 2010

Byung J. Kim
Michael R. Kemme
Mark J. Rood,
Ke Du
Wangki Yuen
Wei Wang
Ram Hashmonay
Ravi Varma
USACE-ERDC

This document has been cleared for public release

SERDP
DOD ▪ EPA ▪ DOE

This report was prepared under contract to the Department of Defense Strategic Environmental Research and Development Program (SERDP). The publication of this report does not indicate endorsement by the Department of Defense, nor should the contents be construed as reflecting the official policy or position of the Department of Defense. Reference herein to any specific commercial product, process, or service by trade name, trademark, manufacturer, or otherwise, does not necessarily constitute or imply its endorsement, recommendation, or favoring by the Department of Defense.

ERDC/CERL TR-10-DRAFT
September 2010

Development of Emission Factors for Dust Generated by Unique Military Activities

Byung J. Kim and Michael R. Kemme

Construction Engineering Research Laboratory (CERL)
U.S. Army Engineer Research and Development Center
2902 Newmark Dr.
Champaign, IL 61822-1076

Mark J. Rood, Ke Du, Wangki Yuen, and Wei Wang

Univeristy of Illinois

Ram Hashmonay and Ravi Varma

ARCADIS, Inc.

Draft Report

Approved for public release; distribution is unlimited.

Prepared for Strategic Environmental Research and Development Program
901 North Stuart Street, Suite 203
Arlington, VA 22203-1821

Under: SERDP Project SI -1400

Keywords: Optical Remote Sensing, Lidar, Particulate Matter, Fugitive Emission, Dust, Extinction, Emission Factor, Artillery Firing, Tracked Vehicle, Wheeled Vehicle, Helicopter

DISCLAIMER: The contents of this report are not to be used for advertising, publication, or promotional purposes. Citation of trade names does not constitute an official endorsement or approval of the use of such commercial products. All product names and trademarks cited are the property of their respective owners. The findings of this report are not to be construed as an official Department of the Army position unless so designated by other authorized documents.

DESTROY THIS REPORT WHEN NO LONGER NEEDED. DO NOT RETURN IT TO THE ORIGINATOR.

Table of Contents

List of Figures and Tables iii

Acronyms and Abbreviations vii

Acknowledgements viii

Abstract ix

1 Objectives 1

2 Background 3

3 Materials and Methods 7

3.1 Optical Remote Sensing Instrumentation 7

3.2 In Plume PM Mass Concentration Measurement 11

3.3 Field Setup 11

3.4 Methodology to Determine PM Emissions 19

3.5 Hybrid Remote Sensing and In-Situ Measurement System to Measure Fugitive Dust Flux 29

3.6 Quality Assurance/Quality Control (QA/QC) 39

4 Results and Discussion 42

4.1 Dust Emissions from Artillery Back Blast 42

4.2 Dust Emissions from Movement of Tracked Vehicles at YTC 44

4.3 Dust Emissions from Approaching and Withdrawing of Flying Helicopters 52

4.4 Dust Emissions from Tracked and Wheeled Vehicles Measured with the Hybrid ORS System at Fort Carson, CO 56

4.5 Comparisons of Emission Factors for Different Military Activities 65

5 Conclusions and Implications for Future Research 67

References 71

Appendix A: Supporting Data 74

Appendix B – List of Scientific/Technical Publications 114

Appendix C – Other Supporting Materials 115

REPORT DOCUMENTATION PAGE 116

List of Figures and Tables

Figures

Figure 1 PM emission factors in relation to the large research framework. 6
Figure 2 Micro-Pulse Lidar instrument 9
Figure 3 IMACC OP-FTIR instrument 10
Figure 4 IMACC OP-LT instrument 10
Figure 5 TSI DustTrakTM Instrument 11
Figure 6 Schematic of the experimental layout for the artillery back-blast tests during the 2005 YPG Field Campaign 12
Figure 7 Field picture for the artillery back blasts test during the 2005 YPG Field Campaign (viewed from MPL) 12
Figure 8 Schematic of the experimental layout for tracked vehicle tests during the 2006 YTC Field Campaign 14
Figure 9 Field picture for tracked vehicle tests during the 2006 YTC Field Campaign (viewed from MPL) 15
Figure 10 Schematic of the experimental layout for measuring dust emissions from the helicopter during the 2007 YPG Field Campaign 16
Figure 11 Field pictures for helicopter tests during the 2007 YPG Field Campaign. (A) instruments (viewed from reflective target); (B) example of an event (viewed from MPL) 16
Figure 12 Schematic of the experimental layout for military vehicle tests during the 2008 Fort Carson Field Campaign 18
Figure 13 Field picture for military vehicle tests during the 2008 Fort Carson Field Campaign (viewed from MPL) 19
Figure 14 Flowchart describing the overall data processing method used during the first three years of the field campaigns (2005 YPG, 2006 YTC, 2007 YPG) 20
Figure 15 Flowchart describing the overall data processing method used during the 2008 Fort Carson field campaign. The differences between Figure 14 and 15 are highlighted in bold text. 20
Figure 16 MPL data correction procedures 22
Figure 17 Schematic of the hybrid dust measurement configuration. The DT pairs consist of one PM_{10} and one $PM_{2.5}$ monitor. 30
Figure 18 OP-LT calibration measurements made at Yuma Proving Grounds - The six dust events with high dust correlations (R > 0.9) 33
Figure 19 Plot of the OP-LT and DM-PM_{10} Calibration Measurements. a) The full 1,840-point data set, b) The six high-correlation events (508 points) data set. 34
Figure 20 Plot of the OP-LT and DM PM_{10} calibration measurements at Fort Carson for events on September 16th 2008. 35
Figure 21 Comparison of PIMC determined with the new method to the PIMC determined from the grid of DT monitors. Top: 5 DT monitors in new method, middle: 3 DT monitors in new method, bottom: 2 DT pairs in new method. 36

Figure 22 Comparison of PIMC determined with the new method to the PIMC determined from the grid of DT monitors for 20 events at Fort Carson. Top: 4 DT monitors in new method, second and third from top: 3 DT monitors in new method (1,2, and 4 and 1,3, and 4), bottom: 2 DT pairs in new method. 38

Figure 23 Experimental setup for ORS mass retrieval method calibration....40

Figure 24 PM_{10} calibration curve for YPG dust (y = 1.00x, R2 = 0.78)....40

Figure 25 $PM_{2.5}$ calibration curve for YPG dust (y = 1.00x, R2 = 0.72)....41

Figure 26 Evolution of a PM10 plume during an artillery-firing event. The letters indicate the order of the time sequence. (projectile model: M107, propelling charge zone: two)....43

Figure 27 Measured emission factors for different types of artillery projectiles during the 2005 YPG Field Campaign....43

Figure 28 Evolution of a plume mass concentration profile for PM_{10} during vehicle travel. The letters indicate the order of the time sequence. 47

Figure 29 (left) Measured emission factors for different types of tracked vehicles, (A) Bradley Fighting Vehicle, (B) M113, and (C) M1A1, on an Unpaved Road during the 2006 YTC Field Campaign. Absence of a thin line (standard deviation) indicates a single data point within the speed interval. (right) Power regressions of the emission factors of these vehicles versus speed 48

Figure 30 (left) Measured emission factors for different types of tracked vehicles, (A) Bradley Fighting Vehicle, and (B) M1A1, on Grassland during the 2006 YTC Field Campaign. Absence of a thin line (standard deviation) indicates that a single data point was available for that vehicle speed interval. (right) Power regressions of the emission factors of these vehicles versus speed 49

Figure 31 Scaling relationship between emission factor and the product of vehicle mass and speed (momentum) for tracked vehicles traveling on (A) Unpaved Road and (B) Grassland during the 2006 YTC Field Campaign. Horizontal axis represents the product of vehicle mass and its speed (kg km/h x10-3). Absence of a thin vertical line (standard deviation) indicates that a single data point was available for that vehicle speed interval. 51

Figure 32 Evolution of plume extinction profile during a helicopter pass. The letters indicate the order of the time sequence. (5/21/2007, Bell 210 Helicopter flying toward the MPL at 30 km/hr over Desert Pavement surface)....54

Figure 33 (left) Measured emission factors on Desert Pavement Surface (Site 1) during the 2007 YPG Field Campaign. (right) Linear regression of emission factor versus helicopter speed. 55

Figure 34 (left) Measured emission factors on Disturbed Soil Surface (Site 2) during the 2007 YPG Field Campaign. (right) Linear regression of emission factor versus helicopter speed. 55

Figure 35 Evolution of plume extinction profiles during vehicle passes at the speed of 15mph towards the MPL: (A) M577 (M113 family)and (B) HEMTT. The time elapsed between two consecutive profiles is 14 seconds. 58

Figure 36 (left) Measured emission factors for different types of tracked vehicles, (A) M270, (B) M577, and (C) M88, at Site 1 during the 2008 Fort Carson Field Campaign. Absence of a thin vertical line (standard deviation) indicates single data point within the speed interval. (right) Power regressions of the emission factors of these vehicles versus speed 61

Figure 37 (left) Measured emission factors for different types of tracked vehicles, (A) M270, (B) M577, and (C) HEMTT, at Site 2 during the 2008 Fort Carson Field

Campaign. Absence of a thin vertical line (standard deviation) indicates single data point within the speed interval. (right) Power regressions of the emission factors of these vehicles versus speed 62

Figure 38 Scaling relationship between emission factor and the product of vehicle mass and vehicle speed for tracked vehicles during the 2008 Fort Carson Field Campaign. Horizontal axis represents the product of vehicle mass and its speed (kg km/h x10^{-3}). 64

Figure 39 Scaling relationship between emission factor and the product of vehicle mass and vehicle speed for the HEMTT wheeled vehicle during the 2008 Fort Carson Field Campaign. Horizontal axis represents the product of vehicle mass and its speed (kg km/h x10-3). Absence of a thin vertical line (standard deviation) indicates that a single data point was available for that speed interval....64

Figure A-1-1 Field map of YPG field campaign on 10/27/05 and 10/28/05....76

Figure A-2-1 Field map of YTC tracked vehicle field campaign on 8/22/06....94

Figure A-2-2 Field map of YTC tracked vehicle field campaign on 8/23/06....95

Figure A-2-3 Field map of YTC tracked vehicle field campaign on 8/24/06....96

Figure A-2-4 Field map of YTC tracked vehicle field campaign on 8/25/06....97

Figure A-3-1 Field map of YPG helicopter field campaign on 5/21/07....103

Figure A-3-2 Field map of YPG helicopter field campaign on 5/23/07....104

Figure A-4-1 Field map of Fort Carson military vehicle field campaign on 9/16/08 and 9/17/08....112

Figure A-4-2 Field map of Fort Carson military vehicle field campaign on 9/19/08....113

Tables

Table 1 MPL specifications....8

Table 2 Positioner specifications....8

Table 3 Summary of PM mass emission factors for the back-blasts from two types of artillery during the 2005 YPG Field Campaign....42

Table 4 Summary of emission factors for Unpaved Road during the 2006 YTC Field Campaign....45

Table 5 Summary of emission factors for Grassland during the 2006 YTC Field Campaign....46

Table 6 Regressions of PM_{10} and $PM_{2.5}$ emission factors (EF, g/vkt) vs. speed (v, km/h) for each vehicle measured in the 2006 YTC Field Campaign. The R^2 values for each regression are also shown....50

Table 7 Summary of emission factors for the Desert Pavement Surface (Site 1) during the 2007 YPG Field Campaign....54

Table 8 Summary of emission factors for the Disturbed Soil Surface (Site 2) during the 2007 YPG Field Campaign....55

Table 9 Regressions of PM10 and PM2.5 emission factors (EF, g/vkt) vs. speed (v, km/h) for the Bell 210 Helicopter in the 2007 YPG Field Campaign. The R2 values for each regression are also shown....56

Table 10 Summary of emission factors for Site 1 during the 2008 Fort Carson Field Campaign....59

Table 11 Summary of emission factors for Site 2 during the 2008 Fort Carson Field Campaign....60

Table 12 Regressions of PM_{10} and $PM_{2.5}$ emission factors (EF, g/vkt) vs. speed (v, km/h) for each vehicle measured in the 2008 Fort Carson Field Campaign. The R2 values for each regression are also shown....63

Table 13 Comparison of measured and modeled emission factors (TV= Tracked Vehicle, WV = Wheeled Vehicle)....66

Table A-1-1 PM mass emission factors for the 2005 YPG Field Campaign....74

Table A-2-1 Physical dimensions of the three tracked vehicles and their tracks....77

Table A-2-2 PM mass emission factors for the 2006 YTC Field Campaign....77

Table A-2-3 Details about tracked vehicle movement based on MPL Data....79

Table A-2-4 Laser Transmissometer data and duration of the plume....81

Table A-2-5 FTIR data....85

Table A-2-6 Wind data....91

Table A-3-1 Specifications of the UH-1 Iroquois (Huey)....98

Table A-3-2 Summary of emission factors for the Desert Pavement Surface during the 2007 YPG Field Campaign....99

Table A-3-3 Summary of emission factors for the Disturbed Soil Surface on 5/23/07 during the 2007 YPG Field Campaign....100

Table A-3-4 Summary of emission factor for the Disturbed Soil Surface on 5/25/07 during the 2007 YPG Field Campaign....101

Table A-4-1 Specifications of tested military vehicles....105

Table A-4-2 Number of tests for select military vehicles....105

Table A-4-3 Detailed test data of military vehicles....106

Table C-1 Sensitivity analysis of K^*, [g/m^2] *§....115

Acronyms and Abbreviations

Term	Definition
1-D	One-Dimensional
2-D	Two-Dimensional
DoD	The Department of Defense
DRI	Desert Research Institute
DT	DustTrak™
FTS	Flux Tower System
HEMMT	Heavy Expanded Mobility Tactical Truck
MPL	Micro-Pulse Lidar
NAAQS	National Ambient Air Quality Standards
NRB	Normalized Relative Backscatter
OP-FTIR	Open-Path Fourier Transform Infrared
OP-LT	Open-Path Visible Laser Transmissometer
ORS	Optical Remote Sensing
PM	Particulate Matter
QA	Quality Assurance
QC	Quality Control
USEPA	United States Environmental Protection Agency
YPG	Yuma Proving Grounds
YTC	Yakima Training Center

Acknowledgements

This study was conducted for the Strategic Environmental Research and Development Program (SERDP) Office as Sustainable Infrastructure Project SI-1400 “Development of Emission Factors for Dust Generated by Unique Military Activities.” The technical monitor was Dr. John Hall who is the Sustainable Infrastructure Program Manager for the SERDP Program Office.

The work was performed in collaboration with SERDP Project SI-1399 “Particulate Matter Emissions for Dust from Unique Military Activities” that was managed and executed by the Desert Research Institute (DRI). All field campaigns described in this report were jointly performed by researchers from both SI-1399 and SI-1400. Key collaborators from DRI include Dr. John Gillies, Dr. Hampden Kuhns, and Dr. Vicken Etyemezian.

The work was managed and executed by the Environmental Processes Branch (CN-E) of the Environmental Division (CN), Construction Engineering Research Laboratory (CERL). The CERL principal investigators were Dr. Byung Kim and Michael Kemme. The authors thank the supporting staff from Yuma Proving Grounds, Yakima Training Center, and Fort Carson for providing support during the field campaigns. Deborah Curtin is Chief, CEERD-CN-E, and John Bandy is Chief, CEERD-CN. The associated Technical Director is Alan Anderson, CEERD-CV-T. The Director of ERDC-CERL is Dr. Ilker R. Adiguzel.

CERL is an element of the U.S. Army Engineer Research and Development Center (ERDC), U.S. Army Corps of Engineers. The Commander and Executive Director of ERDC is COL Gary E. Johnston, and the Director of ERDC is Dr. Jeffery P Holland.

Abstract

The SERDP SI-1400 research team has successfully developed a novel optical remote sensing method to characterize and quantify fugitive particulate matter dust emissions generated by unique military activities. This research team provided Department of Defense installations with results that can be used to estimate the generation of fugitive dust from military activities. Unique military fugitive dust emission sources that were studied during this project include: 1) artillery back blast, 2) rotary wing aircraft and, 3) tracked vehicles.

The optical remote sensing method includes a Micro-Pulse Light detection and ranging device (MPL), an Open Path-Fourier Transform Infrared Spectrometer (OP-FTIR), and an Open Path-Laser Transmissometer (OP-LT). The new analytical technique developed as part of this project quantifies the extinction of light caused by dust plumes passing through the measurement plane of the MPL. The path-integrated OP-FTIR and OP-LT measures the dusts' ability to attenuate light as a function of the dusts' particle size distributions. During the fourth year of this work, the OP-FTIR measurements were replaced with a hybrid system using OP-LT and DustTraks™ to measure the dusts' light extinction efficiencies in a simpler and cost effective manner.

The novel optical remote sensing method was used to quantify PM dust mass emission factors with aerodynamic diameter < 2.5 μm and < 10 μm for artillery back blast, military vehicles, and a flying helicopter. Regressions were developed to determine PM-mass emission factors based on type of fugitive source, speed of the mobile sources, and momentum of the mobile sources. Results from this research are now readily available to develop emission inventories for facilities and to develop more effective environmental compliance and PM control strategies.

1 Objectives

Particulate matter (PM) emissions from fugitive sources are a major concern because of their contribution to the degradation of air quality in many regions of the world. Fugitive dust refers to the re-suspended dust from soil surfaces due to surface disturbance. The objectives of this study were: (1) to identify, characterize, and monitor airborne PM with aerodynamic diameters ≤ 10 μm (PM_{10}) and ≤ 2.5 μm ($PM_{2.5}$) from fugitive dust emissions that are caused by unique military sources; (2) to develop and modify instrumentation, methods, and systems to determine PM emission factors; (3) to determine PM dust emission factors for artillery back blasts, the movement of tracked and wheeled vehicles, and flying helicopters; (4) to develop model components that better describe the generation of the Department of Defense (DoD)'s fugitive PM; and (5) to quantify the variability and uncertainty of these emissions.

These objectives related directly correspond to the following objectives found in SERDP's SON "CPSON-04-04, Particulate Matter Emission Factors for Dust from Unique Military Activities:"

- Determine PM emission factors from training and operational activities at DoD installations, including quantifying of their variability and uncertainty. PM emissions should be characterized for specific representative activities related to tracked vehicle maneuvers, fixed-wing aircraft landing and take-off, rotary-wing aircraft moving near ground surface and blast emissions from artillery use.
- If necessary to meet the above objective, develop or modify innovative instrumentation to identify, characterize, and monitor in real-time or near real-time, the airborne PM emissions resulting from DoD testing/training activities.
- Develop model components that better describe the generation of the various types of PM listed above.

The execution of this project also involved close collaboration with SERDP Project SI-1399 "Particulate Matter Emissions Factors for Dust from Unique Military Activities" with Dr. Jack Gillies, Desert Research Institute (DRI) as the Principal Investigator. The objectives of SI-1399 were complimentary to SI-1400 and included: 1) carry out field measurement campaigns to quantify dust emissions and develop emission factors for tracked military vehicles, rotary-winged aircraft, and artillery pieces for various

unpaved surfaces, while extending our understanding of the important vehicle, activity, and surface characteristics that influence the magnitude of the observed emissions, 2) carry out measurement campaigns using the DRI flux tower system to develop emission factors of artillery back blast, tracked vehicles, and rotary-winged aircraft, 3) link the measured emission factors with indices of surface dust emission potential using a new portable wind tunnel and an on-vehicle measurement system thereby creating a cost effective mechanism to extend the use of the emission factors into different environments, 4) continue to develop a database from field and laboratory measurements that characterizes the chemical, physical, and optical properties of the dust emissions that are important for assessing source contribution estimates and impacts on regional visibility degradation, 5) further develop a Geographic Information System-based dust dispersion modeling system that integrates the newly-developed emission factors into its user interface, and 6) to disseminate the information, methods, and modeling products generated from this research to the military and civilian user community to improve their abilities to gather information, make decisions based on that information, and develop cost-effective solutions that will enhance military preparedness.

2 Background

Particulate matter (PM) is one of the six pollutants regulated by National Ambient Air Quality Standards (NAAQS) issued by the United States Environmental Protection Agency (USEPA). DoD has been concerned about the emissions of fugitive dust from its training and testing ranges. As previously mentioned, fugitive dust refers to the re-suspended dust from soil surfaces due to surface disturbance. The dust imposes considerable health concerns by carrying virus and bacteria, and being inhaled into humans' respiratory tracts[1, 2]. Studies show that aerosol particle concentrations for PM_{10} and $PM_{2.5}$ have positive correlations with the occurrence of human respiratory and cardiac illnesses[3]. Dust also obscures visibility [4, 5] and can impact the effectiveness of military training. Dust also plays a major role in climate change by scattering and absorbing solar radiation[6-9]. During 2006, the U.S. Environmental Protection Agency (USEPA) made the standards stricter for ambient PM concentration by reducing the 24-hr $PM_{2.5}$ allowable concentration from 65 μg/m^3 to 35 μg/m^3 [10]. To protect visual air quality, the Regional Haze Rule was adopted during 1999 to protect visibility at Class I areas, such as national parks, forests, and wilderness areas[11], by controlling anthropogenic PM emissions[5]. The Regional Haze Rule requires that anthropogenic emissions to the atmosphere be reduced to the extent that visibility is not noticeably degraded more than it would be under natural conditions[5, 11].

However, very little is known about dust emissions from military activities. Therefore, characterizing the PM emissions from typical military activities is among the top priorities of the environmental quality/compliance technology research and development of DoD [12]. The emissions of PM by DoD need to be quantified by developing mass emission factors for these activities that can be readily used to create emission inventories and be integrated as source term components for dispersion models [13]. Methods and systems to quantify these emission factors need to be developed to estimate the complex and large fugitive PM plumes generated by unique military sources.

In this research, the project team developed a method to quantify the PM-mass emissions for dust plumes generated by unique military activities using optical remote sensing (ORS) devices and DustTrak™ (DT) aerosol monitors. There were two versions of the ORS system employed in this

study. The first version consisted of a ground-based Micro-Pulse Lidar (MPL) that was located on a positioner to control the vertical measurement angle of the MPL, two mono-static Open-Path Fourier Transform Infrared spectrometers (OP-FTIRs), and two Open-Path Laser Transmissometers (OP-LTs). The second version, which is also referred to as the hybrid version, consisted of an MPL, an OP-LT and three ground-level DT aerosol monitors. MPL, which is an eye-safe subset of LIght Detection And Ranging (Lidar), is a powerful technology for studying clouds and aerosols in the atmosphere. MPL is able to measure range-resolved extinction profiles and/or transmittance of light measured by the backscatter of light generated by the MPL's laser. OP-FTIR is an ORS instrument that provides path-integrated multi-spectral light extinction in a vertical plane downwind of the fugitive PM source. OP-LT is an ORS instrument that measures the path-integrated light extinction for a particular wavelength of light. The DT aerosol monitor is a point-based laser photometer with real-time PM mass concentration detection capability.

The ORS method developed in this research, first determines the dust's extinction profiles via inversion of the Lidar equation from the normalized relative backscattering (NRB) signals that are corrected from raw MPL signals. The one-dimensional (1-D) extinction profiles are combined to provide two-dimensional (2-D) extinction profiles by interpolating the data along all scan-paths in a scan cycle. These 2-D extinction profiles are then converted into 2-D PM mass concentration profiles by multiplying extinction efficiency factors, which are determined with two algorithms corresponding to the two previously described versions of the ORS systems. Finally, emission factors are determined by integrating all vertical 2-D mass concentration profiles with the duration of each plume event and the wind speeds and directions measured by the co-located anemometers. More detailed information about the ORS method, including differences between these two algorithms, is provided in the next section.

Three types of military activities that generate fugitive dust were characterized during this research project. The activities included firing of artillery, movement of tracked and wheeled vehicles, and flying of helicopters. Fugitive PM emissions were studied during four separate field campaigns using the ORS systems:

(1) 2005 Yuma Proving Grounds (YPG) Field Campaign: dust plumes generated from the shock of artillery back blasts were measured at YPG in

Arizona, which is a desert location in the southwestern USA, during October 2005;

(2) 2006 Yakima Training Center(YTC) Field Campaign: dust plumes generated from the movement of three types of tracked vehicles were measured at YTC in Washington State, during August 2006;

(3) 2007 YPG Field Campaign: dust plumes generated during the flight of rotary winged military aircraft were measured at YPG, during May 2007; and

(4) 2008 Fort Carson Field Campaign: dust plumes generated from the movement of three types of tracked vehicles and one type of wheeled vehicle were measured with a hybrid-ORS system at the Fort Carson location in Colorado, during September 2008.

The sources and surface types were selected to represent the most frequently used dust generating activities and earth surfaces at the DoD training sites. The experimental conditions and sampling methodology for each field campaign are described in Sections 3.3 and 3.4.

Very few studies have determined the emission factors of fugitive dust by military activities. Military activities such as artillery back blast, vehicle movement, and flying helicopters can disturb soil surfaces. However, there are limited studies that have determined the emission factors for military vehicles traveling on roads [14]. There is no available literature that describes fugitive dust emission factors generated from artillery back blasts and helicopter flights. The USEPA emission factor database "AP-42 Compilation of Air Pollutant Emissions" is the only database that provides fugitive dust emission factor estimates for civilian sources. Chapter 13.2.2 of the USEPA's AP-42 Emission Factor database provides emission factor estimates for vehicles travelling on unpaved surfaces. The model describes the PM-mass emission factor (g/vkt) as $281.9k(S/12)^{0.9}(W/3)^{0.45}$, where S is silt content (%), W is mean vehicle weight (tons), and k = 0.15 for $PM_{2.5}$ and k = 1.5 for PM_{10} [15]. The database only provides equations for estimation of fugitive dust from the operation of vehicles, not the operation of artillery or helicopters.

PM emission factors for military activities fit into a larger research framework as described in Figure 1. There are extensive DoD training facilities that are prone to generating fugitive dust emissions. Emission factors are

needed to characterize those sources. The emission factors and the sources' operational records can be used to quantify the amount of fugitive PM dust emitted to the atmosphere. These fugitive dust source profiles can then be combined with other military installation PM emission inventories (e.g., non-fugitive dust emission such as PM emissions from elevated point sources) to provide an overall assessment of the PM emissions from DoD training facilities. These DoD-based PM emission inventories can then be integrated with civilian PM-emission inventories and dispersion models to quantify PM mass concentrations in regions bordering DoD installations. PM-mass concentration profiles can then be input into models (e.g., radiative transfer models) to quantify the impact of all regional PM emissions on visibility, climate and human health.

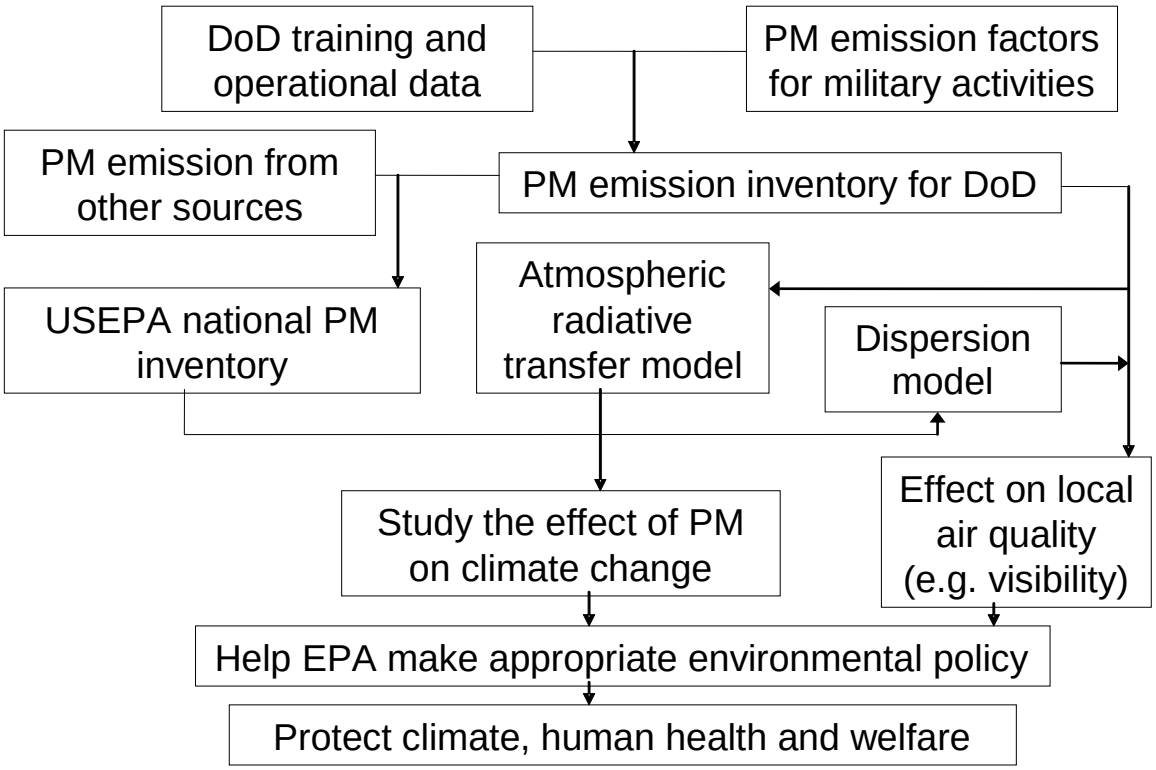

Figure 1 PM emission factors in relation to the large research framework.

This report presents and discusses the results from the field tests when using new ORS methods to characterize fugitive dust plumes and to determine emission factors under select operating conditions for the sources. The effects of operational parameters (e.g., vehicle type and speed) and ground-surface types on the dust emission factors are also presented and discussed.

3 Materials and Methods

3.1 Optical Remote Sensing Instrumentation

3.1.1 Micro-Pulse Lidar (MPL)

The use of pulsed light to detect cloud droplets can be traced back to the 1930s [16]. This type of detection was named as Lidar by Middleton and Spilhaus in 1953 [17]. The invention of the laser during the 1960s allowed Lidar technologies to develop rapidly [18]. During 1992, the Goddard Space Flight Center under the National Aeronautics and Space Administration (NASA) developed the first MPL, which featured eye-safe laser and noise-limited photon counting capabilities [19, 20]. This version of the MPL gave rise to a commercially available Lidar system. MPL was also improved with time to increase the system's reliability [20]. Recently, MPLs have been used to study optical properties of clouds [20-23] and aerosols [20, 24-26]. Currently, the major commercial manufacturers of MPLs are Sigma Space Corporation (www.sigmaspace.com/sigma/micropulseLidar.php) and Science and Engineering Services, Inc (www.sesius.biz).

The MPL used for the field campaigns reported here is an elastic backscatter Lidar operated at a wavelength of 527 nm (Table 1 and Figure 2). This MPL was developed at NASA and manufactured by Sigma Space Corporation, Maryland. The MPL was mounted on a positioner (ORBIT Advanced Technologies, Model: AL-4011-1E with control system AL-1613-3J, Table 2 and Figure 2) to allow the MPL to scan vertically and horizontally. During the field tests, the MPL was located along the same path as the OP-FTIRs and OP-LTs. Backscatter data from the MPL were used to determine the horizontal and vertical light extinction profiles across the scanned cross sectional areas of the plumes.

Table 1 MPL specifications

Wavelength	527 nm
Laser Power	1.0 W
Output Energy	~ 8 μJ
Pulse Repetition Frequency	2.5 kHz
Transceiver Aperture	178 mm
Transceiver Field-of-View	~ 100 μrad
Range Resolution	15 m, 30 m, 75 m
Maximum Range	60 km

Table 2 Positioner specifications

Data Take-off Accuracy	Azimuth	±0.1°
	Elevation	±0.1°
Nominal Speed	Azimuth	12°/s
	Elevation	12°/s
Limit-to-limit Travel	Azimuth	±210°
	Elevation	-5° to 185°

This MPL was chosen for these field campaigns because MPLs determine range resolved, in contrast to path integrated, optical properties of the PM. This feature is possible by measuring the amount of light that is backscattered from the laser's pulsed light source by PM as a function of distance from the MPL. The MPL determines the dust's mass concentration along the MPL's path by integrating the MPL's backscattered light signals with the optical and physical properties of the PM. Moreover, the MPL is designed to emit laser light at low pulse energies (i.e., a few micro-joules), making it safe to human eyes. The MPL's laser can therefore be used to measure in all horizontal and vertical directions with minimal precautions.

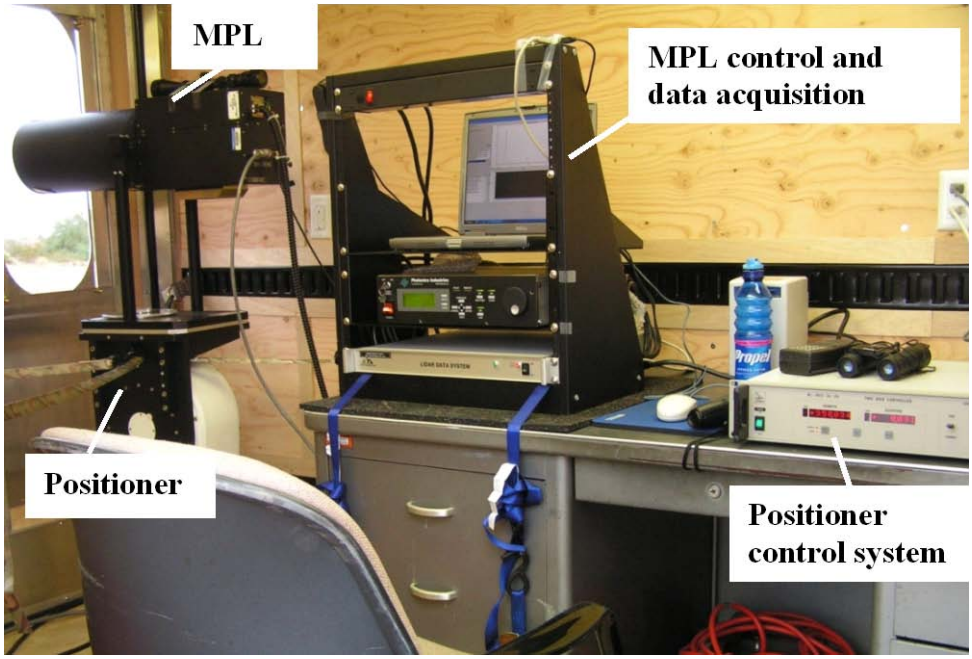

Figure 2 Micro-Pulse Lidar instrument

3.1.2 Open Path-Fourier Transform Infrared (OP-FTIR) Spectrometer

The OP-FTIR spectrometers (IMACC, Inc. and Midac Inc.) used for this project consist of an infrared light beam (wavelength: 2.3 μm –13.2 μm), modulated by a Michelson interferometer (Figure 3). The light beam is transmitted from a single telescope to a retro-reflecting mirror target (retroreflector), which is usually set up at a nominal distance of 100 m away from the OP-FTIR. The returned light signal is received by the single telescope and directed to a detector. The light that is transmitted between the OP-FTIR and retroreflector is absorbed and scattered by the molecules and particles in the light beam's path. The OP-FTIR instrument was originally designed to identify and quantify chemical species by matching the infrared absorption spectra collected in the field to calibrated spectral measurements of individual compounds (i.e., reference spectra) that are obtained in the laboratory. However, the OP-FTIR was used with the OP-LT during the first three field campaigns to determine the size distributions of the dust particles (Section 3.4.3.1).

Figure 3 IMACC OP-FTIR instrument

3.1.3 Open Path Laser Transmissometer (OP-LT)

The OP-LT contains a modulated He-Ne laser that transmits light over an open path of several hundred meters, and is then reflected by a retroreflector back to a detector. It was custom-built by IMACC especially for this research (Figure 4). Data were acquired during the field campaigns at 1 Hz while operating the OP-LT at a wavelength of 0.67 μm.

Figure 4 IMACC OP-LT instrument

3.2 In Plume PM Mass Concentration Measurement

3.2.1 DustTrak™ (DT)

The DT aerosol monitor (Model 8520, TSI, Inc., Minnesota, USA) is a portable, battery-operated laser photometer that provides real-time mass concentration characterization and data logging capabilities (Figure 5). The monitor measures calibrated PM mass concentration corresponding to PM_{10} or $PM_{2.5}$ when using the corresponding inlet attachments. The ORS method was calibrated against standard mass concentrations, which was completed with a pair of DT aerosol monitors that were calibrated by Dessert Research Institute (DRI). Calibration of the DT aerosol monitors was conducted against filter-based mass concentration measurements.

Figure 5 TSI DustTrakTM Instrument[23]

3.3 Field Setup

3.3.1 2005 YPG Field Campaign – Emissions from Back Blasts due to Firing of Artillery

The YPG field campaign occurred during October 2005 to quantify PM dust emissions from back blasts that occur during the firing of artillery (Figure 6 and Figure 7). Detailed field maps depicting the setup are provided in Appendix A (Figure A-1-1). Tests were carried out on improved gun placements (i.e., surfaces where artillery were located had been modified to enhance ease of firing and potentially mitigate dust emissions).

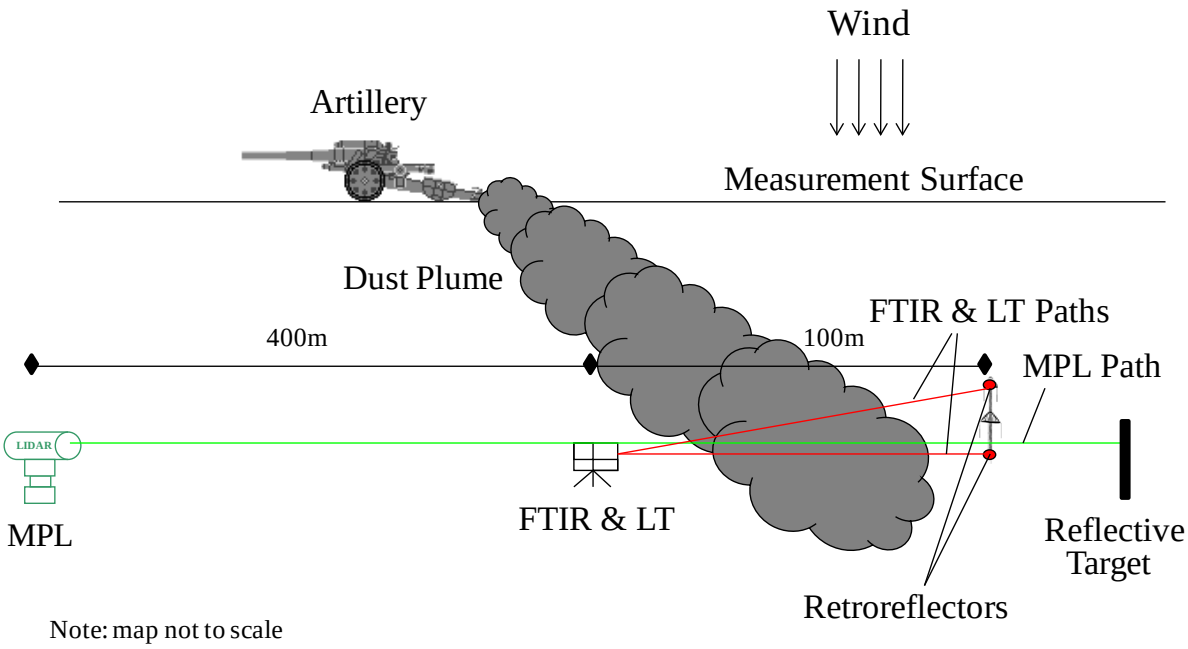

Figure 6 Schematic of the experimental layout for the artillery back-blast tests during the 2005 YPG Field Campaign

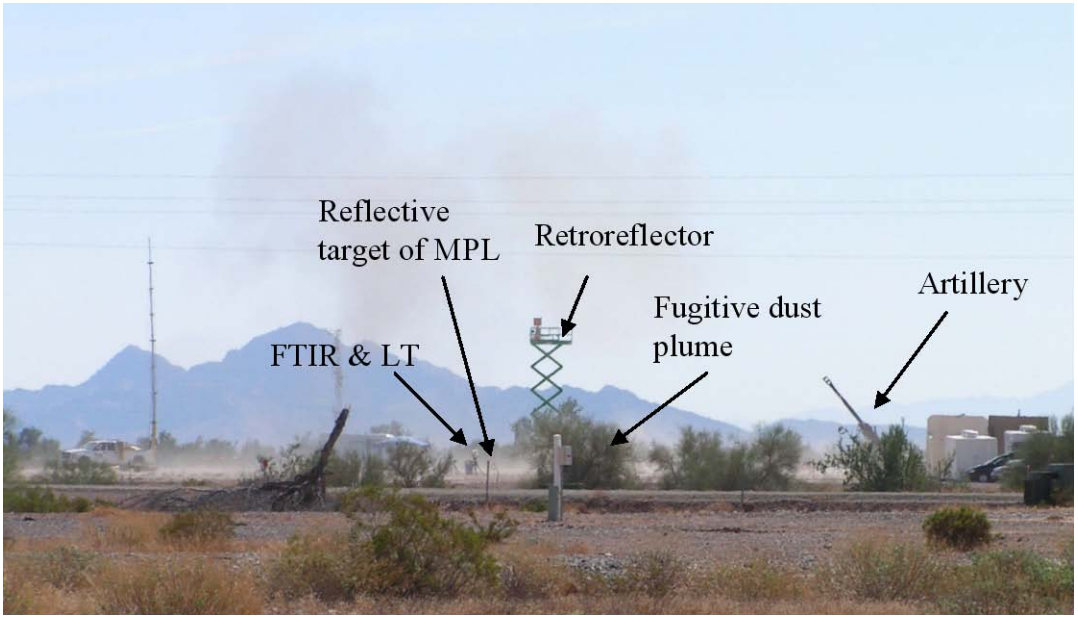

Figure 7 Field picture for the artillery back blasts test during the 2005 YPG Field Campaign (viewed from MPL)

The MPL was operated in a temperature-controlled trailer with stabilizers at each corner of the trailer to allow for stable operation of the instrument. The MPL was operated at only one horizontal angle in contrast to multiple horizontal angles during the vehicle and helicopter field campaigns. The trailer was located 400 m away from the artillery to reduce the magnitude of corrections to the MPL signal when detecting the dust plume and for

safety requirements required by the facility. The laser beam was nominally located perpendicular to the wind direction and downwind from the source. A 0.5 ft x 8 ft (1.27 cm x 244 cm) metal pole was used as a reflective target and was located in the optical path of the MPL. The MPL continuously collected data while the artillery was firing its projectiles. Two sets of OP-FTIR and OP-LT systems, located 1.5 m above the ground, were operated co-linearly with the MPL's beam and 50 m downwind from the artillery firing point. These sets of devices detected dust along two paths, one set was directed horizontally to a retroreflector and the other set was directed to a retroreflector that was located 10 m above the ground. The horizontal distance between the OP-FTIRs/OP-LTs and their corresponding retroreflectors was 100 m.

Two types of artillery with projectile models of M549A1 and M107 were tested during the October 2005 artillery tests. The propelling charge zone was 8S for the M549A1 and the propelling charge zones were 2 and 3 for the M107. Such artillery types were selected based on the artillery testing schedule at YPG and the amount of their use to represent a wide range of artillery training activities by DoD.

3.3.2 2006 YTC Field Campaign – Emissions from Movement of Tracked Vehicles

The YTC field campaign occurred during August 2006 to quantify dust emissions caused by the movement of tracked vehicles on unpaved surfaces (Figure 8 and Figure 9). Detailed field maps depicting the setup are provided in Appendix A (Figure A-2-1 to Figure A-2-4). The MPL's optical path was co-located with the two sets of the OP-FTIR/OP-LT systems described above with their optical paths located parallel to an unpaved road and grassland surfaces where the vehicles traveled. The reflective targets for the MPL consisted of 8 ft (244 cm) high and 4 ft (122 cm) wide custom metal mesh racks that were located along the MPL's path and beyond the opposite edge of where the plumes were measured. The reflective mesh targets were detected more reliably than the reflective metal poles used during the 2005 YPG field campaign. The two OP-FTIR/OP-LT systems were operated in the same manner as described for the artillery field campaign except that their retroreflectors were located 89 m away horizontally, with the retroreflectors located 1.5 m and 15 m above the ground. The MPL was operated on the Orbit positioner, which was programmed to scan vertically at four elevation angles: 0° (horizontal), 1.378°, 2.754°, and 4.127°, corresponding to 1.5 m, 11.5 m, 21.5 m, and 31.5 m at the retroref-

lector. The MPL and FTIR-LT systems were continuously collecting data during the movement of the tracked vehicles.

The M113 tank (12,349 kg), Bradley Fighting Vehicle (29,937 kg), and M1A1 tank (60,909 kg) were the three types of tracked vehicles that were tested. Such tracked vehicles were selected based on the amount of their use and range of vehicle mass and speed to represent a wide range of DoD training activities for tracked vehicles. Detailed specifications of these three vehicles are available in Appendix A (Table A-2-1). Plumes were generated at vehicle speeds of 8, 16, 24, 32, and 40 km/hr (5, 10, 15, 20, and 25 mph), which represent the range of reasonable speeds for these vehicles.

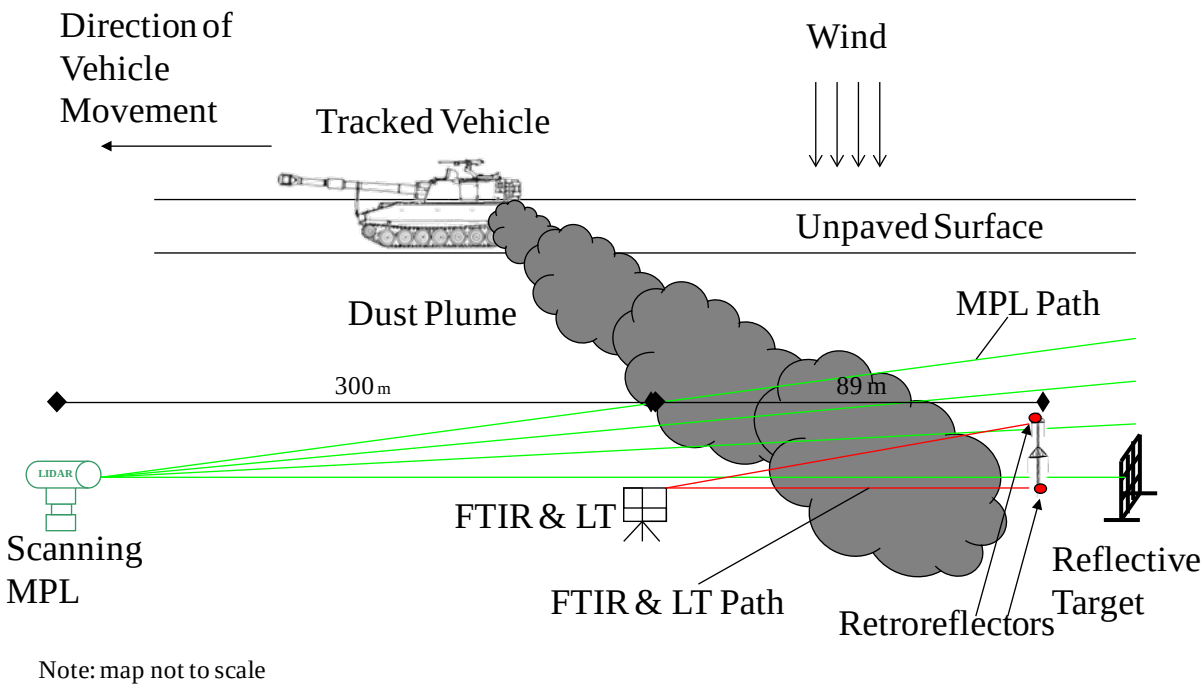

Figure 8 Schematic of the experimental layout for tracked vehicle tests during the 2006 YTC Field Campaign

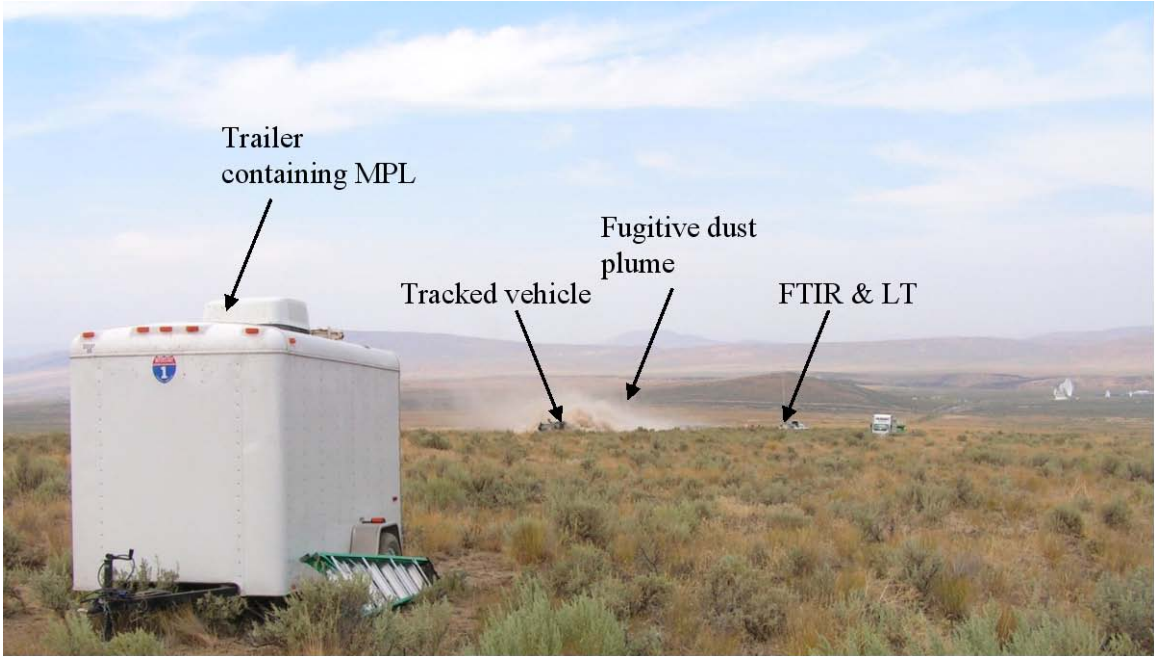

Figure 9 Field picture for tracked vehicle tests during the 2006 YTC Field Campaign (viewed from MPL)

3.3.3 2007 YPG Field Campaign – Emissions from Flying Helicopters

Concentrations and mass fluxes of PM_{10} and $PM_{2.5}$ for dust plumes generated from rotary wing military aircraft were determined with the ORS system during May 2007 at the YPG location (Figure 10 and Figure 11). Detailed field maps depicting the setup are provided in Appendix A (Figure A-3-1 and Figure A-3-2). PM dust emissions were evaluated from a rotary wing aircraft (Model: Bell 210). The Bell 210 is a civilian helicopter that has a military counterpart in the UH-1 (Huey) which is used as a utility helicopter. Detailed specifications of the UH-1 are provided in Appendix A (Table A-3-1). The helicopter flew at speeds ranging from 15 to 60 km/hr (9 to 38 mph) over two surface types: desert pavement and disturbed desert soils. Two-dimensional (2-D) extinction profiles across the dust plumes were constructed by vertically scanning the MPL that was located on the Orbit positioner. Dust plumes generated from the helicopter were monitored continuously.

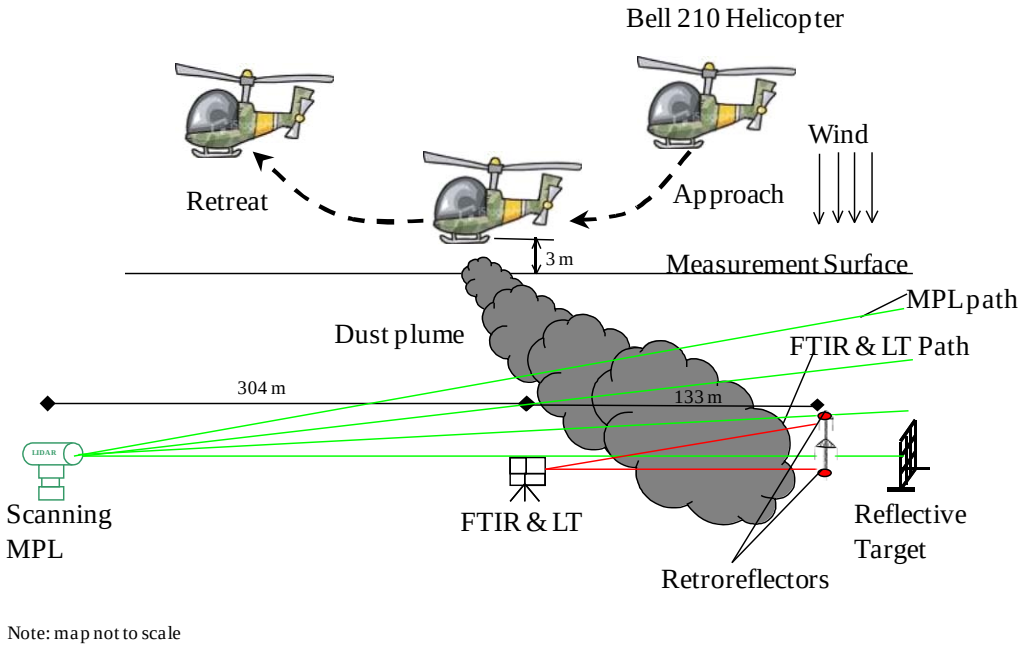

Figure 10 Schematic of the experimental layout for measuring dust emissions from the helicopter during the 2007 YPG Field Campaign

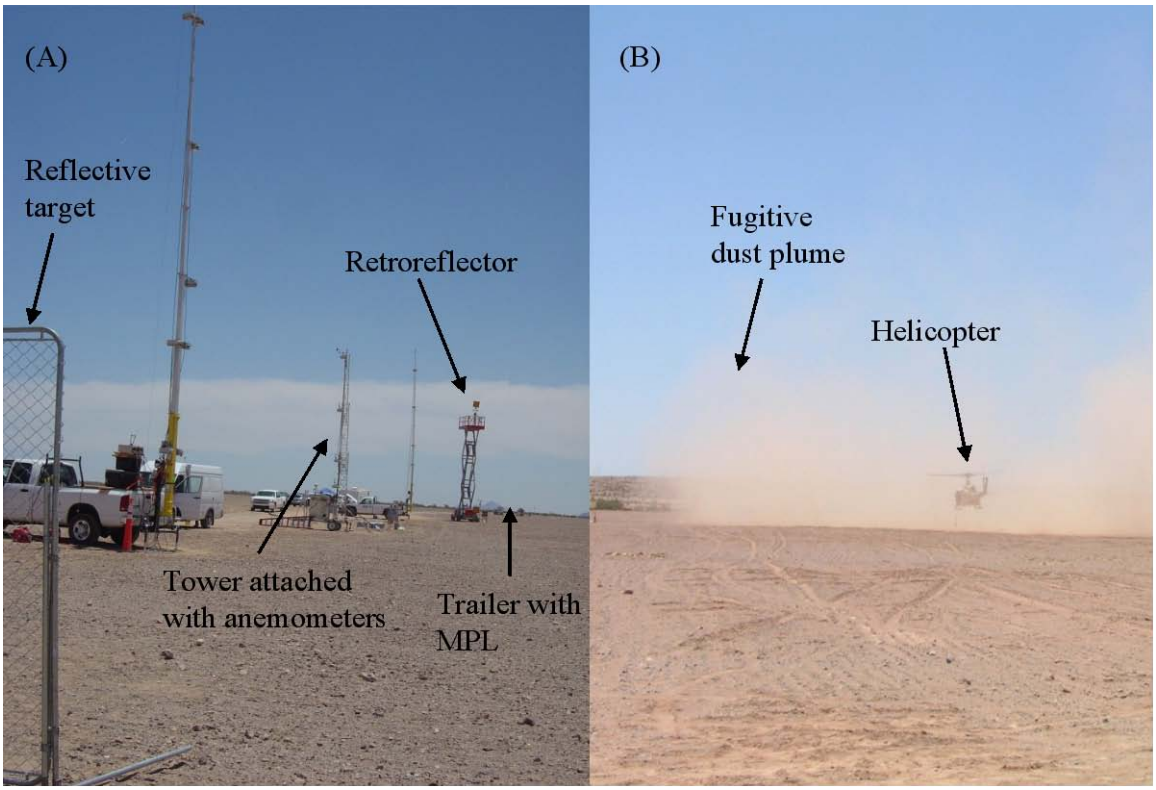

Figure 11 Field pictures for helicopter tests during the 2007 YPG Field Campaign. (A) instruments (viewed from reflective target); (B) example of an event (viewed from MPL)

The MPL was located along the same path as the other ORS systems, but oriented in the opposite direction from those ORS instruments (Figure 10 and Figure 11). Two pairs of OP-FTIR/OP-LT instruments were used to measure light extinction across the plumes generated during helicopter flights. Both pairs of these OP-FTIR/OP-LT instruments were located next to each other and their beams paths were 50 m to 200 m downwind of the helicopter path. The helicopter path was varied depending on the expected concentrations of the dust plumes generated by the helicopter to optimize the PM concentration in the ORS measurement planes. The first path-integrated OP-FTIR/OP-LT beam path was oriented parallel to the ground and directed towards a retroreflector that was placed at the bottom of a tower (i.e., scissor lift) and 130 m away from the location of the first pair of OP-FTIR/OP-LT. The second OP-FTIR/OP-LT pair was directed at a retroreflector that was 15 m above the ground on the same tower. The dust plume generated from each successful helicopter pass was transported by the wind in a generally perpendicular orientation to the measurement plane.

3.3.4 2008 Fort Carson Field Campaign – Emissions from Movement of Tracked and Wheeled Vehicles Measured with the Hybrid ORS System

The hybrid ORS system was implemented to quantify fugitive PM mass emissions that were generated during the movement of tracked and wheeled vehicles during September 2008 at Fort Carson. The similarities and differences between the two versions of the ORS system are apparent by comparing the field schematics shown in Figure 8 and Figure 12. A field picture from the Fort Carson field campaign is also shown in Figure 13. During the 2008 Fort Carson Field Campaign, two unpaved roads were selected for the measurement sites to accommodate changes in wind direction during the field campaign. Detailed field maps depicting the setup are provided in Appendix A (Figure A-4-1 and Figure A-4-2). The MPL continuously scanned in the vertical direction at Site 1 using one of two sets of angles (i.e., 0°, 1.519°, 3.036°, and 4.045° or 0°, 2.025°, 4.045°, and 6.054°) depending on the expected plume elevation. The MPL scanned at angles of 0°, 4.588°, 9.119°, and 12.080° at Site 2. The durations of each vertical scan cycle were 10 s and 14 s for Sites 1 and 2 respectively. The horizontal distances between the MPL system and the OP-LT system were 185 m for Site 1 and 105 m for Site 2. The locations of the OP-LT and retroreflector were switched for Site 2 such that the MPL and OP-LT lasers were emitting light in the same plane but in opposite directions. This change in location was due to differences in topography between the two sites which mandated the locations of the equipment and reflective targets.

The three types of tracked vehicles tested were, the M88A2 (HERCULES, 31,800 kg), the M270 (MLRS, 25,000 kg), and the M577 (12,700 kg) which is part of M113 family of vehicles. The wheeled vehicle tested was a Heavy Expanded Mobility Tactical Truck (HEMTT, 20,000 kg). These vehicles were operated in both directions on the unpaved roads. For each direction, plumes were generated by each vehicle traveling at 8, 16, 24, and 32 km/hr (5, 10, 15, and 20 mph) and their maximum speed. Details about the military vehicles tested during this field study are provided in Appendix A (Table A-4-1).

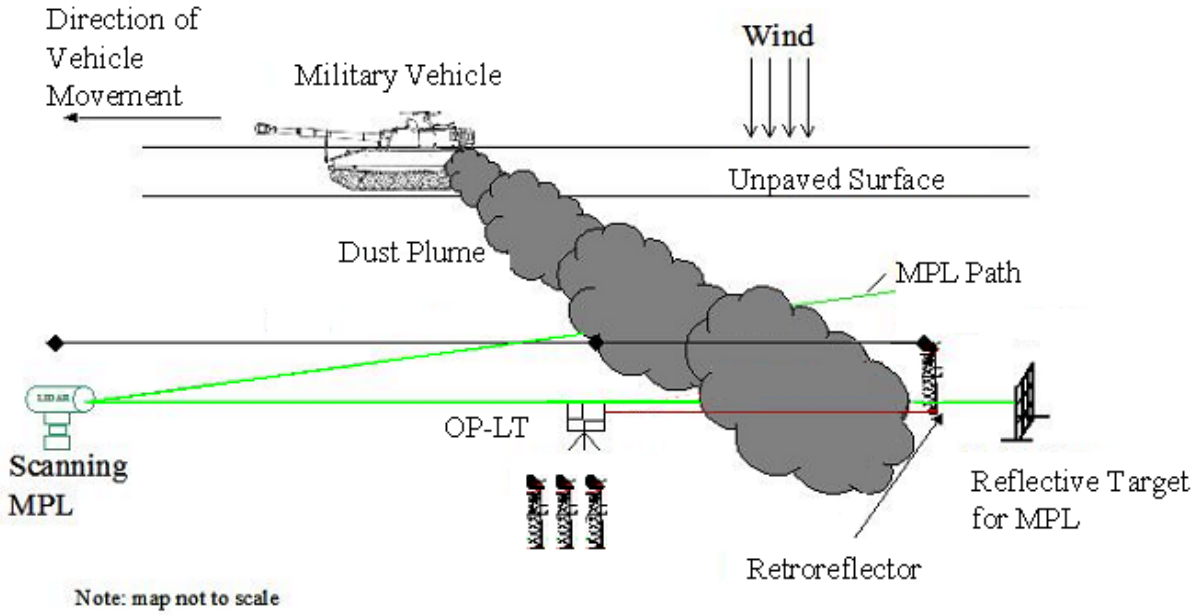

Figure 12 Schematic of the experimental layout for military vehicle tests during the 2008 Fort Carson Field Campaign

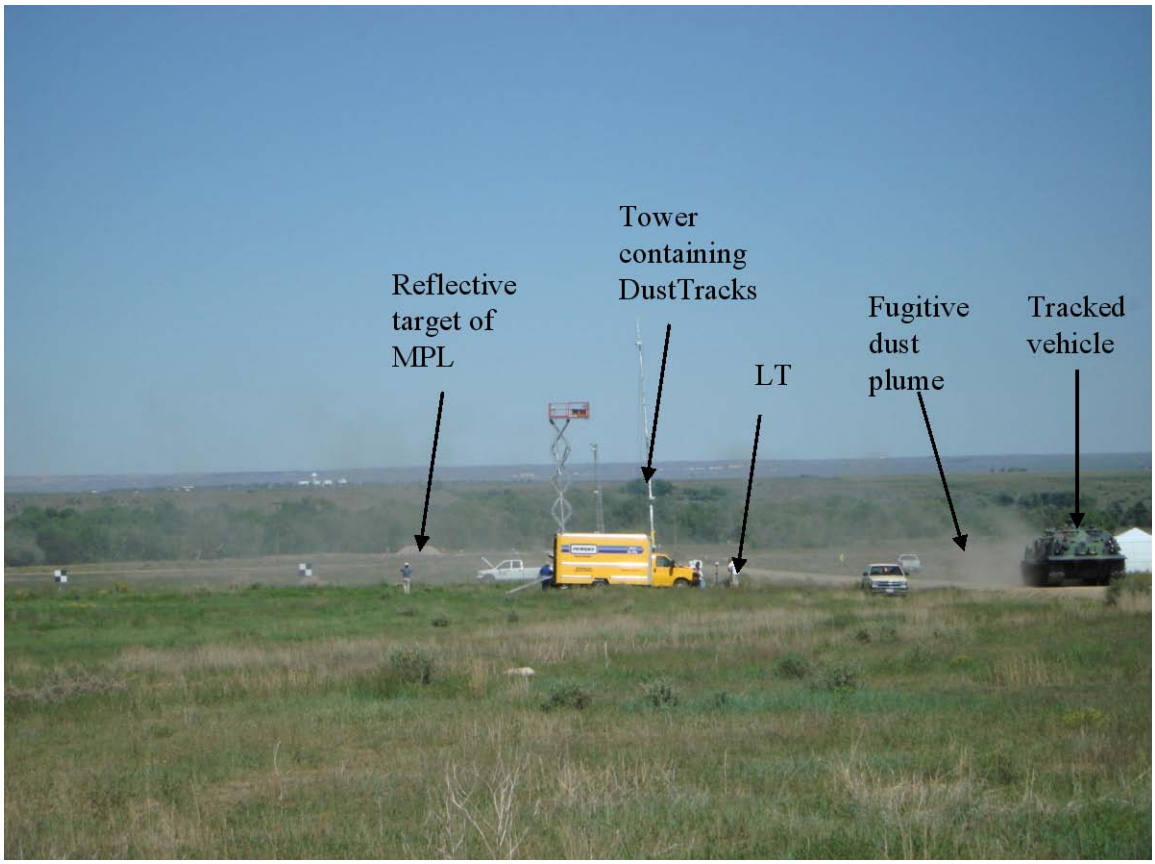

Figure 13 Field picture for military vehicle tests during the 2008 Fort Carson Field Campaign (viewed from MPL)

3.4 Methodology to Determine PM Emissions

3.4.1 Methodology Overview

Figure 14 depicts the overall data processing procedures used for the first three years of the field campaigns and Figure 15 depicts the overall data processing procedures for the Fort Carson field campaign that occurred during the fourth year of the project. The major difference between the two methods is the technique used to determine the mass concentration to light extinction efficiency factor, K*.

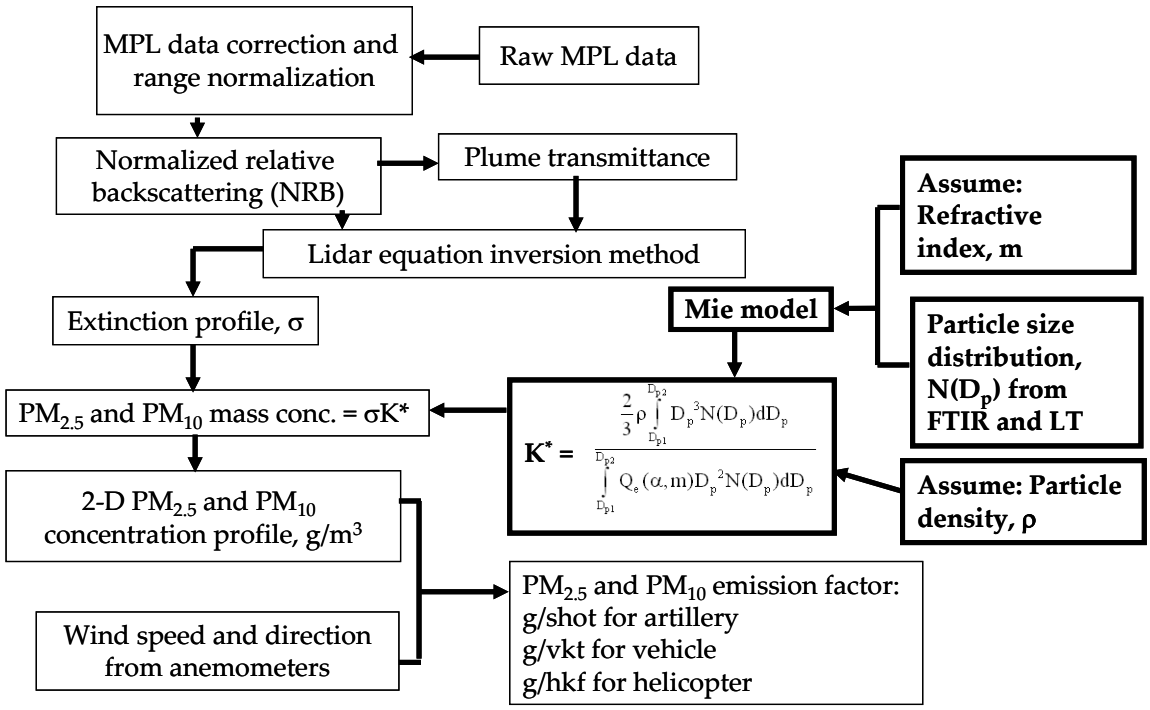

Figure 14 Flowchart describing the overall data processing method used during the first three years of the field campaigns (2005 YPG, 2006 YTC, 2007 YPG)

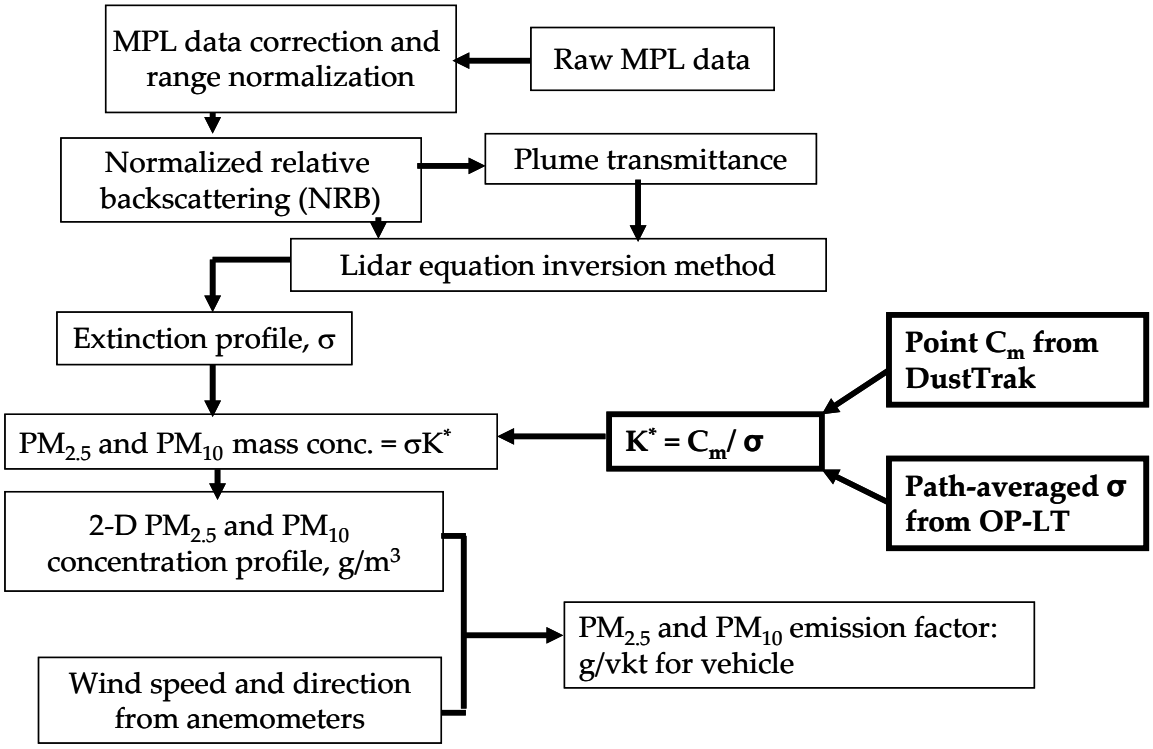

Figure 15 Flowchart describing the overall data processing method used during the 2008 Fort Carson field campaign. The differences between Figure 14 and 15 are highlighted in bold text.

3.4.2 Inversion of MPL Data to Obtain Extinction Profiles through Dust Plumes

3.4.2.1 Conversion of the raw Lidar signal to the normalized relative backscattering signal

As previously mentioned, the MPL detects aerosol particles by emitting pulses of laser light into the atmosphere and then detecting the light that is backscattered by the PM. The raw Lidar signal p(r) in photon counts/sec represents intensity of the received laser light that is backscattered by the PM at a distance of r. The objective of the MPL data calibration is to correct the raw Lidar signal to obtain the NRB signal, which accounts for dark count, dead time, background noise, afterpulse artifact, overlap, and distance corrections.

A summary of the procedure to convert p(r) values to NRB values is described in Figure 16. The dead time correction factor, D[p(r)], corrects p(r) values to account for the MPL underestimating the actual photon counts at high counting rates (e.g. > 5 Mcounts/sec). This correction is a function of the magnitude of the raw p(r) values and is achieved by using a table of values provided by the manufacturer of the MPL. The resulting p(r) values are then corrected for dark counts ($p_{dc}(r)$) because the MPL's photon counting module detects energy, as photon counts, even when the unit's laser is off. Dark counts are measured when the laser is off, and its mean value is subtracted from the p(r) values. The resulting p(r) values are then corrected for the afterpulse signal, $p_{ap}(r)$. The afterpulse signal is caused by internal reflections of the laser light within the instrument that saturate the detector diode at the beginning of the sampling period and the small leakage of photon count signal that is detected for the remaining period of the pulse. Afterpulse signals are obtained by covering the outlet of the transceiver with the laser powered on, and the resulting photon counts are subtracted from the dark count corrected Lidar data. The MPL also detects background photon counts, p_{bg}, which are detected from background light, laser detector noise, and the remaining afterpulse at large distances away from the MPL. The value for p_{bg} is determined by recording the photon counts corresponding to a 40 km distance where no laser light remains to provide backscattered light. The signal is averaged between a distance of 40 km and 55 km, and is then subtracted from the afterpulse corrected Lidar data. The background corrected Lidar signal is then distance corrected due to divergence of the laser signal by multiplying the background corrected Lidar signal by the square of the distance where the Lidar signal is detected. This signal is then modified with the overlap correction factor,

$O_c(r)$, because the MPL has a narrow field of view for its receiver, 100 µrad, that results in a compromised optical efficiency when detecting the backscattered laser light in the near field. The field of view of the receiver cannot "observe" the entire laser beam in the near field until a distance where the more rapidly diverging field of view is able to cover the entire cross-section of the more slowly diverging laser beam (~50 µrad) [28]. Finally the overlap corrected Lidar signals are energy normalized by dividing those values by the initial pulse energy of the laser (E) to provide the NRB signals, as described in Equation 1:

$$NRB(r) = \{(p(r)\times D[p(r)]) - p_{dc} - p_{bg} - p_{ap}(r)\} \times \frac{r^2}{E} \times \frac{1}{O_c(r)} \quad (1)$$

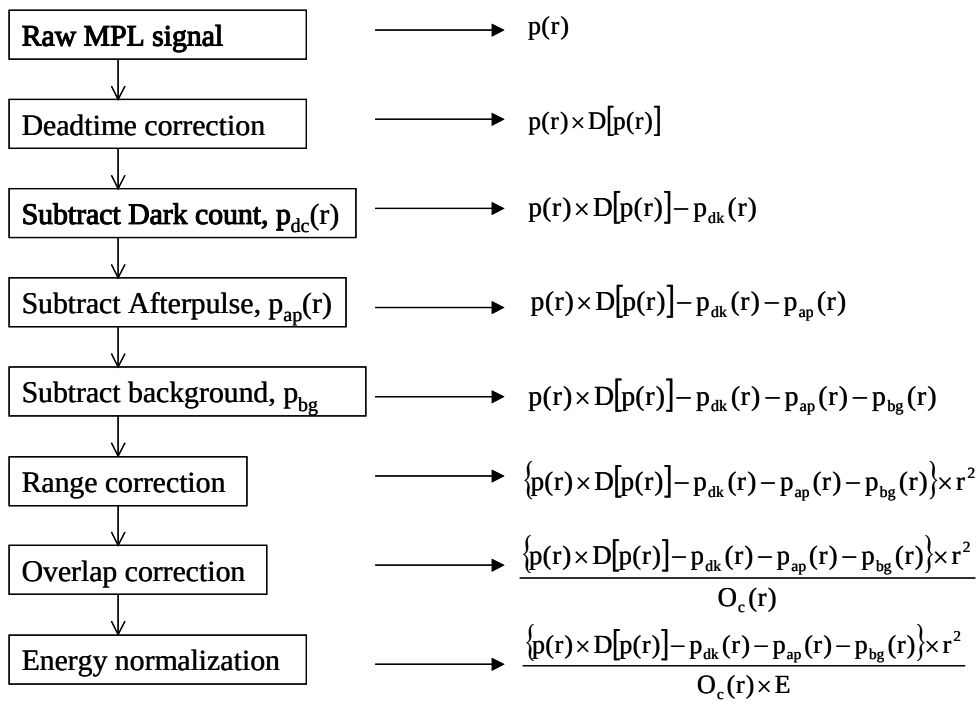

Figure 16 MPL data correction procedures

3.4.2.2 Inversion of Lidar equation to get the extinction profile from NRB data

The extinction of the Lidar signal that is caused by PM can now be described with known values of NRB(r) and the "Lidar equation" (Equation 2). The "Lidar equation" relates NRB(r) to the aerosol's backscatter cross-section (β), transmittance of the laser's light pulses (T) and a Lidar system constant (C) (Equation 2).

$$NRB(r) = \beta(r)\times(T^2(r))\times C \quad (2)$$

From Beer-Lambert Law, $T^2(r)$ is related to the aerosol's extinction coefficient (σ) and distance (r) by:

$$T^2(r) = \exp\left[-2\int_0^r \sigma(r')dr'\right] = \exp\left[-2S\int_0^r \beta(r')dr'\right] \tag{3}$$

where S is the "Lidar ratio" or the "extinction-to-backscatter ratio" and is defined as σ/β, and is determined by the optical properties of dust particles and the incident light's wavelength. S is assumed constant throughout the plume. The analytical solution to the Lidar equation was derived by Fernald [29] and Roy *et. al.* [30] to determine the extinction profile from the NRB profile by Equation 4.

$$\sigma(r) = \frac{NRB(r)}{C^* - 2\int_0^r NRB(r')dr'} \tag{4}$$

where C^* is defined as: $C^* \equiv C/S$.

The minimum resolution of the NRB(r) signal from the MPL for this research is 15 m. Hence, the integral part in Equation 4 can be approximated by the summation:

$$\int_0^r NRB(r)dr \approx \sum_{i=1}^{r/15}\left[NRB(i)\times 15\right] \tag{5}$$

where i = 1, 2, ..., r/15. Therefore, the extinction profile through a dust plume, which spreads over $\tilde{N}$ bins that each 15 m wide, is determined from the discrete NRB(r) profile and C^* by Equation 6 (non-plume extinction and backscattering are neglected):

$$\sigma(n) = \frac{NRB(n)}{C^* - 2\sum_{i=1}^{n}\left[NRB(i)\times 15\right]} \tag{6}$$

where n = 1, 2, ..., $\tilde{N}$. The integral part in Equation 3 can also be approximated by summation to determine the transmittance of the entire dust plume:

$$T = \exp\left[-\sum_{i=1}^{\tilde{N}}\left(\sigma(i)\times 15\right)\right] \tag{7}$$

During the field campaigns, a reflective target was located behind each of the dust plumes. Therefore, the transmittance of laser light through the dust plumes can be determined from the reflective target's NRB signals before and after the dust passes through the MPL's optical path[31]:

$$T = \sqrt{\frac{NRB_t}{NRB_{t0}}} \tag{8}$$

where NRB_t is the NRB signal from the reflective target during a plume event and NRB_{t0} is the NRB signal from the reflective target before the plume event.

Finally, the light extinction profile through a dust plume can be determined by solving a system of ($\tilde{N}$ +1) equations with $\tilde{N}$ +1 unknowns (i.e. σ_1, σ_1, ..., $\sigma_{\tilde{N}}$, and C^*):

$$\begin{cases} \sigma(1) = \dfrac{NRB(1)}{C^* - 30NRB(1)} \\ \sigma(2) = \dfrac{NRB(2)}{C^* - 30\left(NRB(1) + NRB(2)\right)} \\ \vdots \\ \sigma(\tilde{N}) = \dfrac{NRB(\tilde{N})}{C^* - 30\left(NRB(1) + NRB(2) + ... + NRB(\tilde{N})\right)} \\ \sqrt{\dfrac{NRB_t}{NRB_{t0}}} = \exp\left[-\left(\sigma(1) + \sigma(2) + \ldots + \sigma(\tilde{N}) \cdot 15\right]\right. \end{cases} \tag{9}$$

3.4.3 Determination of PM Mass Emissions for the First Three Field Campaigns

3.4.3.1 Conversion from 1-D extinction profiles to 1-D mass concentration profiles

The initial version of the ORS system was implemented during the first three field campaigns, during which the extinction efficiency factor K^* was determined to convert the light extinction profiles from the MPL to PM mass concentration profiles. As previously mentioned, K^* is defined as the ratio of the PM's mass concentration (C_m) to light extinction coefficient (σ):

$$K^* = \frac{C_m}{\sigma} = \frac{\int_{D_{p\,min}}^{D_{p\,max}} \frac{\pi}{6} D_p^{\,3} \rho N(D_p) dD_p}{\int_{D_{p\,min}}^{D_{p\,max}} Q(\alpha, m) \frac{\pi}{4} D_p^{\,2} N(D_p) dD_p} \tag{10}$$

where D_p is the aerosol particle's diameter; D_{pmin} and D_{pmax} are the minimum and maximum particle diameters respectively; $N(D_p)$ is particle diameter distribution per unit volume of sample; Q is the extinction efficiency; α is the optical size parameter of a particle defined as $\alpha \equiv \pi D_p/\lambda$; and λ is the wavelength of MPL's laser pulses (λ = 527 nm). The particle density, ρ, was determined as 2.5×10^3 kg/m^3, representative for desert dust [32]. The real part of the refractive index (n′) was assumed to be 1.54, which is the mean value of n′ for desert dust that ranges between 1.53 and 1.57[33]. The imaginary part of the refractive index (k) was assumed to be zero.

Size distributions of the dust particles were determined using measurements from the OP-FTIR/OP-LT instruments by applying a method developed by Varma *et. al.*[34]. Six wavelengths (2.26, 2.37, 3.48, 3.96, 4.49, and 12.9 μm) were selected from the OP-FTIR spectrum in addition to the OP-LT's wavelength of 0.67 μm to obtain the extinction values to create a smoothed extinction distribution. These wavelengths were selected to avoid the dust's absorption spectrum and other gaseous absorption peaks so that the light extinction values at each wavelength are only due to the PM's ability to scatter light. A triangle-based cubic interpolation was performed between these wavelengths to generate 64 interpolated data points that were used to compute the extinction efficiency (kernel) matrix, $Q_e(D_p, \lambda)$ (the extinction efficiency for each pair of particle diameter, D_p, and λ with constant refractive index). The interpolated data set enhances the over determination of the inversion problem and ensures a unique solution. The resulting interpolated extinction values define the baseline offset (when dust is encountered by light from the ORS devices) that excludes the extinction caused by H_2O vapor and CO_2 and avoids other gaseous and PM absorption features. Also, 64 bins were used that describe particle diameters ranging from 0.25 μm to 20 μm on a log scale, with the first 23 bins corresponding to $PM_{2.5}$, and the first 43 bins corresponding to PM_{10}. After the extinction efficiency matrix was computed, the matrix was inverted to determine the number concentrations for all of the 64 diameter bins[35, 36]. Mie calculations were then completed in the forward direction to evaluate if the retrieved extinction spectrum from the derived size distribution fit well with the input extinction. $PM_{2.5}$ and PM_{10} were then calculated by adding the mass concentrations in all particle diameter bins up

to 2.5 μm, and to 10 μm, respectively. Finally, the 1-D PM-mass concentration profiles for the dust were quantified from the 1-D extinction profiles and the calculated values of K^* with $\rho = 2.5$ g/cm^3, $n' = 1.54$, $k = 0$, and the dust size distributions provided by the OP-FTIR and OP-LT measurements and data interpretation.

3.4.3.2 Determination of 2-D mass concentration profiles

The method used to convert 1-D PM mass concentration profiles into 2-D PM mass concentration profiles is dependent on the type of source. Operation of the instruments in the field is based on the characteristics of the plumes that are generated by the sources to be able to characterize appropriate cross-sections of the plume. For example, plumes from puff sources (i.e. artillery back blast plumes) can completely pass through the vertical plane that is characterized by the ORS system within 10 to 30 sec. Such short durations prevent the MPL from scanning the entire cross-section of the plume and therefore the MPL was kept at a fixed position. On the other hand, plumes from mobile sources (i.e., tracked/wheeled vehicles and flying helicopters) that travel perpendicular to the wind's direction but parallel to the vertical plane that is characterized by the ORS system will pass through the measurement plane within 100 to 200 sec. Such durations allow the MPL to complete 10 to 20 scans of the plume's cross-section for each plume event. Hence, the methods to characterize these shorter-term and longer-term plumes are different as described below.

3.4.3.2.1 Short-Term Plumes from Puff Sources – Emissions from Back-Blasts of Artillery Firings

Dust plumes generated by the back blasts during the firing of artillery required the optical path of the MPL to be kept at a fixed angle when detecting the plume (Figure 6). The horizontal mass concentration profiles at the ground level were determined based on method described in Sections 3.4.1 and 3.4.2. However, the vertical 2-D mass concentration profiles were constructed based on the horizontal 1-D mass concentration profiles and the vertical mass concentration gradients obtained from the two ground-based OP-FTIR/OP-LT systems with retroreflectors. As previously mentioned, these devices detected dust along two paths, one was directed horizontally to a retroreflector that was colinear with the MPL's optical path that was 1.5 m above the ground and the other was directed to a retroreflector that was located 10 m above the ground. The horizontal distance between the OP-FTIR/OP-LT systems and their corresponding retroreflectors was 100 m. Measure-

ments by the OP-FTIR/OP-LT systems provided path-averaged mass concentrations. The vertical gradient in mass concentration was then calculated by fitting a bivariate Gaussian function to the retrieved concentration data from those two paths[34].

3.4.3.2.2 Longer-Duration Plumes from Mobile Sources – Emissions from Moving Tracked Vehicles and Flying Helicopters

Dust plumes generated by the movement of tracked vehicles during the 2006 YTC Field Campaign and flying helicopters during the 2007 YPG Field Campaign were detected by the MPL by scanning the plumes with fixed elevation angles and placing the MPL at specific horizontal distances from the OP-FTIR/OP-LT instruments (Figure 8 and Figure 10). The dust plumes from both field campaigns were generated from mobile sources moving along a straight line parallel to the optical path of the ORS devices. The duration of each vertical scan of the MPL was 10 sec, allowing 10 to 20 vertical scans per plume event and allowing the MPL to characterize the vertical structure of each of the plumes. The 1-D PM-mass concentration profile along each scanned path of the MPL was determined first. The 2-D PM-concentration profile across the dust plume was then calculated by interpolating the data obtained from the corresponding 1-D PM-concentration profiles.

3.4.3.3 Determination of PM mass emission factors for puff and mobile sources

The ORS system operated continuously during all plume events. The PM-mass concentration profiles across the dust plumes' cross sections were then determined every second or every 10 sec, depending if the MPL was in a fixed position or was scanning through fixed elevation angles, respectively. Wind speed and direction were monitored during each plume event with two anemometers (R.M. Young Inc.). The PM-mass emission factor (EF) for each event was computed by integrating the 2-D mass concentration profiles with the calculated wind speeds that were perpendicular to the ORS observing plane and with the duration of each plume event in a rectangular coordinate system using equations (11) and (12) for artillery back blasts (puff source) and movement of tracked vehicles and flying helicopters (mobile sources), respectively:

$$EF = \sum_{t=0}^{T}\left[\sum_{y=0}^{Y}\sum_{z=0}^{Z} C_m(y,z,t)\Delta y \Delta z\right] u \cos\theta \Delta t \qquad (11)$$

(g-PM/shot)

$$EF = \frac{1000}{Y} \times \sum_{t=0}^{T} \left[\sum_{y=0}^{Y} \sum_{z=0}^{Z} C_m(y,z,t)\Delta y \Delta z \right] u \cos\theta \Delta t \tag{12}$$

(g-PM/vkt or g-PM/hkf)

where T is the duration of the plume event; Y is the width of the ORS path where the plume is located; Z is height of the ORS path where the plume is located; $C_m(y, z, t)$ is the mass concentration of the particles in the plume at location y and z, and time t; Δy and Δz are integration steps in the y and z directions respectively; u and θ are the mean wind speed and the angle between the wind direction and the normal direction of the ORS observing plane during that event, respectively. The acronyms "vkt" and "hkf" represent "vehicle kilometer traveled" and "helicopter kilometer flown" respectively, and 1,000/Y is the conversion factor to covert the PM mass emission along a path of Y meters wide to the PM mass emission for one kilometer when considering plumes generated by the movement of a tracked vehicle or helicopter.

3.4.4 Determination of PM Mass Emissions for the 2008 Fort Carson Field Campaign

3.4.4.1 Determination of mass concentration profiles

As previously mentioned, a "hybrid" ORS system, as described by Hashmonay *et al.*[37], was used during the 2008 Fort Carson Field Campaign. This hybrid system consists of one horizontal ground-level OP-LT and three ground-level DT aerosol monitors without the use of the OP-FTIR instrumentation to determine the light extinction efficiency factor, K*. The four 1-D extinction profiles from the MPL scans were interpolated to provide 2-D extinction profiles. The duration of the MPL vertical scans was 10 or 14 seconds, while the duration of a plume event was between 70 to 120 seconds. Therefore, there were approximately 5 to 10 time-dependent 2-D extinction profiles generated for each plume event. These time-dependent 2-D extinction profiles were converted into time-dependent 2-D mass concentration profiles for both $PM_{2.5}$ and PM_{10} using the K* values from the hybrid system and a second algorithm developed during this research project (Figure 15). For this new algorithm, K* is the ratio of C_m to σ measured by the DT aerosol monitors and the OP-LT respectively. Unlike the first algorithm (Figure 14), only the upper particle diameter limits corresponding to $PM_{2.5}$ or PM_{10} are needed when applying this algorithm.

The corresponding values of K* for $PM_{2.5}$ and PM_{10} were determined from the slope of the linear regressions between the OP-LT measured extinction

values and the DT's measured mass concentration values for $PM_{2.5}$ and PM_{10}. Those K* values were then corrected from their OP-LT measured wavelength of 670 nm to a wavelength of 527 nm that was used by the MPL using Mie theory and typical size distributions measured for the dust. Finally, the wavelength-corrected K* values were multiplied with the corresponding extinction profiles that were measured by the MPL to obtain the 2-D mass concentration profiles for $PM_{2.5}$ and PM_{10}.

3.4.4.2 Determination of PM mass emission factors

Emission factors were determined by integrating all of the time dependent vertical 2-D PM-mass concentration profiles during each plume event with wind speeds and wind directions (equation 13). Unlike the previous three field campaigns, this integration was completed by using a polar coordinate system instead of rectangular coordinate system to match the radial direction of the MPL scans. Moreover, wind speed was treated as a function of height. Power regression fits of the wind speed data at five heights were performed for each vehicle pass, and each regression was used to determine wind speed at a specified elevation during that pass of an MPL scan. Wind direction was treated as a constant in the vertical direction and emission factors calculated using:

$$EF = \frac{1000}{Y} \times \sum_{t=0}^{T} \left(\sum \theta C(A,t) \Delta A \right) u(z) \cos \Delta \quad \text{(g-PM/vkt)} \tag{13}$$

where T and Y are the same as previously defined in Equation 12. $C_m(A, t)$ is the mass concentration of the particles in the plume at time t within the differential area A, ΔA is integration steps in the differential area A, u(z) is the mean wind velocity at the height of the MPL's measured location, and θ is the angle between the wind direction and the normal direction of the ORS observing plane during that event.

3.5 Hybrid Remote Sensing and In-Situ Measurement System to Measure Fugitive Dust Flux

The new hybrid test method for measuring fugitive dust emissions was initially deployed and its performance evaluated by SI-1399 and SI-1400 at YPG during the rotary-winged aircraft testing and at Fort Carson during the tracked vehicle testing. The measurement system included one open path laser transmissometer (OP-LT) operating in the visible wavelength, (at least) two time-resolved DT aerosol monitors, and (at least) two wind speed instruments. Each DT aerosol monitor was capable of measuring

PM_{10} and $PM_{2.5}$ concentrations with a size selective inlet and the configuration normally consists of a co-located pair of separate monitors for PM_{10} and $PM_{2.5}$ concentrations (DM_{10} and $DM_{2.5}$ respectively). Figure 17 shows a schematic of the setup configuration with three DT aerosol monitors mounted on the tower at different elevations. Preferably these DT aerosol monitors would be calibrated to integrated mass filter measurements in a laboratory setup using a gravimetric method. The OP-LT beam path distance from the sensor to the retroreflector can vary according to the expected plume width and possible trajectories. Typically, the path distance will be on the order of several hundred meters. The simplest configuration would use one tower located at the expected plume centerline. The two (or three) DT aerosol monitor pairs and the two wind monitors would be distributed evenly at different heights, the lowest at the same height as the OP-LT beam.

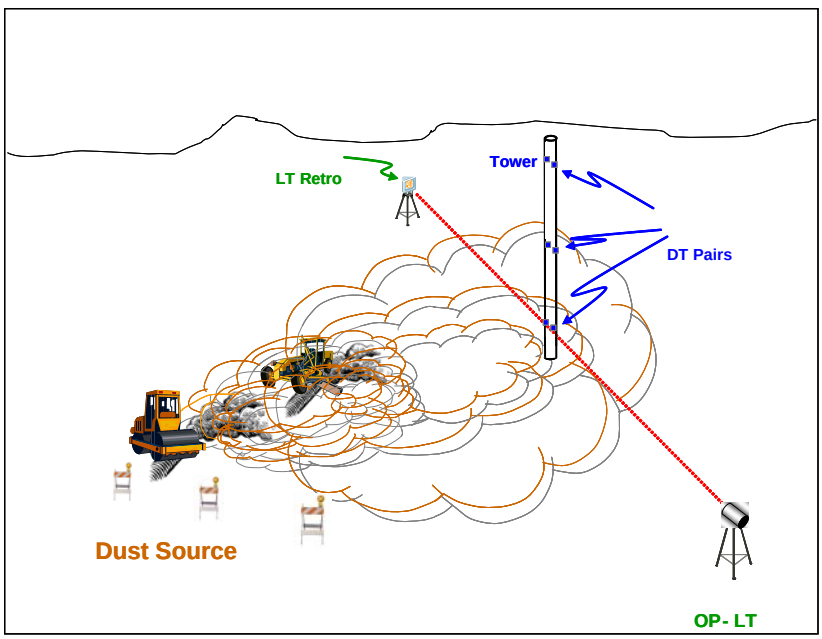

Figure 17 Schematic of the hybrid dust measurement configuration. The DT pairs consist of one PM_{10} and one $PM_{2.5}$ monitor.

3.5.1 Hybrid System Principles

The concept behind this emission measurement method is to use the OP-LT to determine the entire cross-plume, plume-averaged mass concentration of PM_{10} dust at ground level $C_y^{\overline{PM_{10}}}$, and use the vertically distributed PM_{10} DT aerosol monitors to determine the vertical distribution of the dust mass concentration. These two parameters can be used to deter-

mine the plane-integrated PM_{10} mass concentration ($PIMC_{10}$), which is the mass concentration integrated over the vertical downwind measurement plane:

$$PIMC_{10} = \iint C^{PM_{10}}(y,z)\,dy\,dz \tag{14}$$

In order to determine $\overline{C_y^{PM_{10}}}$ from the OP-LT measurements, the OP-LT must be calibrated against the DM_{10} DT aerosol monitors using the procedure described in the next section.

The $PIMC_{10}$ is calculated by the following expression:

$$PIMC_{10} \cong \frac{\overline{C_y^{PM_{10}}}}{C_{z_0}^{DM_{10}}}\,\overline{C_z^{DM_{10}}}\,A \tag{15}$$

where $C_{z_0}^{\overline{DM_{10}}}$ is the measurement of DM_{10} at the same height as the OP-LT beam. $C_z^{\overline{DM_{10}}}$ is the average of all of the measurements by the vertically distributed DM_{10} monitors on the tower, and A is the area of the plane defined by the product of the OP-LT path distance, L, and the height of the top DM on the tower, H. The values for $PIMC_{10}$ are in units of g m^{-1}. The ratio $C_y^{\overline{PM_{10}}} / C_{z_0}^{\overline{DM_{10}}}$ is a correction factor for the horizontal capture of the plume by the single tower. This correction ratio depends on the position and width of the plume. If the ratio has a value of 1, the plume is distributed uniformly over the OP-LT beam path. The correction ratio is <1 when a narrow plume is centered on the tower and the PM_{10} concentrations measured at the tower location overestimate the plane average concentration. This correction ratio is >1 when a narrow plume misses the tower and the PM_{10} concentrations measured at the tower location underestimate the plane average concentration.

The PM_{10} flux, $\varphi_{PM_{10}}^{A}$, through the measurement area is given by:

$$\varphi_{PM_{10}}^{A} = PIMC_{10}\,\overline{U_x} \tag{16}$$

where $\overline{U_x}$ is the normal wind component averaged over the two or three vertically distributed anemometers. If the entire plume is encompassed by the measurement area, $\varphi_{PM_{10}}^{A}$ is equal to the total mass emission rate for

PM_{10} released from the target fugitive source. The flux of $PM_{2.5}$ would be calculated similarly by substituting the measurements from the $DM_{2.5}$ DT aerosol monitors and using the same wind speed data.

3.5.2 Results: Hybrid System Performance

The OP-LT was calibrated, and the validity of the new dust monitoring method was demonstrated with data collected during the rotary-winged aircraft measurement field campaign at YPG in May 2007 and the tracked vehicle measurement campaign at Fort Carson in October 2008. These campaigns provided us with an abundance of OP-LT and DM measurement data with which were used to test and validate the new method. The measurements were event-based with each dust plume originating from the aircraft or tracked vehicle as it passed the instrument array. The PM and extinction data were recorded continuously as the dust plume passed through the measurement plane.

The OP-LT measures the path-integrated extinction (PIE) given by:

$$PIE^{LT} = \int_0^L \varepsilon(y)\,dy \tag{17}$$

where $\varepsilon(y)$ is the extinction value at a location y along the beam path; L is the beam-path distance from the OP-LT sensor to the retroreflector. For fixed particle composition and size distribution, the path-averaged extinction, PAE: PIE^{LT}/L, is proportional to the path-averaged dust concentration.

The OP-LT is calibrated by performing a linear regression fit of the path-averaged extinction to the average value of the PM_{10} measurements by the DT aerosol monitors, distributed along the cross-plume OP-LT beam path $\overline{C_y^{DM_{10}}}$, to compute the calibration factor, $F^{DM\text{-}LT}$

$$\overline{C_y^{DM_{10}}} = F^{DM-LT}\,PAE^{LT} \tag{18}$$

At YPG 1840, one-second dust plume measurements were collected for 32 plume events. For YPG measurements the one-second PM_{10} concentration data (calibrated to gravimetric filter-based measurements) from the lowest DT aerosol monitors (situated along the OP-LT beam path) were spatially averaged ($\overline{C_y^{DM_{10}}}$) and synchronized against the path-averaged extinction.

The Pearson correlation was calculated for each event and six events out the total 32 had a Pearson correlation higher than 0.9 (R >0.9). The other 26 events had Pearson correlation values between 0.6 and 0.9, which indicates a less homogeneous plume along the OP-LT path length. Figure 18 shows an example of the calibration data from YPG for the six events with the highest correlation occurring between the average PM_{10} concentration from the three DT aerosol monitors and the OP-LT path-averaged extinction.

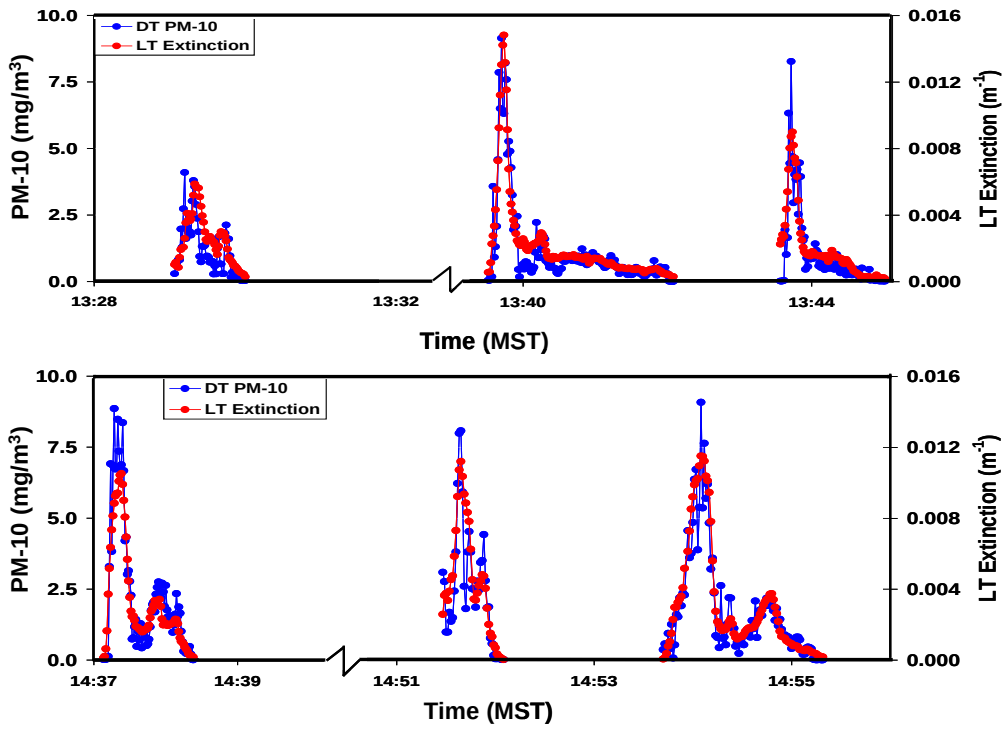

Figure 18 OP-LT calibration measurements made at Yuma Proving Grounds - The six dust events with high dust correlations (R > 0.9)

Plots of $\overline{C_y^{DM_{10}}}$ measurements versus the path-averaged OP-LT extinction measurements are shown in Figure 19. Figure 19-a shows the plot of the entire data set (32 events, 1840 points) and Figure 19-b shows the plot of the measurements made during the six events shown in Figure 18. The slope of the linear plot for the full data set results in a calibration factor (areal mass density) of 551 mg/m^2 and the R^2, the square of the Pearson correlation coefficient, has a value of 0.69. As one may expect, reducing the data set to the six high-correlation events results in much less scatter in the linear plot, as shown in Figure 19-b. The linear plot of the six events resulted in the improved R^2 value of 0.83 and a calibration factor of 592 g/m^2. The six highly correlated events represent the case when the plume is more evenly distributed along the OP-LT beam path and conditions are

favorable for such calibration. It is not necessary to use any preset number of DT aerosol monitors along the OP-LT beam path as long as there are a large number of data sets with Pearson correlation coefficients > 0.9, and an overall $R^2 > 0.8$ in the linear regression calibration curve.

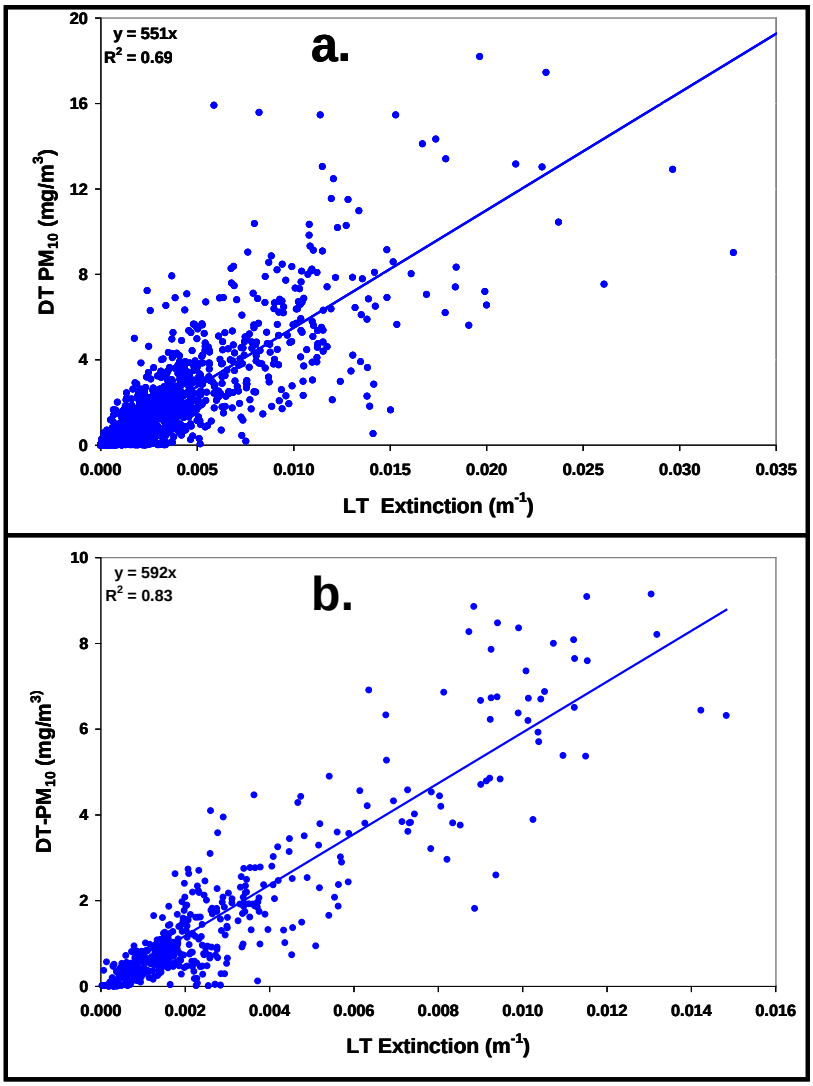

Figure 19 Plot of the OP-LT and DM-PM_{10} Calibration Measurements. a) The full 1,840-point data set, b) The six high-correlation events (508 points) data set.

At Fort Carson, the second by second correlation between the OP-LT extinction and average (3 bottom DT-PM_{10} monitors) PM_{10} concentrations for each event were quite poor ($r < 0.5$). This may be due to the type of fugitive dust source (tracked vehicle). Therefore, the calibration curve was generated for 20 events on September 16th 2008. Figure 20 shows a very strong correlation and a calibration factor almost identical to the Yuma dust. This calibration factor (593 mg/m^2) was used for the dust PIMC calculations for the hybrid method.

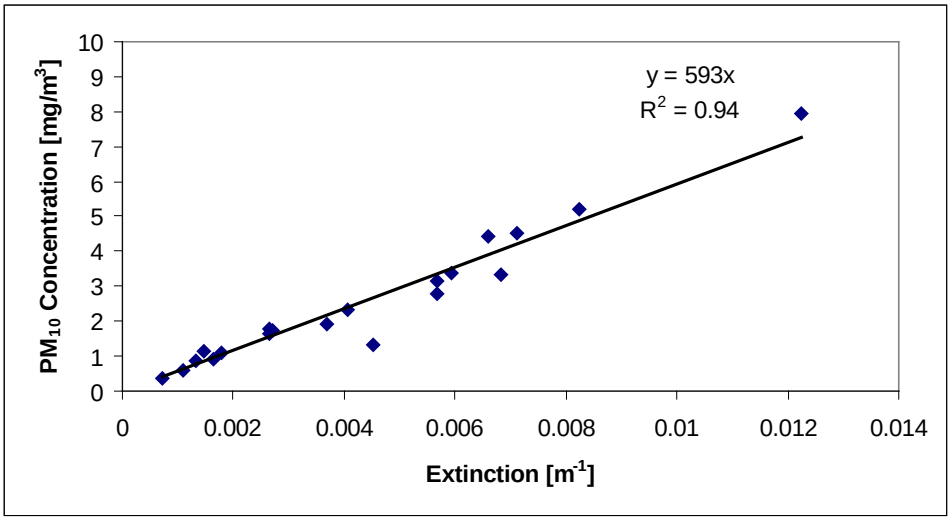

Figure 20 Plot of the OP-LT and DM PM_{10} calibration measurements at Fort Carson for events on September 16th 2008.

3.5.3 Proof-of-Concept of the Hybrid Method

The fifteen DT aerosol monitors used by DRI to measure PM_{10} (DM_{10}s) at YPG formed a 3×5 grid that defined the measurement area, A, as a 105 m wide by 10 m high plane. The $PIMC_{10}$ is calculated as the product of the mean value of the 15 DM_{10}s for the three towers and the area A:

$$PIMC_{10}^{Grid} \cong \overline{DM_{10}^{Grid}}\, A \tag{19}$$

The configuration used at YPG has the elements required for applying the hybrid method if towers one and three are ignored. The calculation of $PIMC_{10}^{Grid}$ can be compared to the $PIMC_{10}$ hybrid method by performing a linear regression for all 32 rotary-winged plume events. We tested the effect of reducing the number of DT aerosol monitor pairs on the $PIMC_{10}$ emission estimate, the results of which are shown in Figure 21 for three cases: five, three, and two DM_{10}s. These results indicate that the new hybrid method's calculations of $PIMC_{10}$ values are comparable (slope close to one with $R^2 > 0.85$) to the calculations of $PIMC_{10}^{Grid}$. Also, it is shown that the use of five DT aerosol monitor instruments on the tower for the hybrid method is not required, as similar results can be obtained by using only two or three DT aerosol monitors. Less DT aerosol monitors simplifies the instrumentation set up and logistics of deployment, making this method an attractive alternative to more costly emission profiling methods.

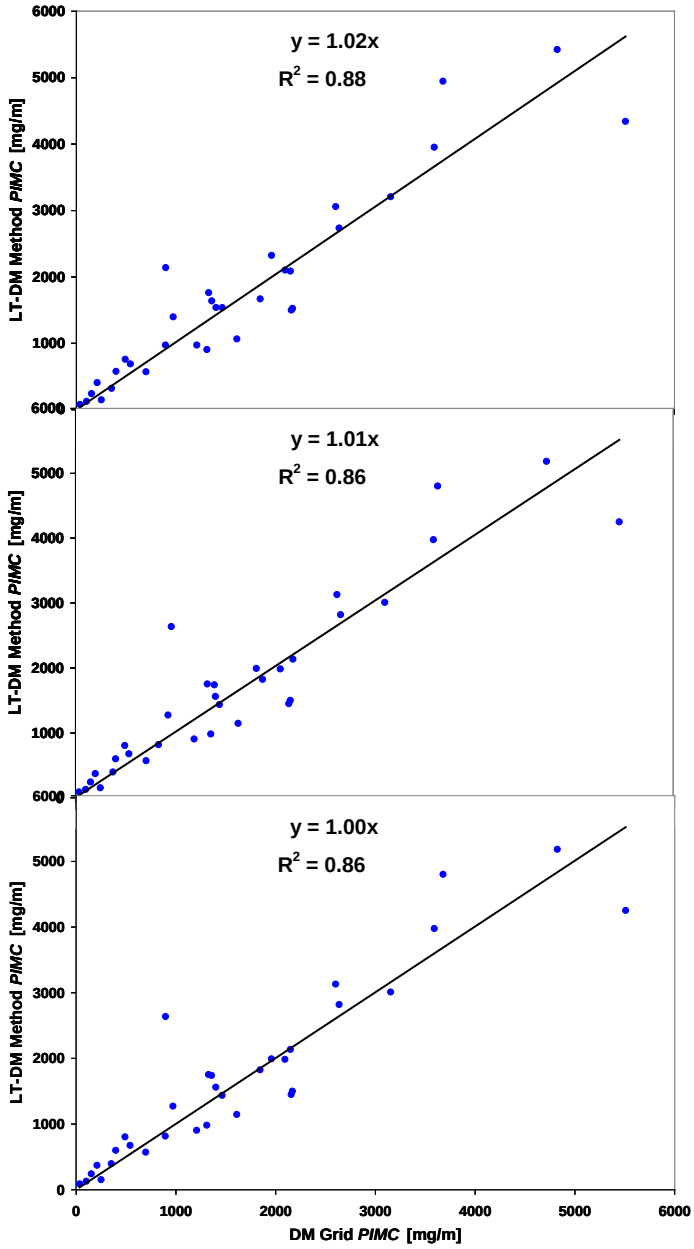

Figure 21 Comparison of PIMC determined with the new method to the PIMC determined from the grid of DT monitors. Top: 5 DT monitors in new method, middle: 3 DT monitors in new method, bottom: 2 DT pairs in new method.

The Fort Carson field campaign offered another chance to evaluate the hybrid approach for tracked vehicles. In this type of source, the variability in the DT data was much larger than the rotary wing data, and there was no single event where the Pearson correlation was > 0.5 between the OP-LT and DT aerosol monitor data (see 6 events in Figure 18 for rotary wing source). Therefore it is expected that the agreement between the Grid and the Hybrid method will be worse and the regression R^2 will be also quite poor. However, the results are quite comparable as can be seen in Figure

22. It is observed that the agreement for plane integrated mass concentration is better with 4 and 3 DT aerosol monitors on the middle tower but the correlation is the best for 2 DT monitors on the middle tower. For tracked vehicle sources, it is recommended to have at least 3 DT aerosol monitors on the single tower when using the hybrid method.

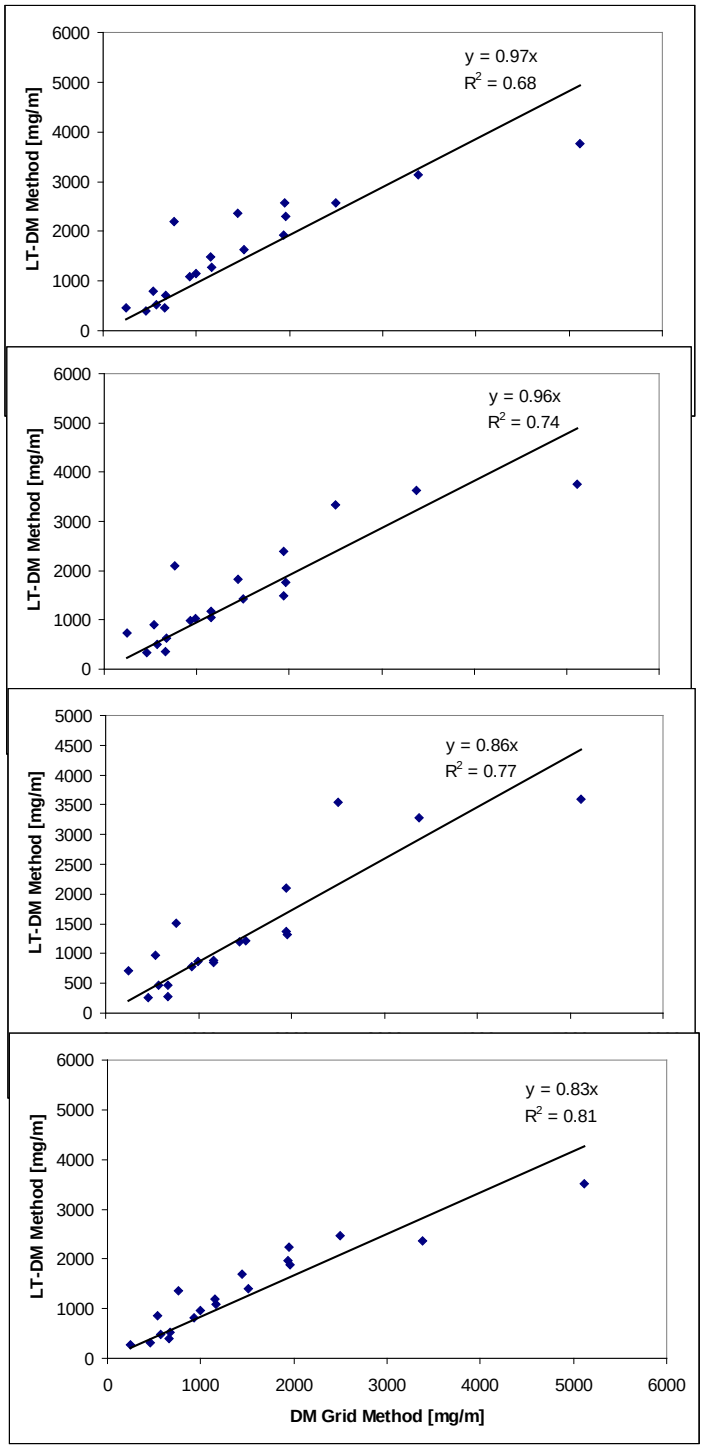

Figure 22 Comparison of PIMC determined with the new method to the PIMC determined from the grid of DT monitors for 20 events at Fort Carson. Top: 4 DT monitors in new method, second and third from top: 3 DT monitors in new method (1,2, and 4 and 1,3, and 4), bottom: 2 DT pairs in new method.

3.5.4 Conclusions: Hybrid Method

As a joint effort between SI-1399 and SI-1400, the research teams compared the results for emission flux determinations using the hybrid in situ

and ORS system to the full in situ flux tower system, which requires multiple (three) towers and 30 DT aerosol monitors. The results indicate that the hybrid system can provide equivalent measurements as compared with the flux tower system.

Acceptance of the new test method would offer an accurate, cost-effective method to acquire dust emission measurement data for the development of fugitive dust emission factors. The hybrid method brings closure to an issue that has hindered the development of other ORS techniques used to define fugitive dust emission flux. The issue in the past has been the highly uncertain relationship between open path extinction (or opacity) and PM mass concentration for specific dust plumes. This new method provides a calibration relationship between ORS and in situ PM measurements that will allow for the development and eventual deployment of other open path extinction measurements tools such as Lidar or digital cameras, which can be used to develop fugitive PM emission factors.

3.6 Quality Assurance/Quality Control (QA/QC)

3.6.1 Calibration of ORS method

Calibration of the ORS method was done with a two-step approach by comparing $PM_{2.5}$ and PM_{10} values retrieved by the ORS method to the $PM_{2.5}$ and PM_{10} measured values that were obtained by a pair of calibrated DT aerosol monitors. The first step in the ORS calibration is to retrieve the right apportionment of $PM_{2.5}$ and PM_{10} in the dust plume. The second step is to determine the correct PM-mass concentration values for $PM_{2.5}$ and PM_{10}.

The calibration experiment was performed with a controlled release of dust from the measurement sites in a tent with a 4 m beam path (Figure 23). The tent was used to enclose the optical path of the ORS to avoid influence from ambient wind, and to ensure as uniform a dust plume as possible throughout its beam path. The OP-FTIR and the OP-LT were placed close to each other so that the combined optical beams form the ORS optical beam path for the experiment. The dust plume was generated and introduced into the ORS beam path using a blower to entrain the dust and a fan to disperse the dust uniformly in the beam path.

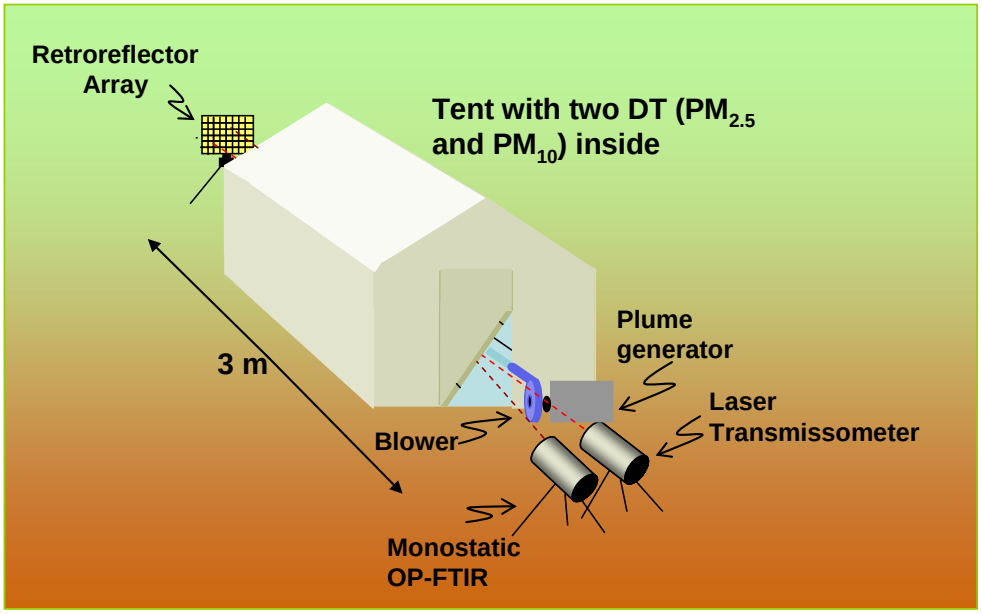

Figure 23 Experimental setup for ORS mass retrieval method calibration

The DT aerosol monitors were placed inside the tent mid-way along the ORS beam path, with one DT having a $PM_{2.5}$ inlet and the other having a PM_{10} inlet. The ORS and DT measurements were temporally synchronized so that each data point was an average of 10 seconds. The $PM_{2.5}$ and PM_{10} mass concentrations were retrieved from ORS extinction measurements, as explained in Section 3.4.3.1. The $PM_{2.5}$ and PM_{10} data collected by the DT aerosol samplers were calibrated against filter-based mass concentration measurements that were averaged for the same period as the ORS data. Figure 24 and Figure 25 show examples of the calibration curves for YPG dust collected during the artillery back blast field campaign.

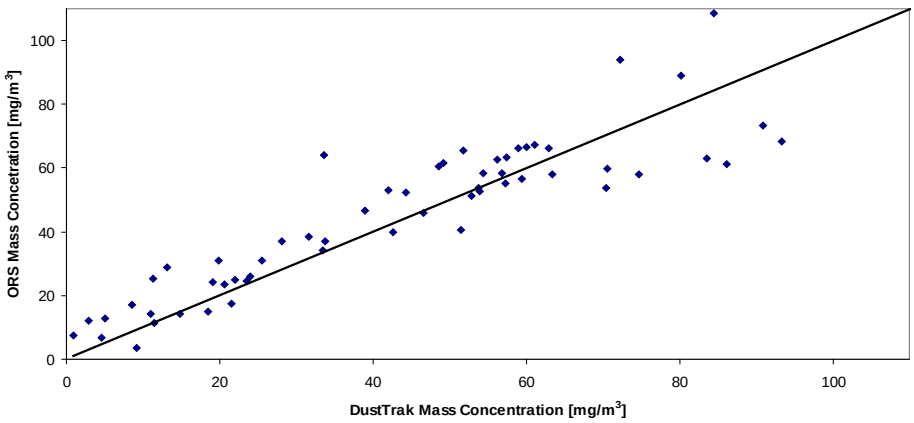

Figure 24 PM_{10} calibration curve for YPG dust (y = 1.00x, R2 = 0.78)

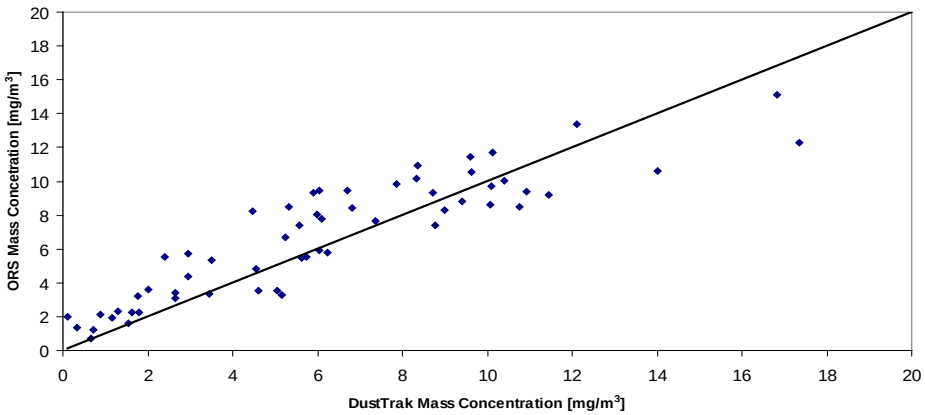

Figure 25 $PM_{2.5}$ calibration curve for YPG dust (y = 1.00x, R2 = 0.72)

3.6.2 Background corrections using MPL reflective target and FTIR/LT retroreflectors

During the field campaigns, a reflective target was located such that the plume's measurement plane was located between the MPL and the reflective target. Similarly, the OP-FTIRs, OP-LTs and their retroreflectors bounded the measurement area. The reflective target and retroreflectors not only allow the determination of optical measurements, but also measured the background optical properties. With this information, the background contribution to the optical measurements of plumes can be eliminated.

4 Results and Discussion

4.1 Dust Emissions from Artillery Back Blast

A summary of the results obtained from the ORS measurements of PM-mass emissions due to artillery back blast using the method described in Section 3.4 for select types of artillery and charge zones are presented in Table 3. The detailed PM-mass emission factor results are provided in Appendix A (Table A-1-1). Results in Table 3 describe mean $PM_{2.5}$ and PM_{10} emission factors in g-PM/shot for projectile models M107 and M549A1 and their standard deviations. Note that a larger charge zone value means that the propulsion force is stronger. Figure 26 shows the evolution of a plume of PM_{10} during an artillery firing event by projectile model M107. Figure 27 shows the bar chart displaying the results in Table 3. These results indicate the trend that increasing the level of charge zone increases the quantity of dust emissions from the artillery back blasts.

Table 3 Summary of PM mass emission factors for the back-blasts from two types of artillery during the 2005 YPG Field Campaign

Projectile Model	Propelling Charge Model	Propelling Charge Zone	Number of Events	Mass Emission Factor (g-PM/shot)			
				PM_{10}		$PM_{2.5}$	
				Mean	Standard Deviation	Mean	Standard Deviation
M549A1	M203A1	8S	30	173	113	52	43
M107	M3A1	3	8	90	51	57	37
M107	M3A1	2	10	70	35	8	7

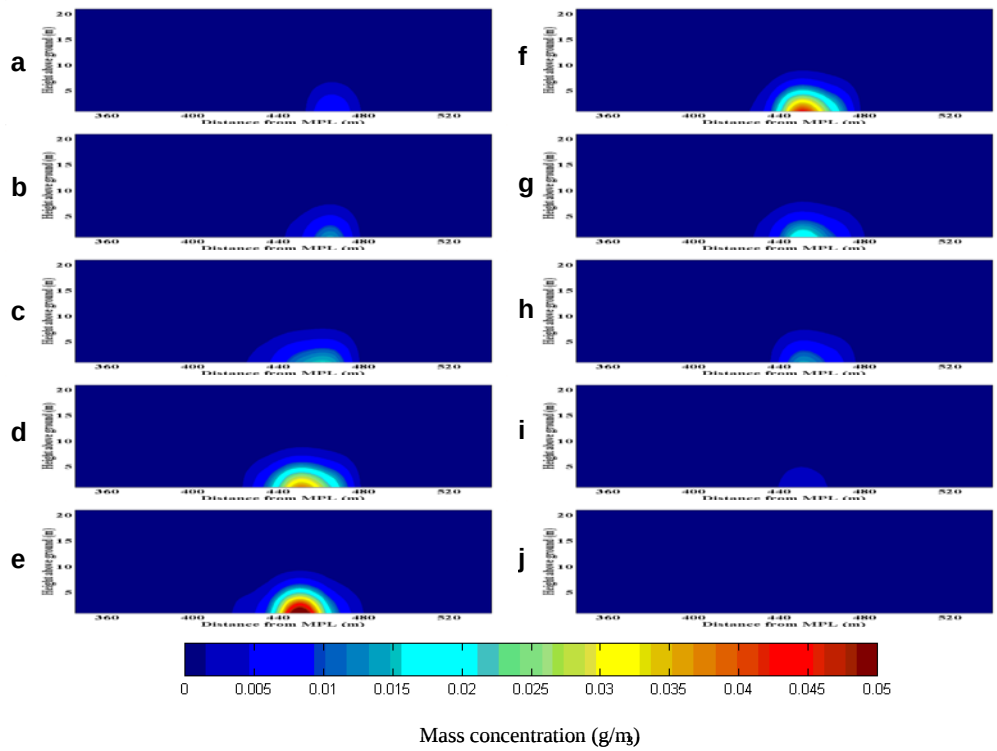

Figure 26 Evolution of a PM10 plume during an artillery-firing event. The letters indicate the order of the time sequence. (projectile model: M107, propelling charge zone: two)

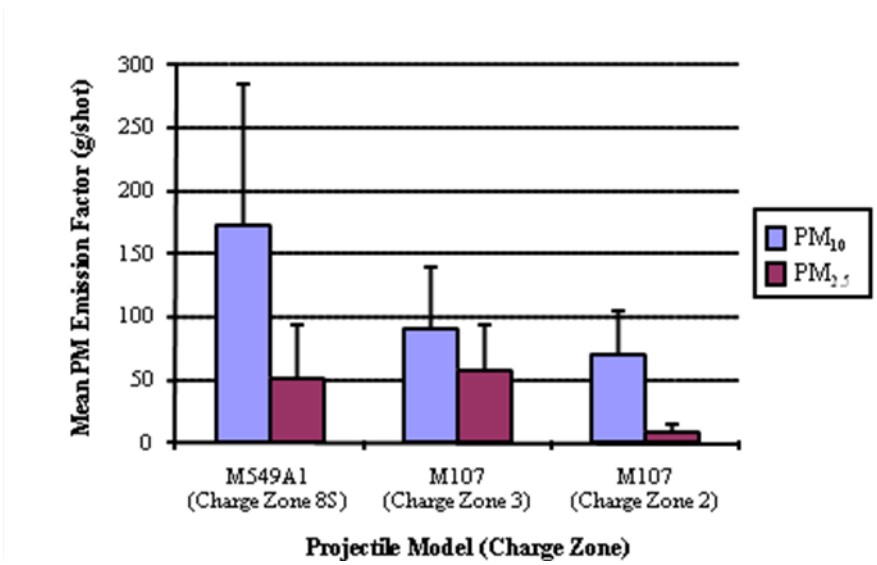

Figure 27 Measured emission factors for different types of artillery projectiles during the 2005 YPG Field Campaign

Artillery back blast was selected for the first year field campaign in part because it was expected to be the smallest PM generator out of the four

operations listed in CPSON-04-04. As a result of extensive Army wide coordination, YPG was selected for the field campaign site. Since YPG is a testing facility, the artillery firing sites had improved (stabilized soil) surfaces. Figure 27 shows that the amounts of PM_{10} and $PM_{2.5}$ were minimal (less than 180 g-PM/shot). However, these emission factors are only applicable for firing points with improved soil surfaces.

Artillery back blast is a small contributor when compared to other military fugitive dust sources. This source results in a single puff plume emission and its impact is much smaller than a continuous line source from vehicle movement. For example, using the average emission factor from Table 3 of 111 g PM_{10}/shot and the vehicular emission factor data for Fort Carson from Table 11, the estimated distances required to generated 111 g PM_{10} for three military vehicles travelling at about 25 km/hr is shown below:

- M270 – 173 m
- M577 – 106 m
- HEMTT – 81 m

At Fort Carson in FY03, the Army's Operating and Support Management Information System reports that M577s travelled about 98,000 km. This distance for a single vehicle type at Fort Carson corresponds to the PM_{10} generated by 929,000 average artillery shots (i.e., 111 g PM_{10}/shot). At the time of the back blast testing, research team members concluded that the artillery back blasts emitted less PM than the munitions delivery truck used to carry projectiles to the firing point site during testing. It's clear that even if artillery back blast emissions from unimproved surfaces are an order of magnitude higher than from improved surfaces, their impact on base-wide PM emissions would still be small in comparison with other fugitive PM sources.

4.2 Dust Emissions from Movement of Tracked Vehicles at YTC

The ORS method was implemented using the initial version of the system to determine PM mass emissions caused by the movement of tracked vehicles at YTC during August 2006. Mean and standard deviation values for PM-mass emission factors in units of g-PM/vkt for the specified tracked vehicles moving on unpaved roads are provided in Table 4. Corresponding values for the specified tracked vehicles moving on grassland at the same test site are provided in Table 5. As previously mentioned, more detailed results are provided in Appendix A (Table A-2-2).

Figure 28 provides an example of the evolution of a plume's mass concentration profile for PM_{10} during movement of a Bradley Fighting Vehicle. The impact of vehicle speed on the mass emission factors for PM_{10} and $PM_{2.5}$ are presented for two road surfaces: an unpaved road consisting of volcanic ash and a section of grassland that is also covering volcanic ash. Figure 29 describes PM-mass emission factors for M113, M1A1 and Bradley Fighting Vehicle tracked vehicles traveling on the unpaved road, and Figure 30 describes PM-mass emission factors for M1A1 and Bradley Fighting Vehicle tracked vehicles traveling on the grassland. Regressions of emission factors for each vehicle are also shown in both figures. As an alternative representation, the vehicle speeds were divided into five groups with an interval of 8 km/h (5 mph). For example, the speed range for the first group is from 4 km/h to 12 km/h and the median value is 8 km/h, as shown on the horizontal axis. The mean value of the emission factors was calculated for each speed group and then shown on the vertical axis of the plot. In addition, the power regressions of emission factor versus vehicle speed are shown in Table 6. The regression between PM-mass emission factor and the product of vehicle mass and speed (momentum) for tracked vehicles traveling on these two surface types are described with a linear model in Figure 31. Similarly, the median value of the momentum term is shown on the horizontal axis and the interval of each momentum group is 200 (10^3 kg by km/hr). These regression lines were force-fit through the origin because it was reasonable to assume that stationary vehicles did not generate fugitive dust.

Table 4 Summary of emission factors for Unpaved Road during the 2006 YTC Field Campaign

Vehicle Type	Vehicle Speed (km/h)	Number of Events	Mass Emission Factor (g-PM/vkt)			
			PM_{10}		$PM_{2.5}$	
			Mean	Standard Deviation	Mean	Standard Deviation
Bradley (tracked)	8	2	12,432	11,427	1,840	1,572
	16	3	9,366	8,907	932	978
	24	2	24,036	12,705	584	825
	32	2	40,198	9,056	4,907	2,957
	40	4	26,349	25,778	2,230	3,372
M113 (tracked)	8	0	---	---	---	---
	16	2	5,695	348	1,202	308
	24	0	---	---	---	---
	32	1	20,768	---	3,782	---
	40	3	19,168	10,020	3,755	2,244

M1A1 (tracked)	8	3	21,503	12,442	1,193	314
	16	5	22,788	9,915	3,382	2,164
	24	4	44,989	19,024	4,096	2,919
	32	2	56,295	19,962	6,710	2,421
	40	2	53,944	7,390	7,151	6,455

Table 5 Summary of emission factors for Grassland during the 2006 YTC Field Campaign

Vehicle Type	Vehicle Speed (km/h)	Number of Events	Mass Emission Factor (g-PM/vkt)			
			PM_{10}		$PM_{2.5}$	
			Mean	Standard Deviation	Mean	Standard Deviation
Bradley (tracked)	8	1	10,710	---	989	---
	16	1	415	---	74	---
	24	2	5,256	2,347	763	0
	32	4	10,495	5,807	1,848	1,606
	40	2	6,161	314	2,045	187
M1A1 (tracked)	8	1	6,902	---	797	---
	16	1	11,980	---	1,073	---
	24	1	31,943	---	5,715	---
	32	3	35,062	14,814	8,124	3,546
	40	1	7,191	---	450	---

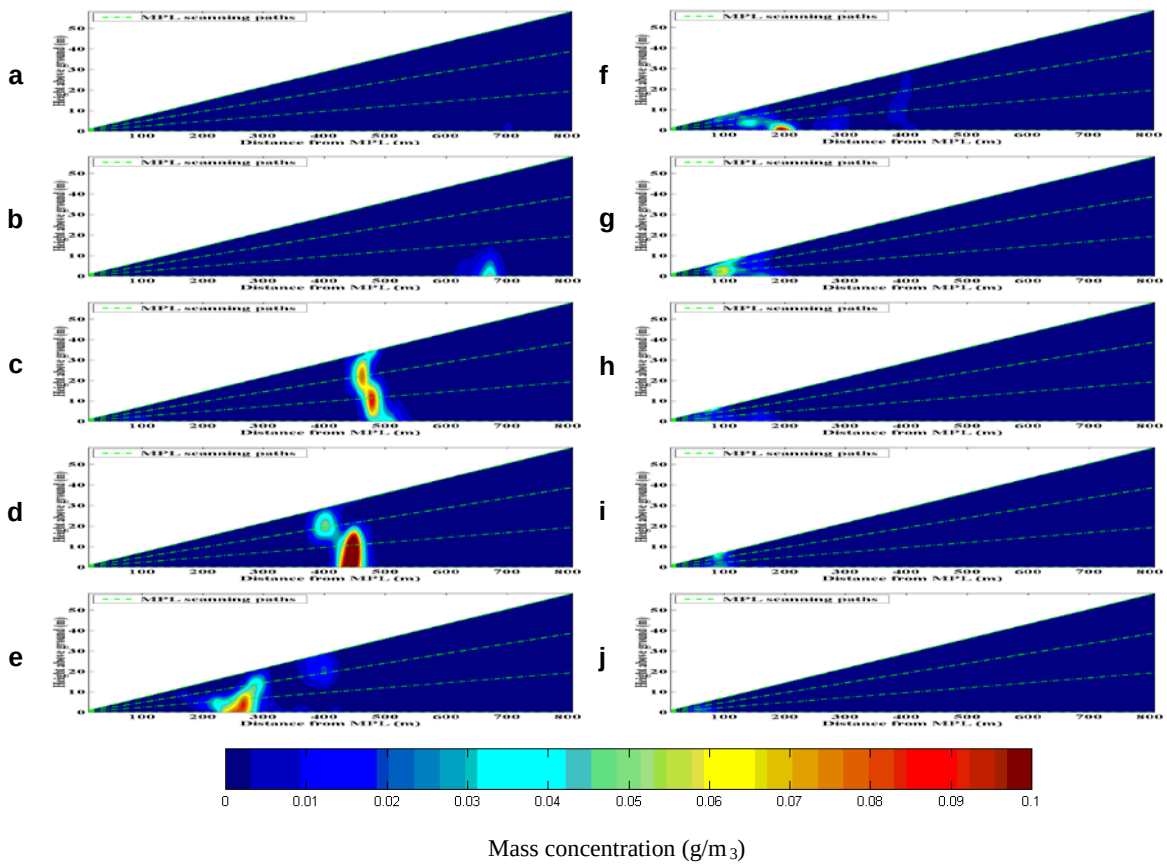

Figure 28 Evolution of a plume mass concentration profile for PM_{10} during vehicle travel. The letters indicate the order of the time sequence.
(Bradley Fighting Vehicle, moving to the left at 20 mph)

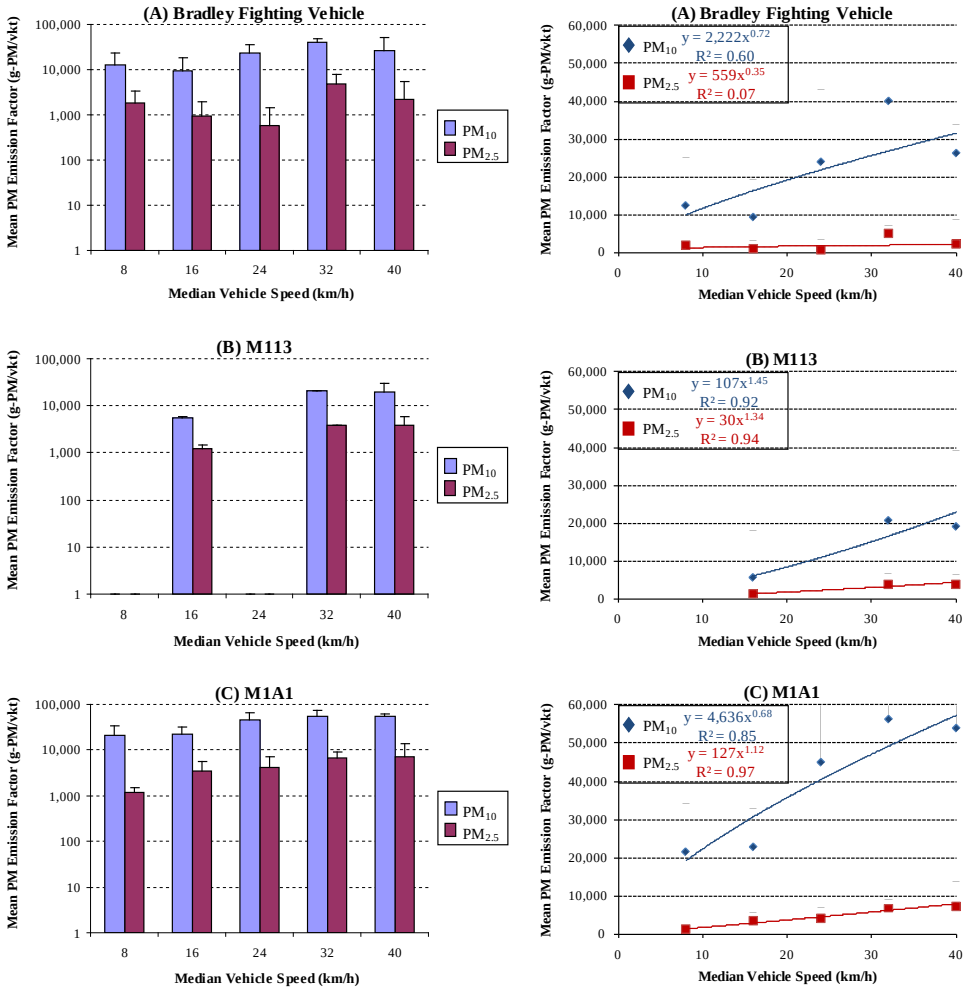

Figure 29 (left) Measured emission factors for different types of tracked vehicles, (A) Bradley Fighting Vehicle, (B) M113, and (C) M1A1, on an Unpaved Road during the 2006 YTC Field Campaign. Absence of a thin line (standard deviation) indicates a single data point within the speed interval. (right) Power regressions of the emission factors of these vehicles versus speed

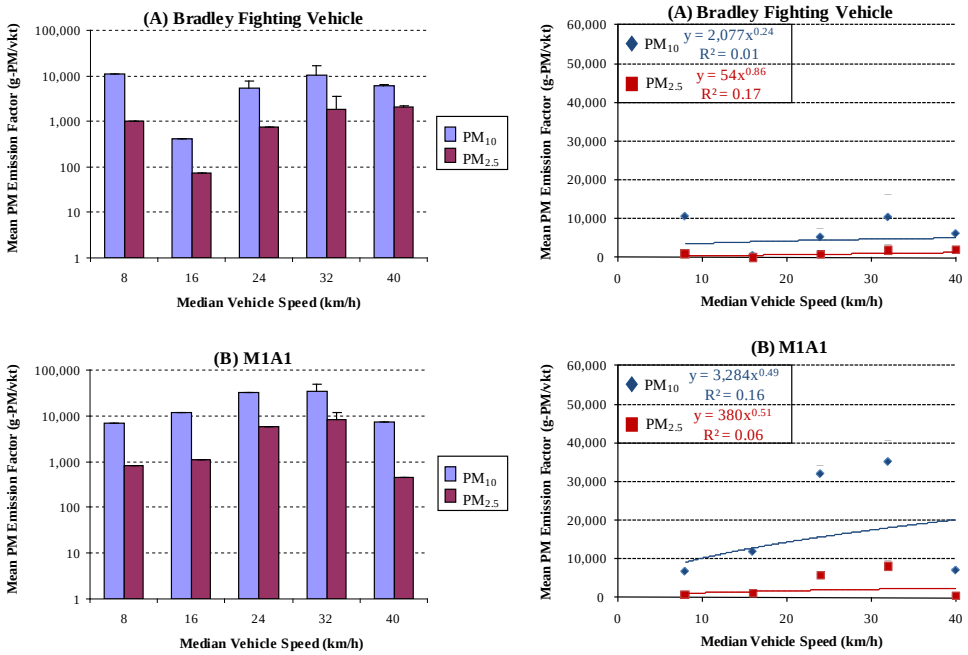

Figure 30 (left) Measured emission factors for different types of tracked vehicles, (A) Bradley Fighting Vehicle, and (B) M1A1, on Grassland during the 2006 YTC Field Campaign. Absence of a thin line (standard deviation) indicates that a single data point was available for that vehicle speed interval. (right) Power regressions of the emission factors of these vehicles versus speed

Table 6 Regressions of PM_{10} and $PM_{2.5}$ emission factors (EF, g/vkt) vs. speed (v, km/h) for each vehicle measured in the 2006 YTC Field Campaign. The R^2 values for each regression are also shown

Surface Type	Vehicle Type	Particle Size	Regression	R^2
Unpaved Road	Bradley (tracked)	PM_{10}	$EF= 2{,}222v^{0.72}$	0.60
		$PM_{2.5}$	$EF= 559v^{0.35}$	0.07
	M113 (tracked)	PM_{10}	$EF= 107v^{1.45}$	0.92
		$PM_{2.5}$	$EF= 30v^{1.34}$	0.94
	M1A1 (tracked)	PM_{10}	$EF= 4{,}636v^{0.68}$	0.85
		$PM_{2.5}$	$EF= 127v^{1.12}$	0.97
Grassland	Bradley (tracked)	PM_{10}	$EF= 2{,}077v^{0.24}$	0.01
		$PM_{2.5}$	$EF= 54v^{0.86}$	0.17
	M1A1 (tracked)	PM_{10}	$EF= 3{,}284v^{0.49}$	0.16
		$PM_{2.5}$	$EF= 380v^{0.51}$	0.06
Unpaved Road	Combined (tracked)	PM_{10}	$EF= 81.88v^{0.74}$	0.94
		$PM_{2.5}$	$EF= 46.38v^{0.61}$	0.52
Grassland	Combined (tracked)	PM_{10}	$EF=740.85v^{0.38}$	0.15
		$PM_{2.5}$	$EF= 38.95v^{0.53}$	0.16

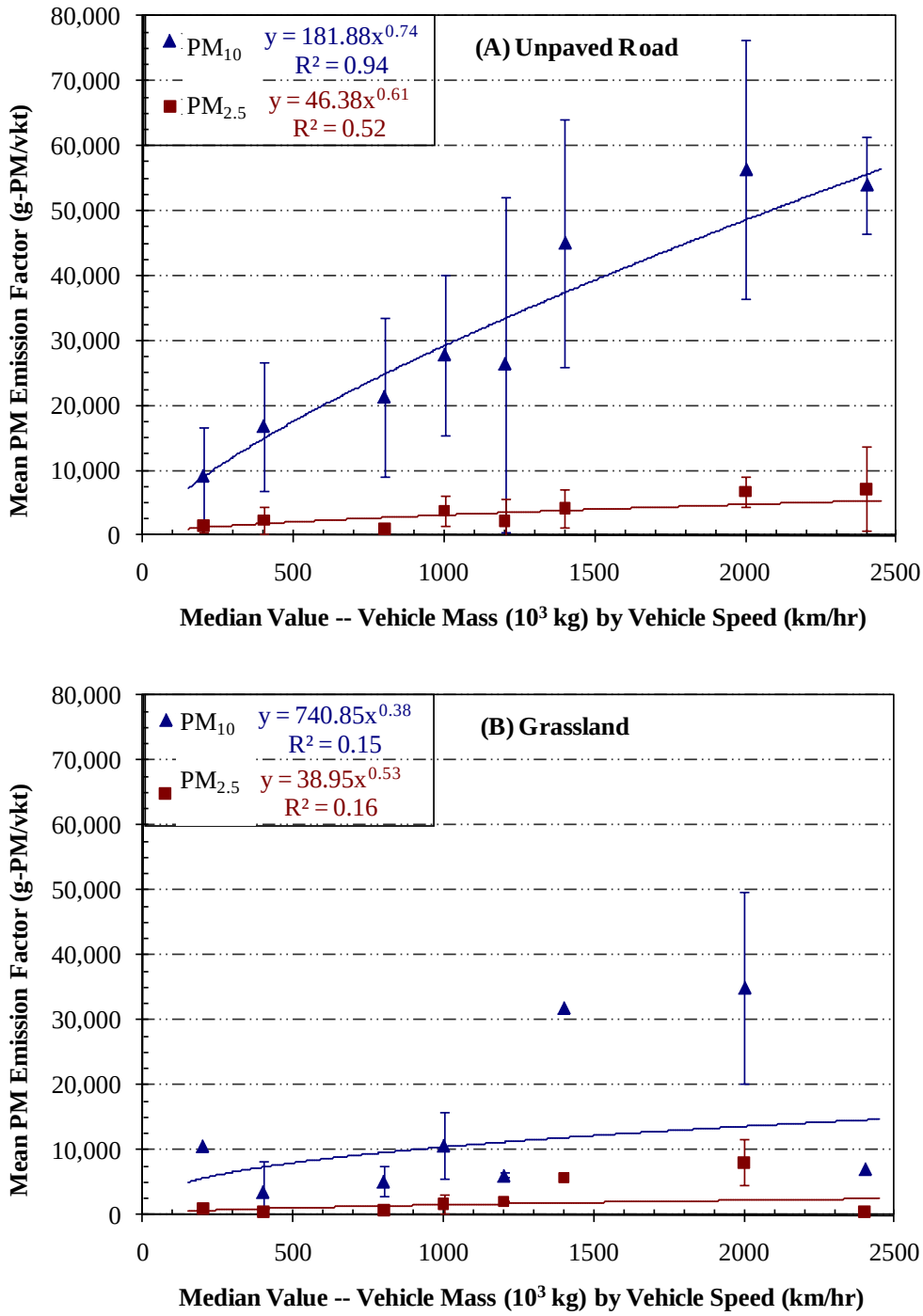

Figure 31 Scaling relationship between emission factor and the product of vehicle mass and speed (momentum) for tracked vehicles traveling on (A) Unpaved Road and (B) Grassland during the 2006 YTC Field Campaign. Horizontal axis represents the product of vehicle mass and its speed (kg km/h x10-3). Absence of a thin vertical line (standard deviation) indicates that a single data point was available for that vehicle speed interval.

Factors affecting the PM-mass emission factor during movement of the tracked vehicles include vehicular speed, weight, and type, and surface

type (i.e., unpaved road or grassland). Figure 29 and Figure 30 show the general trend of increasing PM-mass emission factor with increasing vehicle speed, especially for vehicle speeds of 16, 24, and 32 km/h (10, 15, and 20 mph). The correlations between the PM mass-emission factor and vehicle momentum (vehicle mass × speed) for unpaved road and grassland surfaces are described in Figure 31. The correlations for the unpaved road surface are larger than for the grassland surface for all tracked vehicles tested. The larger slopes for both PM_{10} and $PM_{2.5}$ in Figure 31 (A) compared to corresponding slopes in Figure 31 (B) suggests that vegetation restrains the dust emissions. Furthermore, PM_{10} consistently demonstrated better correlation than $PM_{2.5}$, irrespective of vehicle or surface type. However, the correlations between dust emissions and the product of vehicle mass and speed for tracked vehicles are not as large as for the wheeled vehicles as shown by Gillies [14]. One possible reason for these results is that track patterns of tracked vehicles may act as an additional factor to control dust emissions, which does not exist for wheeled vehicles. A comparison of emission factors from Figure 31 (A) and (B) shows that surface type affects the correlations between emission factor and vehicle momentum. Therefore, it is necessary to develop calibration curves that take into consideration different surface types. Alternatively, surface characteristics should be considered to predict emission factors. For instance, the fugitive dust equation shown in USEPA's AP-42 uses silt content on the surface as a parameter to predict emission factors [15].

4.3 Dust Emissions from Approaching and Withdrawing of Flying Helicopters

More than 90% of the helicopter passes from the 2007 YPG field campaign were able to be analyzed for PM_{10} and $PM_{2.5}$ emission factors. This was due to the very good field conditions and the horizontal and vertical plume capture capability of the MPL system. Figure 32 shows an example of the evolution of a plume extinction profile during a helicopter pass.

The summary mean and standard deviation values for PM_{10} and $PM_{2.5}$ mass emission factors (in units of g/hkf, where hkf describes "helicopter kilometer flown") for each helicopter speed category for the desert pavement surface type are provided in Table 7. Figure 33 provides the graphical representation of the values given in Table 7 as well as linear regressions from these data. Table 8 provides the summary of the mean and standard deviation values for PM_{10} and $PM_{2.5}$ mass emission factors for each helicopter speed category for the disturbed soil surface type. Figure 34 provides the graphical representation of the information given in Table

8 as well as linear regressions from the emission factor data. Table 9 provides the linear regressions of PM_{10} and $PM_{2.5}$ emission factors versus travelling speed for both surface types.

In summary, this study demonstrates that PM-mass emission factors for the disturbed soil surface type measured at Site 2 are larger than PM-mass emission factors for the desert pavement surface type measured at Site 1 for all helicopter speed categories. At both sites, the PM-mass emission factor decreases dramatically with increasing helicopter speed. One logical explanation for the increased PM emission factors at lower helicopter speeds is the resulting angle (pitch) of the main rotor blades that is required to change the horizontal helicopter speed while keeping the helicopter airborne. More energy is dissipated vertically by the main rotor blades at lower horizontal helicopter velocities resulting in larger vertical downward wind speeds and larger durations of exposure of the dust to those larger vertical wind speeds.

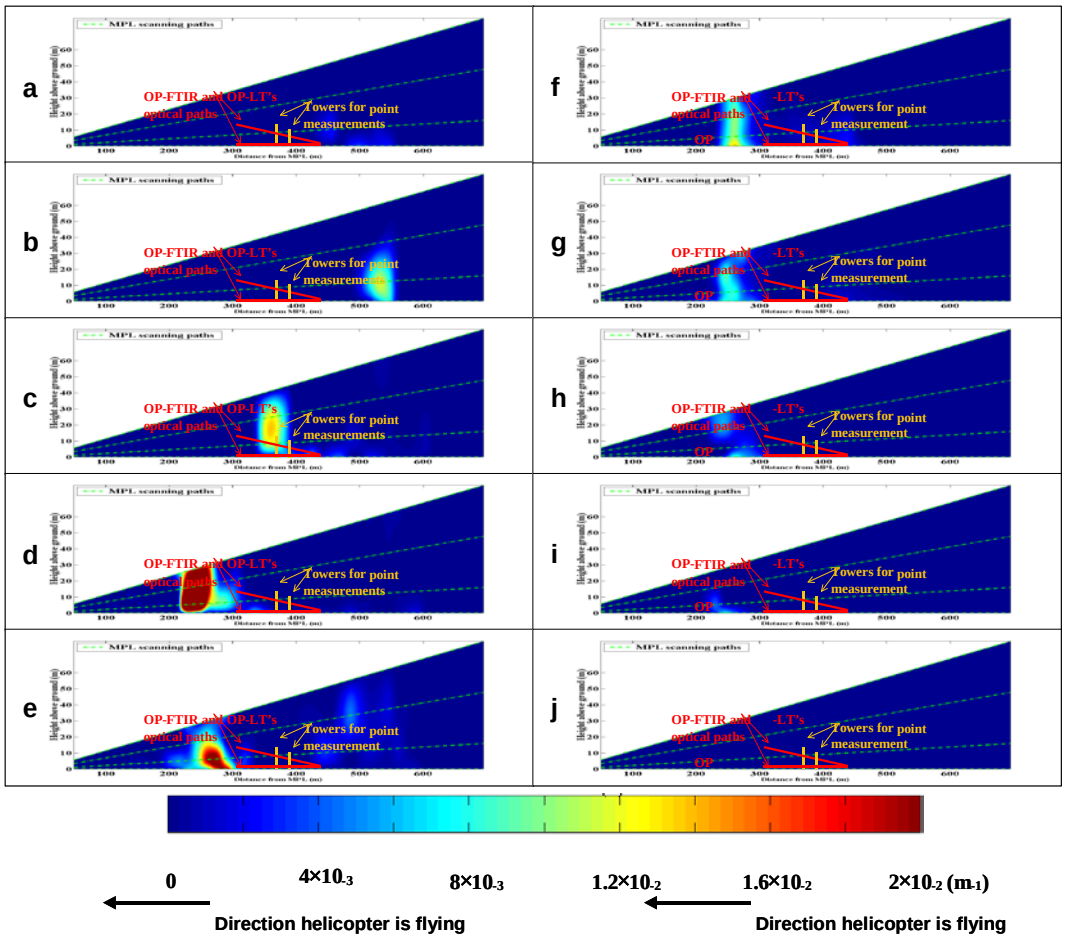

Figure 32 Evolution of plume extinction profile during a helicopter pass. The letters indicate the order of the time sequence. (5/21/2007, Bell 210 Helicopter flying toward the MPL at 30 km/hr over Desert Pavement surface)

Table 7 Summary of emission factors for the Desert Pavement Surface (Site 1) during the 2007 YPG Field Campaign

Median Helicopter Speed (km/h)	Number of Events	Mass Emission Factor (g-PM/hkf)			
		PM_{10}		$PM_{2.5}$	
		Mean	Standard Deviation	Mean	Standard Deviation
15	8	54,887	112,782	26,316	52,632
30	10	18,797	33,083	9,023	15,789
60	7	1,278	1,880	602	902

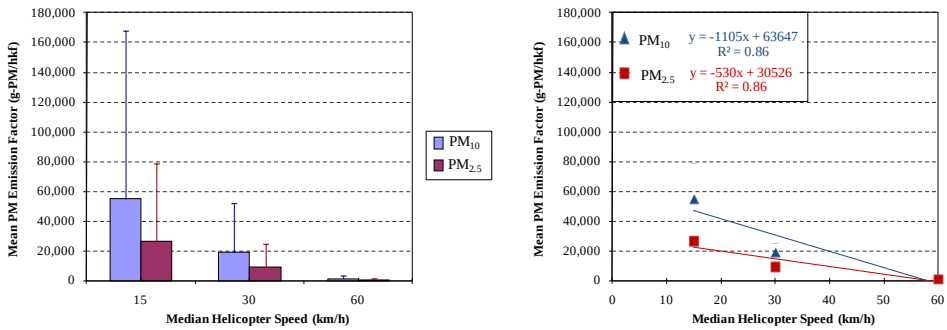

Figure 33 (left) Measured emission factors on Desert Pavement Surface (Site 1) during the 2007 YPG Field Campaign. (right) Linear regression of emission factor versus helicopter speed.

Table 8 Summary of emission factors for the Disturbed Soil Surface (Site 2) during the 2007 YPG Field Campaign

Median Helicopter Speed (km/h)	Number of Events	Mass Emission Factor (g-PM/hkf)			
		PM_{10}		$PM_{2.5}$	
		Mean	Standard Deviation	Mean	Standard Deviation
15	14	98,214	205,357	25,893	53,571
27.5	16	33,036	63,393	8,482	16,964
35	8	15,179	33,036	3,839	8,571
52.5	9	1,250	1,607	357	446

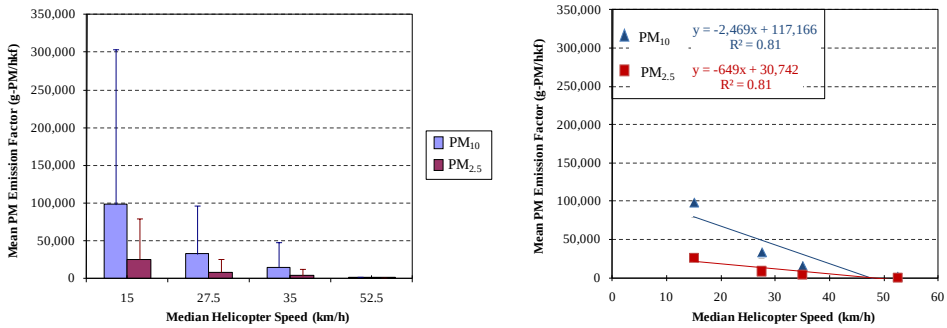

Figure 34 (left) Measured emission factors on Disturbed Soil Surface (Site 2) during the 2007 YPG Field Campaign. (right) Linear regression of emission factor versus helicopter speed.

Table 9 Regressions of PM_{10} and $PM_{2.5}$ emission factors (EF, g/vkt) vs. speed (v, km/h) for the Bell 210 Helicopter in the 2007 YPG Field Campaign. The R2 values for each regression are also shown.

Surface Type	Particle Size	Regression	R^2
Desert Pavement	PM_{10}	EF= -1,105v+ 63,647	0.86
	$PM_{2.5}$	EF= - 530v+ 30,526	0.86
Disturbed Soil	PM_{10}	EF= -2,469v+117,166	0.81
	$PM_{2.5}$	EF= - 649v+ 30,742	0.81

4.4 Dust Emissions from Tracked and Wheeled Vehicles Measured with the Hybrid ORS System at Fort Carson, CO

As previously mentioned, PM-mass emissions from tracked and wheeled vehicles were measured with the hybrid ORS system during the Fort Carson Field Campaign using the methodology described in Section 3.4.4. Detailed information including the estimated PM-emission factors for each test event is provided in Appendix A (Table A-4-3) for both sites at Fort Carson. Note that monitoring of the meteorological parameters was undertaken continuously throughout the field study to ensure continuity and completeness of the measurements. Therefore, data collected during unfavorable meteorological conditions (e.g., plumes travelling parallel to the ORS observing plane) were also measured. In addition, the ORS instruments (i.e., OP-LT, DT, and MPL) were operated separately; and the plumes were occasionally contaminated by external non-tracked vehicle sources. These factors altogether resulted in 49% of the data being valid for data analysis and interpretation.

Based on these results, the effects of vehicle speed and vehicle type on dust emission factor were investigated. Figure 35 shows two examples of the evolution of plume extinction profiles during the pass of a M577 vehicle and a HEMTT vehicle traveling from right to left. The tabular and graphical forms of the PM-mass emission factors for Site 1 and Site 2 are presented in Table 10 and Table 11 and Figure 36 and Figure 37, respectively. Figure 36 and Figure 37 also show the power regressions of emission factors versus vehicle speeds. The mean PM-mass emission factor values (vertical bars) and their standard deviations (vertical lines) for each speed range are shown on the vertical axes with vehicle speed located along the horizontal axes. Vehicle speed was first categorized into a select speed ranges and the mean value of emission factors for that specified speed range was then determined for each vehicle type. The vehicle speeds

shown in horizontal axes are the medians of the speed ranges. The power regressions of the PM-mass emission factors versus vehicle speed for each vehicle and measurement site are shown in Table 12. The correlations between PM-mass emission factors and vehicle momentum (vehicle mass × speed) for tracked and wheeled vehicles measured during this field campaign are described in Figure 38 and Figure 37 respectively. The treatment of PM-mass emission factor data versus vehicle momentum is the same as the treatment of the emission factor data versus vehicle speed for each individual vehicle.

It is observed that the PM-mass emission factors for both $PM_{2.5}$ and PM_{10} increased with vehicle speeds for almost all situations except for the M270 and M577 vehicles measured at Site 2. The increase in emission factors with increasing vehicle speed was more evident at smaller rather than larger values of vehicle speeds. When the results were compared between different vehicle types, it is observed that heavier vehicles re-suspended more PM than the lighter vehicles. As described previously, the order of vehicle weight for these vehicles ranging from heavier to lighter is: M88 > M270 > HEMTT > M577. It is also observed that the effect of vehicle weight on dust emissions became less apparent at larger vehicle speeds. In addition, the wheeled vehicle (HEMTT) was shown to have larger PM-mass emission factors than the tracked vehicles (M270 and M577) at Site 2. Figure 39 also shows an excellent fit for the HEMTT to the developed power law PM emission factor equations. However, the differences due to testing site were not observable when comparing the PM-mass emission factors for the M270 and M577 between Site 1 and Site 2.

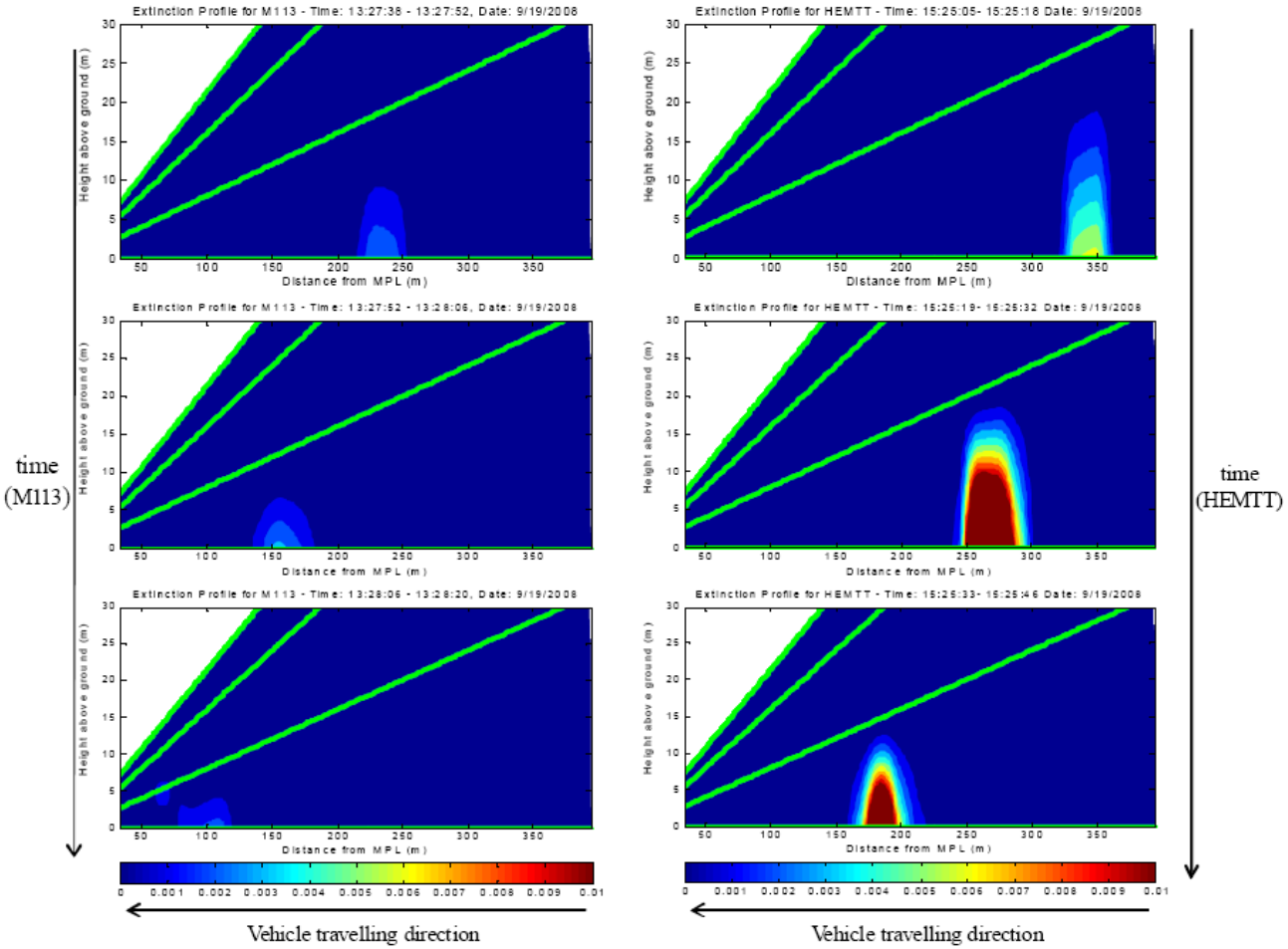

Figure 35 Evolution of plume extinction profiles during vehicle passes at the speed of 15mph towards the MPL: (A) M577 (M113 family)and (B) HEMTT. The time elapsed between two consecutive profiles is 14 seconds.

Table 10 Summary of emission factors for Site 1 during the 2008 Fort Carson Field Campaign

Vehicle Type	Vehicle Speed Range (km/h)	Median Vehicle Speed (km/h)	Vehicle Speed (km/h)		Number of Events	Mass Emission Factor (g-PM/vkt)			
						PM_{10}		$PM_{2.5}$	
			Mean	σ		Mean	σ	Mean	σ
M270 (tracked)	4--12	8	---	---	0	---	---	---	---
	12--20	16	17.6	0.8	4	386	262	179	155
	20--28	24	25.8	1.5	5	738	448	320	216
	28--36	32	33.1	1.0	3	1,094	87	482	109
	36--44	40	---	---	0	---	---	---	---
	44--52	48	49.3	0.7	2	1,276	375	517	127
M577 (tracked)	4--12	8	---	---	0	---	---	---	---
	12--20	16	19.3	0.6	2	206	102	78	21
	20--28	24	24.5	2.6	4	264	63	102	39
	28--36	32	32.9	0.9	5	1,047	436	495	284
	36--44	40	---	---	0	---	---	---	---
	44--52	48	---	---	0	---	---	---	---
M88 (tracked)	4--12	8	---	---	0	---	---	---	---
	12--20	16	16.4	3.2	6	744	425	375	154
	20--28	24	25.4	2.7	5	856	265	452	133
	28--36	32	30.2	3.7	4	975	391	535	297
	36--44	40	---	---	0	---	---	---	---
	44--52	48	---	---	0	---	---	---	---

σ – standard deviation

Table 11 Summary of emission factors for Site 2 during the 2008 Fort Carson Field Campaign

Vehicle Type	Vehicle Speed Range (km/h)	Median Vehicle Speed (km/h)	Vehicle Speed (km/h)		Number of Events	Mass Emission Factor (g-PM/vkt)			
						PM_{10}		$PM_{2.5}$	
			Mean	σ		Mean	σ	Mean	σ
M270 (tracked)	4–12	8	---	---	0	---	---	---	---
	12–20	16	17.8	---	1	89	---	45	---
	20–28	24	26.3	0.3	2	642	569	369	377
	28–36	32	---	---	0	---	---	---	---
	36–44	40	42.9	---	1	489	---	188	---
	44–52	48	---	---	0	---	---	---	---
	52–60	56	---	---	0	---	---	---	---
	60–68	64	---	---	0	---	---	---	---
M577 (tracked)	4–12	8	---	---	0	---	---	---	---
	12–20	16	18.9	0.5	2	569	260	103	77
	20–28	24	25.4	0.6	3	1,052	1,171	347	400
	28–36	32	31.4	1.1	4	1,844	1,249	712	400
	36–44	40	42.6	---	1	1,566	---	536	---
	44–52	48	45.6	---	1	1,738	---	684	---
	52–60	56	---	---	0	---	---	---	---
	60–68	64	---	---	0	---	---	---	---
HEMTT (wheeled)	4–12	8	---	---	0	---	---	---	---
	12–20	16	18.6	0.9	3	223	110	44	30
	20–28	24	25.2	1.8	5	1,378	1,463	356	344
	28–36	32	32.0	1.2	5	2,737	2,317	712	581
	36–44	40	---	---	0	---	---	---	---
	44–52	48	---	---	0	---	---	---	---
	52–60	56	---	---	0	---	---	---	---
	60–68	64	62.9	4.1	3	4,339	1,319	1,627	224

σ – standard deviation

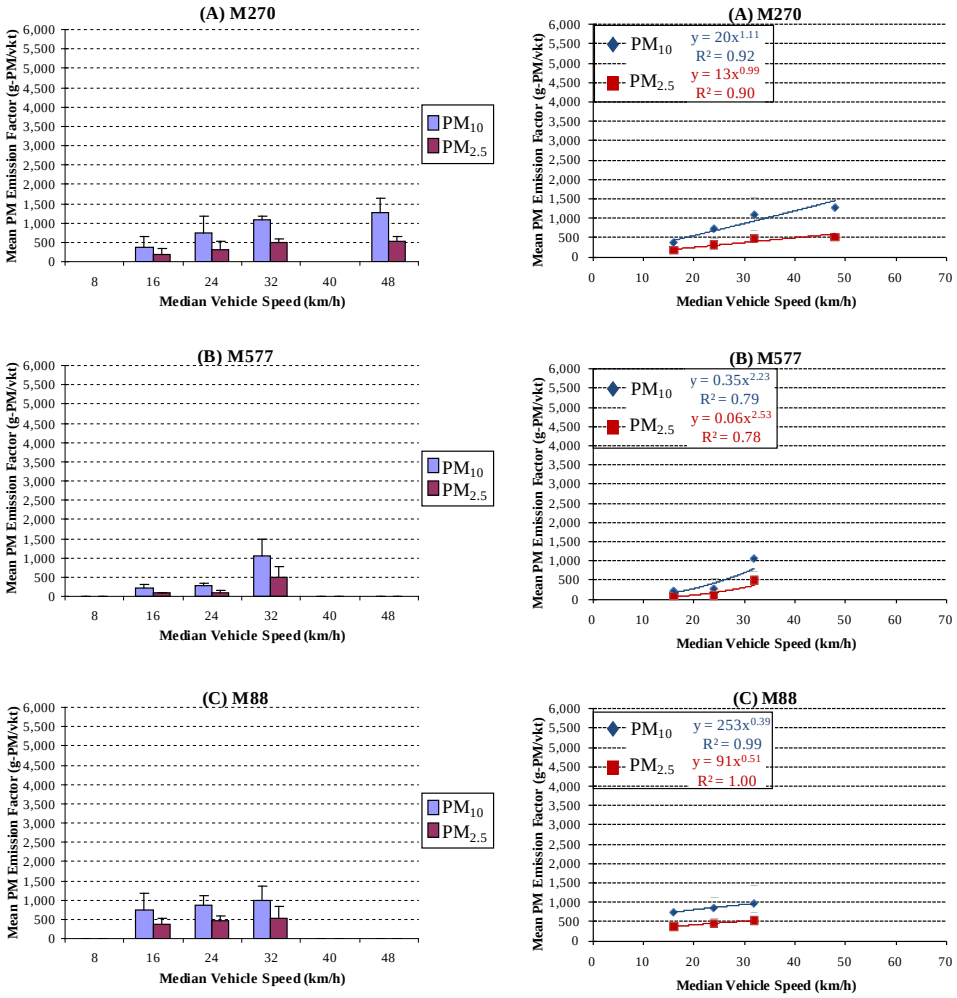

Figure 36 (left) Measured emission factors for different types of tracked vehicles, (A) M270, (B) M577, and (C) M88, at Site 1 during the 2008 Fort Carson Field Campaign. Absence of a thin vertical line (standard deviation) indicates single data point within the speed interval. (right) Power regressions of the emission factors of these vehicles versus speed

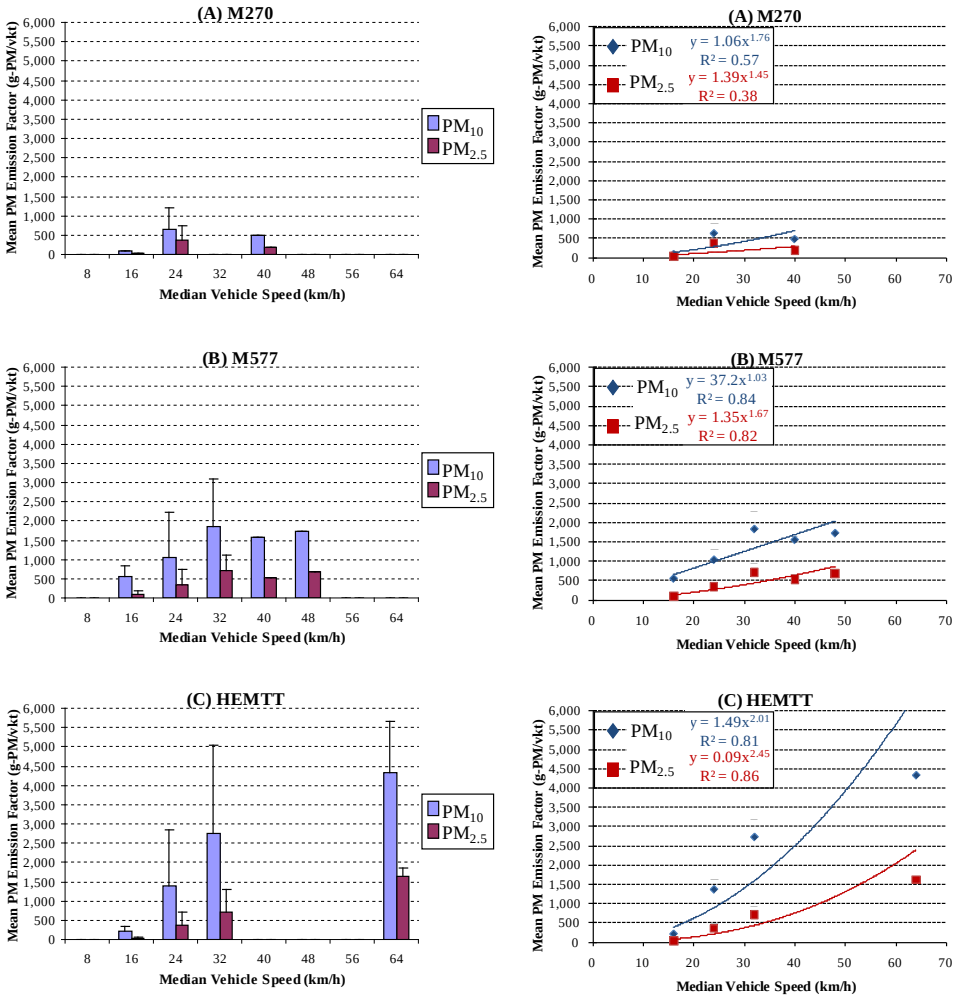

Figure 37 (left) Measured emission factors for different types of tracked vehicles, (A) M270, (B) M577, and (C) HEMTT, at Site 2 during the 2008 Fort Carson Field Campaign. Absence of a thin vertical line (standard deviation) indicates single data point within the speed interval. (right) Power regressions of the emission factors of these vehicles versus speed

Table 12 Regressions of PM_{10} and $PM_{2.5}$ emission factors (EF, g/vkt) vs. speed (v, km/h) for each vehicle measured in the 2008 Fort Carson Field Campaign. The R2 values for each regression are also shown.

Site #	Vehicle Type	Particle Size	Regression	R^2
1	M270 (tracked)	PM_{10}	$EF= 20v^{1.11}$	0.92
		$PM_{2.5}$	$EF= 13v^{0.99}$	0.90
	M577 (tracked)	PM_{10}	$EF= 0.35v^{2.23}$	0.79
		$PM_{2.5}$	$EF= 0.06v^{2.53}$	0.78
	M88 (tracked)	PM_{10}	$EF= 253v^{0.39}$	0.99
		$PM_{2.5}$	$EF= 91v^{0.51}$	1.00
2	M270 (tracked)	PM_{10}	$EF= 1.06v^{1.76}$	0.57
		$PM_{2.5}$	$EF= 1.39v^{1.45}$	0.38
	M577 (tracked)	PM_{10}	$EF= 37.2v^{1.03}$	0.84
		$PM_{2.5}$	$EF= 1.35v^{1.67}$	0.82
	HEMTT (wheeled)	PM_{10}	$EF= 1.49v^{2.01}$	0.81
		$PM_{2.5}$	$EF= 0.09v^{2.45}$	0.86
	Combined (tracked)	PM_{10}	$EF= 21.07v^{0.57}$	0.68
		$PM_{2.5}$	$EF= 0.79v^{0.94}$	0.76
	Combined (wheeled, only HEMTT)	PM_{10}	$EF= 1.78v^{1.08}$	0.94
		$PM_{2.5}$	$EF= 0.04v^{1.46}$	0.96

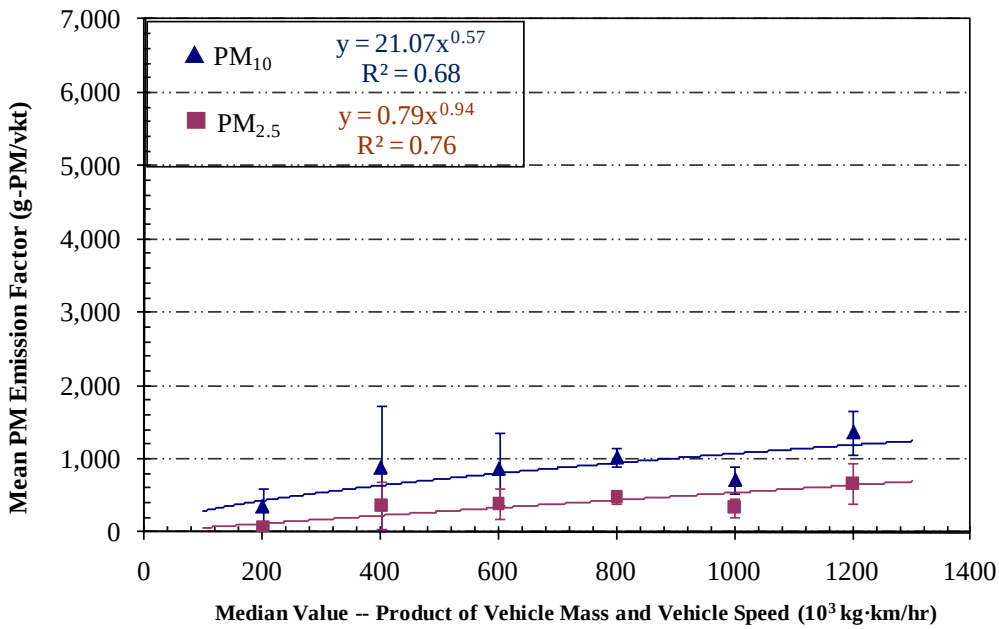

Figure 38 Scaling relationship between emission factor and the product of vehicle mass and vehicle speed for tracked vehicles during the 2008 Fort Carson Field Campaign. Horizontal axis represents the product of vehicle mass and its speed (kg km/h x10^{-3}).

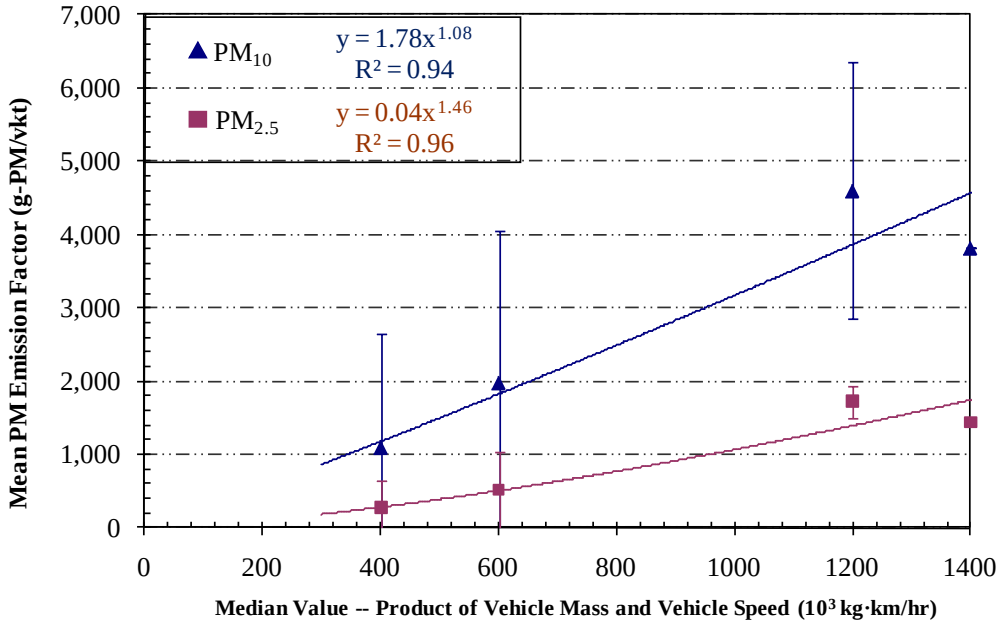

Figure 39 Scaling relationship between emission factor and the product of vehicle mass and vehicle speed for the HEMTT wheeled vehicle during the 2008 Fort Carson Field Campaign. Horizontal axis represents the product of vehicle mass and its speed (kg km/h x10-3). Absence of a thin vertical line (standard deviation) indicates that a single data point was available for that speed interval.

4.5 Comparisons of Emission Factors for Different Military Activities

It is very difficult to provide a meaningful comparison of PM-mass emission factors between puff sources (e.g. artillery back blast) and mobile sources (e.g. vehicles and helicopters) due to the differences in the source types (i.e. puff compared to continuous emission). However, it is reasonable to compare the trend of emission factors from military vehicles and helicopters. Tracked vehicle emission factors measured during two separate field campaigns can also be compared. Measured emission factors of military vehicles can also be compared with existing emission factor models, such as those provided by USEPA's AP-42 emission factors [15] that were developed for civilian wheeled vehicles.

Comparing the relationships between emission factor and vehicle speed for military vehicles (Figure 29, Figure 30, Figure 36 and Figure 37) and for helicopters (Figure 33 and Figure 34), it is observed that their relationships are different. Emission factors for PM_{10} and $PM_{2.5}$ generally increase with speed for military vehicles, while the emission factors decrease noticeably with increasing speed of the helicopter. Unlike EPA's AP-42 equation which only includes the vehicle weight[15], we have discovered that both the vehicle's speed and weight are important and that emission factors are correlated with vehicle momentum. Helicopters generate fugitive dust from blowing surface soil by rotary wings that spin at a fairly constant rate. This means that by slowing helicopter movement, the duration of forcing air downward to the earth's surface and the energy required to keep the helicopter aloft blowing per unit distance traveled is larger, resulting in larger PM-mass emission factors.

Comparing the emission factors between two military vehicle field campaigns (Figure 29 and Figure 30 versus Figure 36 and Figure 37), it is observed that the emission factors from the YTC field campaign are systematically larger than those from the Fort Carson field campaign.

USEPA's AP-42 emission factor database provides emission factor estimates for vehicles travelling on unpaved surfaces[15]. The model describes the PM-mass emission factor (g/vkt) as $281.9k(S/12)^{0.9}(W/3)^{0.45}$, where S is silt content (%), W is mean vehicle weight (tons), and k = 0.15 for $PM_{2.5}$ and k = 1.5 for PM_{10}. Silt content of the unpaved road was not monitored as part of this study. However, one study observed that the silt content of an unpaved road ranged from 4 to 7%[14], while another study observed that the silt content of another unpaved road range from 39 to 56%[38].

Therefore, modeled PM-mass emission factors were calculated assuming silt content of 4% and 56% to see if the measured PM-mass emission factors are bounded by these two modeled values. The measured emission factors are the emission factors averaged by vehicle speeds reported from the four field campaigns described in this report.

Table 13 compares the PM-mass emission factors for vehicles traveling on unpaved roads as measured during the two field campaigns studied as part of this research project and corresponding PM-mass emission factors modeled by USEPA AP-42. It was observed that measured emission factors from YTC Field Campaign are 4 to 8 times larger than the AP-42 modeled value (i.e., at 56% silt). However, emission factors from Fort Carson Field Campaign mostly fall within the 4% to 56% modeled value range. Exceptions are two $PM_{2.5}$ values that exceed the 56% silt modeled value by less than 100%. The unusually high emission factors from the YTC field campaign are most likely the result of surface volcanic ash that fell over the Yakima region after the 1980 Mount Saint Helens eruption. It is therefore unlikely that the YTC emission factors are representative of other DoD facilities.

Table 13 Comparison of measured and modeled emission factors (TV= Tracked Vehicle, WV = Wheeled Vehicle)

YTC field campaign			Mass Emission Factor of $PM_{2.5}$			Mass Emission Factor of PM_{10}		
Vehicle	Weight (kg)	Weight (ton)	4% silt (g/vkt)	56% silt (g/vkt)	Measured (g/vkt)	4% silt (g/vkt)	56% silt (g/vkt)	Measured (g/vkt)
Bradley (TV)	29,937	33	46	498	2,029	463	4,976	22,064
M113 (TV)	12,349	14	31	334	2,908	311	3,341	14,944
M1A1 (TV)	60,909	67	64	685	4,037	637	6,851	36,180

Fort Carson field campaign			Mass Emission Factor of $PM_{2.5}$			Mass Emission Factor of PM_{10}		
Vehicle	Weight (kg)	Weight (ton)	4% silt (g/vkt)	56% silt (g/vkt)	Measured (g/vkt)	4% silt (g/vkt)	56% silt (g/vkt)	Measured (g/vkt)
M88 (TV)	63,504	70	65	698	443	649	6,980	843
M270 (TV)	24,948	28	43	458	320	426	4,584	718
M113 (TV)	12,338	14	31	334	379	311	3,339	985
HEMTT (WV)	19,958	22	39	415	647	386	4,146	2,141

5 Conclusions and Implications for Future Research

The SI-1400 project team has successfully developed and implemented a novel ORS technique to quantify fugitive dust PM emissions from unique military operations. These operations include the firing of artillery, the movement of tracked and wheeled vehicles, and the flying of helicopters in arid regions of the United States.

Two versions of the ORS system were developed as part of this research. The initial version utilized OP-FTIRs and OP-LTs with Mie-Lorenz theory to determine PM's light extinction efficiency values that were then used with the MPL, and wind directions and velocities to determine mass emission factors. The second version replaced the OP-FTIRs and OP-LTs with simpler and less expensive DustTraks™ and an OP-LT to determine the light extinction efficiencies.

Specific results from the four field campaigns include:

1. Fugitive dust emission factors for artillery back blast were quantified for $PM_{2.5}$ and PM_{10}. Larger PM-mass emission factors were observed with increased charge zone.

2. Fugitive dust emission factors for tracked and wheeled vehicles were quantified for $PM_{2.5}$ and PM_{10} and statistical trends were established based on vehicle speed and momentum providing two options to model the PM-mass emission factors when developing PM-mass emission inventories for DoD installations.

3. The tested wheeled vehicle (i.e., HEMTT) generates approximately twice the amount of dust in comparison to the tested tracked vehicles (i.e., M88, M270, M113, and M1A1). This suggests that the properties of the wheel and their enclosures are important considerations when determining methods to reduce dust emissions from select types of vehicles.

4. Helicopter dust emission factors were successfully quantified with their dependence on helicopter speed with correlation coefficients $\geq$ 0.81. In contrast to vehicular travel, faster traveling helicopters

generated less dust per unit distance traveled than slower traveling helicopters.

The latest field campaign performed at Fort Carson measured PM-mass emission factors in the same order of magnitude as values provided by existing AP-42 emission factors. These results are encouraging seeing that ORS techniques can be applied to a much larger range of PM sources than typical point-based measurements (i.e., plumes generated by rotary winged aircraft, fixed winged aircraft, open burning and open detonation of energetic materials, and ships). However, additional baseline measurements and comparisons need to be made for a wider range of sources and field conditions to develop a greater degree of confidence when comparing results based on point and path dependent measurement techniques.

The emission factor data generated by this project could be added to AP-42, if USEPA or any applicants would propose its addition for any of the tested fugitive PM sources (i.e., artillery back blast, helicopter flight, or military vehicle movement). However, the test data quality would be "C" rated because the tests were based on a new methodology and the AP-42 emission factor quality would be "D" rated because the test data were from a small number of facilities. To receive "A" ratings for test data quality and AP-42 emission factor quality, the test methodology should be widely used and data should be taken from many randomly chosen facilities in the population to minimize variability.

During all field campaigns, researchers from both SI-1400 and SI-1399 collected data from the same military activity events to develop emission factors for those activities. SI-1399 used a flux tower sampling system developed by DRI, as part of SERDP project CP-1191 that included up to three mobile towers to measure the flux of particles emitted from fugitive PM sources [14]. Two of the towers were vehicle-mounted (1/2-ton pick-up truck) and one was trailer-mounted. The flux tower sampling system measured both PM_{10} and $PM_{2.5}$ concentrations using DT aerosol monitors (i.e., TSI 8520 DustTraks). The DRI system also included a Tapered Element Oscillating Microbalance (TEOM) measurement unit collocated with two DustTraks as an additional check on PM_{10} and $PM_{2.5}$ concentrations.

The DRI system has the following strengths and weaknesses:

- The system is based on the "Upwind / Downwind" method that is accepted as a U.S. EPA approved technique for measuring road dust.

- Real-time in situ measurements can be linked with gravimetric mass measurements.
- Excellent choice for line sources, and for plumes approximating the scale of the monitoring system.
- Difficult to implement for plumes larger than those generated from vehicle line sources.
- Difficult to adequately capture "wandering" type plumes. Orientation with respect to wind direction is very important for non-line sources.
- Does not capture complete plume, relies on inference of point measurements to represent plume characteristics.

The original ORS system has the following strengths and weaknesses:

- Path integrated measurements of PM mass flux and size distribution across the entire plume.
- Capability to map plume height and width across measurement plane.
- Excellent for large fugitive PM sources where it is difficult to measure average plume conditions with in situ measurements.
- Remote technology allows the instrumentation to be placed outside of plume and away from field activity.
- Large offset requirement for MPL and the requirement for placement of equipment on both sides of plume may be difficult to achieve under some field conditions.
- Difficult for the MPL to map small instantaneous PM releases due to return bin width and vertical scanning speed.
- Dependence on consistent wind speed and direction during testing.

This report was not intended to directly compare results between SI-1399 and SI-1400. However, the close coordination between two projects resulted in field campaign cost savings. A limited review of data from both projects during the field campaigns and during meetings before and after the field campaigns revealed that both methods resulted in reasonably close emission factors. Differences are due to the inherently different measurement technologies employed and to the large variability found in fugitive PM plumes.

Although the Hybrid Method described in this report did not come from the combination of SI-1400 (ORS) and SI-1399 (in-situ) measurement systems, it does borrow measurement technology from both systems. The data presented in this report indicates that the Hybrid Method can produce reasonable PM_{10} and $PM_{2.5}$ emission measurements at lower costs. The system benefits from path integrated measurements from the OP-LT and is a type of "Upwind / Downwind" method accepted by EPA. The system is however limited to plume sizes not much larger than the top of the tower containing the DT aerosol monitor pairs and is best suited to line PM source such as vehicular movement.

Future applications of these ORS techniques include the rapid and real-time characterization of PM and gaseous plumes that are generated by large and complex DoD sources such as open burning and open detonation of energetic materials from demilitarization operations, monitoring of air quality along facility borders, and evaluation of closure between dust transport models and ORS measurement techniques. Also it is important to evaluate the use of lower cost ORS techniques such as digital still cameras as established by American Society Testing Materials (ASTM) International [39] and the Hybrid Method as described in this report. Overall, this research project successfully developed novel ORS technologies to quantify PM mass concentrations and emission factors from complex DoD sources. These results are now available for DoD and USEPA to better characterize PM sources and complete PM emission inventories for artillery back blasts, tracked and wheeled vehicle movement, and flying rotary winged aircraft.

References

1. Xia, T. K., M.; Nel, A. E., Impairment of Mitochondrial Function by Particulate Matter (PM) and Their Toxic Components: Implications for PM-induced Cardiovascular and Lung Disease. Frontiers in Bioscience 2007. **12**(1): p. 1238-1246.
2. Dockery, D., Xu, X., Spengler, J., Ware, J., Fay, M., Ferris Jr., B., and Speizer, E., An Association Between Air Pollution and Mortality in Six U.S. Cities. New Eng. J. of Medicine, 1993. **329**(24): p. 1753-1759.
3. Burnett, R. T. S.-D., M.; Stieb, D.; Cakmak, S.; Brook, J. R. , Effects of particulate and gaseous air pollution on cardiorespiratory hospitalizations. Archives Environ Health, 1999. **54**(2): p. 130-139.
4. Boylan, J. W. O., M. T.; Wilkinson, J. G.; Russell, A. G., Integrated Assessment Modeling of Atmospheric Pollutants in the Southern Appalachian Mountains: Part II. Fine Particulate Matter and Visibility. J. Air Waste Manage. Assoc. , 2006. **56**(1): p. 12-22.
5. Watson, J. G., Visibility: Science and Regulation. J. Air Waste Manage. Assoc. , 2002. **52**: p. 628-712.
6. Charlson, R. J., Schwartz, S. E., Hales, J. M., Cess, R. D., Coakley, J., J.A., Hansen, J. E., and Hoffmann, D. J., Climate Forcing by Anthropogenic Aerosols. Science, 1992. **255**(423-428).
7. Carrico, C. M., Kus, P., Rood, M. J., Quinn, P. K., and Bates, T. S., Mixtures of pollution, dust, seasalt and volcanic aerosol during ACE-Asia: Aerosol Radiative properties as a function of relative humidity. J. of Geophysical Research-Atmospheres, 2003: p. 44.
8. Rood, M. J., Covert, D. S., and Larson, T. V., Hygroscopic Properties of Atmospheric Aerosols in Riverside, California. Tellus, 1987. **39B**(4): p. 383-397.
9. Kus, P., Physical and Chemical Properties of Laboratory and Ambient Aerosols Related to Climate Change. 2003, University of Illinois at Urbana-Champaign: Urbana, IL.
10. USEPA. PM Standards Revision - 2006. 2006; Available from: http://epa.gov/pm/naaqsrev2006.html.
11. USEPA, Regional Haze Regulations; Final Rule, in 40 CFR Part 51. 1999.
12. Kemme, M., et. al. , Nonfacility Particulate Matter Issues in the Army - A Comprehensive Review in ERDC-CERL Technical Report TR-01-50 2001.
13. Schnelle, K. B. and Dey, P. R., Atmospheric Dispersion Modeling Compliance Guide. 2000: McGraw-Hill, New York.
14. Gillies, J. A., Etyemezian, V., Kuhns, H., Nikolic, D., and Gillette, D. A., Effect of vehicle characteristics on unpaved road dust emissions. Atmospheric Environment, 2005. **39**(13): p. 2341-2347.
15. USEPA. AP-42. Miscellaneous Sources (Chapter 13) 2006 9/5/2008; 5th:[Available from: http://www.epa.gov/ttn/chief/ap42/ch13/final/c13s0202.pdf.
16. Wandinger, U., Introduction to Lidar, Chapter 1 in Lidar: Range-Resolved Optical Remote Sensing of the Atmosphere, C. Weitkamp, Editor. 2005. Springer. p. 2.

17. Middleton, W. E. K. and Spilhaus, A. F., Meteorological Instruments. 1953, Toronto: University of Toronto Press.

18. Wandinger, U., Introduction to Lidar, in Lidar: Range-Resolved Optical Remote Sensing of the Atmosphere, Weitkamp, C., Editor. 2005, Springer. p. 1-18.

19. Spinhirne, J. D., Micro Pulse Lidar. IEEE Transactions on Geoscience and Remote Sensing, 1993. **31**(1): p. 48-55.

20. Campbell, J. R., Hlavka, D. L., Welton, E. J., Flynn, C. J., Turner, D. D., Spinhirne, J. D., Scott III, V. S., and Hwang, I. H., Full-time, Eye-safe Cloud and Aerosol Lidar Observation at Atmospheric Radiation Measurement Program Sites: Instruments and Data Processing. Journal of Atmospheric and Oceanic Technology, 2002. **19**(4): p. 431-442.

21. Shiobara, M., Yabuki, M., and Kobayashi, H., A polar cloud analysis based on Micro-pulse Lidar measurements at Ny-Alesund, Svalbard and Syowa, Antarctica. Physics and Chemistry of the Earth, 2003. **28**(28-32): p. 1205-1212.

22. Campbell, J. R. and Sassen, K., Polar stratospheric clouds at the South Pole from 5 years of continuous lidar data: Macrophysical, optical, and thermodynamic properties. Journal of Geophysical Research - Atmospheres, 2008. **113**(D20).

23. Cordoba-Jabonero, C., Gil, M., Yela, M., Maturilli, M., and Neuber, R., Polar Stratospheric Cloud Observations in the 2006/07 Arctic Winter by Using an Improved Micropulse Lidar. Journal of Atmospheric and Oceanic Technology, 2009. **26**(10): p. 2136-2148.

24. Anderson, T. L., Masonis, S. J., Covert, D. S., Charlson, R. J., and Rood, M. J., In situ Measurement of the Aerosol Extinction-to-backscatter Ratio at a Polluted Continental Site. Journal of Geophysical Research, 2000. **105**(D22): p. 26,907-26,915.

25. Welton, E. J., Voss, K. J., Quinn, P. K., Flatau, P. J., Markowicz, K., Campbell, J. R., Spinhirne, J. D., Gordon, H. R., Johnson, J. E., Measurements of aerosol vertical profiles and optical properties during INDOEX 1999 using micropulse lidars. Journal of Geophysical Research, 2002. **107**(D19): p. 8019-8038.

26. Voss, K. J., Welton, E. J., Quinn, P. K., Johnson, J., Thompson, A., and H., G., Lidar Measurements During Aerosols99. J. Geophys. Res., 2001. **106**: p. 20821-20832.

27. Weir, A., Jones, D. G., Papay, L. T., Calvert, S., and Yung, S. C., Factors Influencing Plume Opacity. Environmental Science & Technology, 1976. **10**(6): p. 539-544.

28. Campbell, J. R. H., D. L.; Welton, E. J.; Flynn, C. J.; Turner, D. D.; Spinhirne, J. D.; Scott III, V. S.; Hwang, I. H., Full-time, Eye-safe Cloud and Aerosol Lidar Observation at Atmospheric Radiation Measurement Program Sites: Instruments and Data Processing. Journal of Atmospheric and Oceanic Technology, 2002. **19**(4): p. 431-442.

29. Fernald, F. G. H., B. M.; John, A. R., Determination of Aerosol Height Distributions by Lidar. Journal of Applied Meteorology, 1972. **11**(3): p. 482-489.

30. Roy, G., Vallee, G., and Marcelin, J., LIDAR-Inversion Technique Based on Total Integrated Backscatter Calibrated Curves. Applied Optics, 1993. **32**(33): p. 6754-6763.

31. Du, K., Rood, M. J., Kim, B. J., Kemme, M., Hashmonay, R., and Varma, R. Optical Remote Sensing of Dust Plumes Using Micropulse Lidar. in 99th Annual Meeting of the Air & Waste Management Association. 2006. New Orleans, LA.

32. Volz, F. E., Infrared Optical Constants of Ammonium Slfate, Sahara Dust, Volcanic Pumice, and Flyash. Applied Optics, 1973. **12**(3): p. 564-568.

33. Sokolik, I., Andronova, A., and Johnson, T. C., Complex refractive index of atmospheric dust. Atmospheric Environment, 1993. **27A**(16): p. 2495-2502.

34. Varma, R. M., Hashmonay, R. A., Du, K., Rood, M. J., Kim, B. J., Kemme, M. R., A Novel Methodology for Fugitive Dust Emission Estimation using Optical Remote Sensing, in Advanced Environmental Monitoring, Kim, Y. J., Platt, U., Editor. 2007, Springer-Verlag GmbH.

35. Hashmonay, R. A. and Harris, D. B. Particulate Matter Measurements Using Open-Path Fourier Transform Infrared Spectroscopy. in 94th A&WMA Annual Conference & Exhibition. 2001. Orlando, FL.

36. Wickramasinghe, N. C., Light Scattering Functions for Small Particles with Applications in Astronomy. 1973, London: Adam Hilger. 25-27.

37. Hashmonay, R. A., Kagann, R. H., Rood, M. J., Kim, B. J., Kemme, M. R., Gillies, J., An Advanced Test Method for Measuring Fugitive Dust Emissions Using a Hybrid System of Optical Remote Sensing and Point Monitor Techniques, in Atmospheric and Biological Environmental Monitoring, Y. J. Kim, U. P., M. B. Gu, H. Iwahashi, Editor. 2009, Springer Netherlands. p. 73-81.

38. Williams, D. S., Shukla, M. K., Ross, J., Particulate matter emission by a vehicle running on unpaved road. Atmospheric Environment, 2008. **42**(16): p. 3899-3905.

39. ASTM, D 7520: Standard Test Method to Determine the Opacity of a Plume in the Outdoor Ambient Atmosphere. 2010, ASTM International. p. 22.

Appendix A: Supporting Data

Appendix A-1: Supporting Data for Artillery Blast Events during the 2005 YPG Field Campaign

Table A-1-1 PM mass emission factors for the 2005 YPG Field Campaign

Date	Event #	Projectile Model	Propelling Charge Model	Propelling Charge Zone	PM Emission Factor (g-PM/shot)	
					PM_{10}	$PM_{2.5}$
10/27/2005	150	M549A1	M203A1	8S	152	26
10/27/2005	151	M549A1	M203A1	8S	67	9
10/27/2005	152	M549A1	M203A1	8S	561	91
10/27/2005	153	M549A1	M203A1	8S	258	31
10/27/2005	154	M549A1	M203A1	8S	111	21
10/27/2005	155	M549A1	M203A1	8S	49	3
10/27/2005	156	M549A1	M203A1	8S	193	32
10/27/2005	157	M549A1	M203A1	8S	81	9
10/27/2005	158	M549A1	M203A1	8S	331	46
10/27/2005	159	M549A1	M203A1	8S	182	50
10/27/2005	160	M549A1	M203A1	8S	183	42
10/27/2005	161	M549A1	M203A1	8S	74	18
10/27/2005	162	M549A1	M203A1	8S	39	15
10/27/2005	163	M549A1	M203A1	8S	31	9
10/27/2005	165	M549A1	M203A1	8S	152	46
10/27/2005	166	M549A1	M203A1	8S	64	30
10/27/2005	167	M549A1	M203A1	8S	113	40
10/27/2005	168	M549A1	M203A1	8S	287	117
10/27/2005	169	M549A1	M203A1	8S	167	38
10/27/2005	170	M549A1	M203A1	8S	321	96
10/27/2005	172	M549A1	M203A1	8S	175	63
10/27/2005	173	M549A1	M203A1	8S	100	60
10/27/2005	174	M549A1	M203A1	8S	107	21
10/27/2005	175	M549A1	M203A1	8S	175	65
10/27/2005	176	M549A1	M203A1	8S	109	50
10/27/2005	177	M549A1	M203A1	8S	133	35
10/27/2005	178	M549A1	M203A1	8S	313	197
10/27/2005	179	M549A1	M203A1	8S	288	149
10/27/2005	180	M549A1	M203A1	8S	158	81
10/27/2005	181	M549A1	M203A1	8S	209	61
10/27/2005	182	M107	M3A1	2	62	21

Date	Event #	Projectile Model	Propelling Charge Model	Propelling Charge Zone	PM Emission Factor (g-PM/shot)	
					PM_{10}	$PM_{2.5}$
10/27/2005	183	M107	M3A1	2	78	8
10/27/2005	184	M107	M3A1	2	119	2
10/27/2005	185	M107	M3A1	2	50	0
10/27/2005	186	M107	M3A1	2	48	3
10/27/2005	187	M107	M3A1	2	80	6
10/27/2005	188	M107	M3A1	2	50	9
10/27/2005	189	M107	M3A1	2	142	20
10/27/2005	190	M107	M3A1	2	45	3
10/27/2005	191	M107	M3A1	2	30	9
10/28/2005	205	M107	M3A1	3	121	50
10/28/2005	206	M107	M3A1	3	103	60
10/28/2005	207	M107	M3A1	3	67	47
10/28/2005	209	M107	M3A1	3	154	104
10/28/2005	210	M107	M3A1	3	44	36
10/28/2005	211	M107	M3A1	3	57	36
10/28/2005	212	M107	M3A1	3	155	118
10/28/2005	214	M107	M3A1	3	19	8

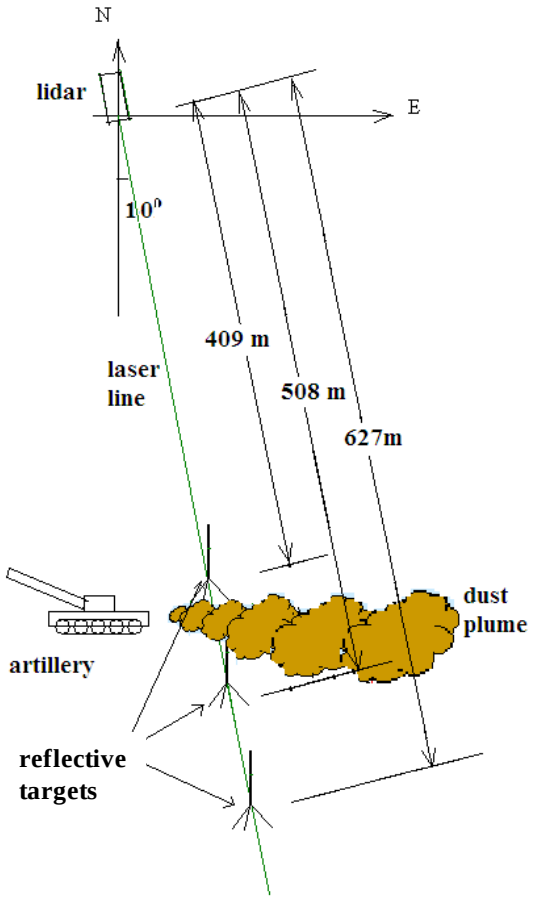

Figure A-1-1 Field map of YPG field campaign on 10/27/05 and 10/28/05

Appendix A-2: Supporting Data for Tested Tracked Vehicles during the 2006 YTC Field Campaign

Table A-2-1 Physical dimensions of the three tracked vehicles and their tracks

Vehicle Type	M113	Bradley	M1A1
Length (m)	5.32	6.45	7.57
Width (m)	2.53	3	3.67
Height-Front (m)	1.91	1.6	1.2
Height-Back (m)	1.91	1.6	1.6
Ground Clearance (m)	0.52	0.46	0.48
Vehicle Mass (kg)	12,349	29,937	60,909
Ground Pressure (kgf/cm^2)	0.61	0.7	0.98
Track Width (m)	0.4	0.55	0.65
Track Contact Length (m)	2.97	4.1	5.1
Pad Length (m)	0.18	0.12	0.16
Pad Width (m)	0.14	0.25	0.22
# Pads/Contact Length	6.4	6.4	4.9

(Source: Gillies, J. A.; Etyemezian, V.; Kuhns, H.; Moosmuller, H.; Engelbrecht, J.; Sweeney, M.; Uppapalli, S.; Gillette, D. A.; Allwine, K. J.; Rutz, F. C.; Chapman, E. G. *Particulate Matter Emissions for Dust from Unique Military Activities*, 2006.)

Table A-2-2 PM mass emission factors for the 2006 YTC Field Campaign

Date	Event #	Surface Type	Vehicle Type	Speed (mph)	Speed (km/h)	Mass Emission Factor (g-PM/vkt)	
						PM_{10}	$PM_{2.5}$
8/25/2006	1	Grassland	Bradley	15	24	6,915	763
8/25/2006	2	Grassland	Bradley	20	32	12,771	1,407
8/25/2006	3	Grassland	Bradley	20	32	11,563	4,094
8/25/2006	4	Grassland	Bradley	25	40	6,383	2,177
8/25/2006	5	Grassland	Bradley	25	40	5,939	1,913
8/25/2006	6	Grassland	Bradley	20	32	2,143	287
8/25/2006	7	Grassland	Bradley	20	32	15,503	1,605
8/25/2006	8	Grassland	Bradley	15	24	3,596	763
8/25/2006	9	Grassland	Bradley	10	16	415	74
8/25/2006	10	Grassland	Bradley	5	8	10,710	989
8/25/2006	11	Grassland	M1A1	20	32	48,615	10,287
8/25/2006	12	Grassland	M1A1	21	34	19,247	4,032
8/25/2006	13	Grassland	M1A1	25	40	7,191	450

Date	Event #	Surface Type	Vehicle Type	Speed (mph)	Speed (km/h)	Mass Emission Factor (g-PM/vkt)	
						PM_{10}	$PM_{2.5}$
8/25/2006	14	Grassland	M1A1	20	32	37,323	10,053
8/25/2006	15	Grassland	M1A1	15	24	31,943	5,715
8/25/2006	16	Grassland	M1A1	10	16	11,980	1,073
8/25/2006	17	Grassland	M1A1	5	8	6,902	797
8/24/2006	18	Unpaved Road	M113	10	16	5,449	984
8/24/2006	19	Unpaved Road	M113	20	32	20,768	3,782
8/24/2006	20	Unpaved Road	M113	10	16	5,941	1,419
8/24/2006	22	Unpaved Road	M113	25	40	16,314	4,178
8/24/2006	23	Unpaved Road	M113	25	40	30,306	5,757
8/24/2006	24	Unpaved Road	M113	25	40	10,885	1,329
8/23/2006	28	Unpaved Road	M1A1	10	16	27,380	3,037
8/23/2006	29	Unpaved Road	M1A1	10	16	37,769	7,008
8/23/2006	30	Unpaved Road	M1A1	15	24	52,965	4,238
8/23/2006	31	Unpaved Road	M1A1	15	24	16,548	702
8/23/2006	32	Unpaved Road	M1A1	15	24	56,618	7,813
8/23/2006	33	Unpaved Road	M1A1	20	32	70,411	4,998
8/23/2006	34	Unpaved Road	M1A1	20	32	42,180	8,422
8/23/2006	35	Unpaved Road	M1A1	25	40	48,718	11,716
8/23/2006	36	Unpaved Road	M1A1	25	40	59,169	2,586
8/23/2006	47	Unpaved Road	M1A1	5	8	27,546	875
8/23/2006	48	Unpaved Road	M1A1	7.5	12	29,769	1,502
8/23/2006	49	Unpaved Road	M1A1	7.5	12	7,194	1,203
8/23/2006	50	Unpaved Road	M1A1	10	16	15,334	1,169
8/23/2006	62	Unpaved Road	M1A1	15	24	53,823	3,633
8/23/2006	63	Unpaved Road	M1A1	10	16	13,669	2,823
8/23/2006	64	Unpaved Road	M1A1	10	16	19,788	2,872
8/22/2006	65	Unpaved Road	Bradley	5	8	4,352	728
8/22/2006	83	Unpaved Road	Bradley	10	16	7,285	818
8/22/2006	85	Unpaved Road	Bradley	5	8	20,512	2,952
8/22/2006	86	Unpaved Road	Bradley	10	16	1,684	15
8/22/2006	87	Unpaved Road	Bradley	10	16	19,129	1,962
8/22/2006	88	Unpaved Road	Bradley	15	24	33,021	0
8/22/2006	89	Unpaved Road	Bradley	15	24	15,052	1,167
8/22/2006	90	Unpaved Road	Bradley	20	32	33,794	2,816
8/22/2006	91	Unpaved Road	Bradley	20	32	46,601	6,998
8/22/2006	92	Unpaved Road	Bradley	25	40	44,915	7,270
8/22/2006	93	Unpaved Road	Bradley	25	40	2,808	215
8/22/2006	94	Unpaved Road	Bradley	25	40	52,100	922
8/22/2006	95	Unpaved Road	Bradley	25	40	5,574	513

Table A-2-3 Details about tracked vehicle movement based on MPL Data

Date	Event #	Vehicle	Plume	Plume	Vehicle	Vehicle
8/25/2006	1	12:17:22	12:18:09	12:19:41	BFV	15.0
8/25/2006	2	12:20:10	12:20:20	12:22:01	BFV	20.0
8/25/2006	4	12:27:35	12:27:45	12:30:27	BFV	25.0
8/25/2006	5	12:30:29	12:30:58	12:33:49	BFV	25.0
8/25/2006	7	12:49:51	12:50:15	12:53:17	BFV	20.0
8/25/2006	10	13:05:38	13:06:31	13:09:53	BFV	5.0
8/25/2006	11	14:33:39	14:34:28	14:36:19	M1A1	20.0
8/25/2006	12	14:37:28	14:37:59	14:39:40	M1A1	21.0
8/25/2006	13	14:42:45	14:44:08	14:47:09	M1A1	25.0
8/25/2006	14	14:47:31	14:48:02	14:50:40	M1A1	20.0
8/25/2006	15	14:50:58	14:51:44	14:54:21	M1A1	15.0
8/25/2006	16	14:54:43	14:55:50	14:59:24	M1A1	10.0
8/25/2006	17	14:59:09	14:59:52	15:05:16	M1A1	5.0
8/24/2006	18	13:55:21	13:55:53	13:58:29	M113	10.0
8/24/2006	19	14:18:07	14:18:50	14:20:17	M113	20.0
8/24/2006	20	14:28:03	14:28:20	14:31:13	M113	10.0
8/24/2006	21	14:56:40	14:57:51	14:59:59	M113	15.0
8/24/2006	22	15:07:45	15:09:00	15:10:39	M113	25.0
8/24/2006	23	15:13:11	15:13:46	15:16:00	M113	25.0
8/24/2006	24	15:17:03	15:18:20	15:20:43	M113	25.0
8/24/2006	25	15:22:19	15:22:58	15:26:05	M113	25.0
8/23/2006	28	10:36:00	10:37:01	10:39:02	M1A1	10.0
8/23/2006	29	10:42:21	10:42:24	10:46:04	M1A1	10.0
8/23/2006	30	10:46:45	10:47:19	10:50:37	M1A1	15.0
8/23/2006	32	10:54:10	10:54:08	10:56:59	M1A1	15.0
8/23/2006	33	10:57:11	10:57:40	10:59:10	M1A1	20.0
8/23/2006	34	11:04:35	11:04:42	11:07:33	M1A1	20.0
8/23/2006	35	11:07:55	11:08:23	11:09:54	M1A1	25.0

Date	Event #	Vehicle	Plume	Plume	Vehicle	Vehicle
8/23/2006	36	11:16:47	11:17:07	11:19:28	M1A1	25.0
8/23/2006	37	11:21:50	11:22:09	11:24:49	M1A1	25.0
8/23/2006	38	12:28:31	11:28:40	11:31:40	M1A1	25.0
8/23/2006	39	11:32:10	11:32:22	11:33:52	M1A1	20.0
8/23/2006	40	11:39:34	11:39:45	11:41:45	M1A1	20.0
8/23/2006	41	11:42:30	11:42:46	11:44:56	M1A1	15.0
8/23/2006	42	11:48:53	11:49:08	11:53:40	M1A1	15.0
8/23/2006	43	11:53:30	11:53:50	11:58:42	M1A1	10.0
8/23/2006	44	11:58:50	11:59:02	12:01:53	M1A1	10.0
8/23/2006	45	12:02:30	12:04:15	12:05:13	M1A1	5.0
8/23/2006	46	12:10:58	12:11:07	12:14:28	M1A1	5.0
8/23/2006	47	13:37:21	13:39:05	13:40:06	M1A1	5.0
8/23/2006	48	13:43:30	13:44:27	13:45:28	M1A1	7.5
8/23/2006	49	13:48:15	13:48:48	13:51:39	M1A1	7.5
8/23/2006	50	13:57:10	13:57:32	13:59:58	M1A1	10.0
8/23/2006	51	14:03:15	14:03:51	14:05:39	M1A1	15.0
8/23/2006	52	14:12:20	14:12:22	14:15:28	M1A1	15.0
8/23/2006	53	14:15:33	14:16:15	14:17:40	M1A1	20.0
8/23/2006	56	14:28:23	14:28:52	14:31:32	M1A1	25.0
8/23/2006	57	14:32:03	14:32:53	14:34:23	M1A1	25.0
8/23/2006	58	14:36:30	14:36:55	14:39:35	M1A1	25.0
8/23/2006	59	14:40:20	14:41:16	14:42:17	M1A1	20.0
8/23/2006	60	14:44:11	14:44:38	14:46:47	M1A1	20.0
8/23/2006	61	14:52:10	14:52:10	14:54:00	M1A1	15.0
8/23/2006	63	15:00:33	15:01:03	15:03:44	M1A1	10.0
8/22/2006	65	10:15:10	10:15:13	10:20:20	BFV	5.0
8/22/2006	73	11:39:30	11:39:40	11:41:26	BFV	20.0
8/22/2006	77	11:56:25	11:56:34	11:58:23	BFV	25.0
8/22/2006	78	12:01:18	12:01:28	12:04:06	BFV	20.0

Date	Event #	Vehicle	Plume	Plume	Vehicle	Vehicle
8/22/2006	81	12:21:19	12:21:24	12:23:44	BFV	15.0
8/22/2006	82	12:30:27	12:30:32	12:34:06	BFV	10.0
8/22/2006	88	14:45:20	14:45:17	14:47:57	BFV	15.0
8/22/2006	89	14:50:36	14:50:58	14:52:50	BFV	15.0
8/22/2006	90	14:53:30	14:53:30	14:55:00	BFV	20.0
8/22/2006	91	14:59:13	14:59:22	15:02:02	BFV	20.0
8/22/2006	92	15:02:34	15:02:57	15:04:45	BFV	25.0
8/22/2006	94	15:09:27	15:09:46	15:12:06	BFV	25.0
8/22/2006	96	15:18:56	15:19:09	15:21:09	BFV	25.0
8/22/2006	97	15:23:08	15:23:31	15:25:51	BFV	20.0
8/22/2006	98	15:29:36	15:30:03	15:31:53	BFV	20.0
8/22/2006	99	15:34:02	15:34:15	15:36:15	BFV	15.0
8/22/2006	100	15:43:29	15:43:38	15:45:08	BFV	15.0
8/22/2006	101	15:46:06	15:46:18	15:49:20	BFV	10.0
8/22/2006	102	15:56:00	15:55:01	15:58:03	BFV	5.0
8/22/2006	103	16:02:40	16:02:56	16:06:16	BFV	5.0

Table A-2-4 Laser Transmissometer data and duration of the plume

Date	Event #	Optical Path at 670 nm (Un-		Plume Duration (sec)
		Lower Path	Upper Path	
8/25/2006	1	0.160	0.160	25
8/25/2006	2	0.300	0.300	41
8/25/2006	3	0.485	0.485	41
8/25/2006	4	0.368	0.309	56
8/25/2006	5	0.244	0.234	61
8/25/2006	6	0.126	0.111	39
8/25/2006	7	0.314	0.241	82
8/25/2006	8	0.116	0.127	52
8/25/2006	9	0.071	0.062	15

Date	Event #	Optical Path at 670 nm (Un-		Plume Duration (sec)
		Lower Path	Upper Path	
8/25/2006	10	0.160	0.160	55
8/25/2006	11	0.763	0.882	76
8/25/2006	12	0.558	0.645	40
8/25/2006	13	0.258	0.192	67
8/25/2006	14	0.949	0.960	61
8/25/2006	15	0.728	1.004	50
8/25/2006	16	0.214	0.213	51
8/25/2006	17	0.180	0.210	41
8/24/2006	18	0.442	0.398	54
8/24/2006	19	0.826	0.907	55
8/24/2006	20	0.361	0.399	43
8/24/2006	22	0.790	0.847	52
8/24/2006	23	1.460	1.372	49
8/24/2006	24	0.767	0.725	47
8/23/2006	28	0.553	0.704	47
8/23/2006	29	0.678	0.713	59
8/23/2006	30	0.795	0.793	87
8/23/2006	31	0.416	0.288	41
8/23/2006	32	1.285	1.292	46
8/23/2006	33	1.396	1.212	57
8/23/2006	34	1.698	1.471	53
8/23/2006	35	1.052	1.126	66
8/23/2006	36	0.888	0.519	72
8/23/2006	47	0.535	0.426	43
8/23/2006	48	0.793	0.847	42
8/23/2006	49	0.253	0.312	72
8/23/2006	50	0.504	0.486	39
8/23/2006	62	0.614	0.536	98

Date	Event #	Optical Path at 670 nm (Un-		Plume Duration (sec)
		Lower Path	Upper Path	
8/23/2006	63	0.397	0.370	44
8/23/2006	64	0.599	0.511	46
8/22/2006	65	0.600	0.358	52
8/22/2006	66	0.600	0.348	55
8/22/2006	67	0.872	0.893	42
8/22/2006	69	1.224	1.008	60
8/22/2006	70	1.047	1.027	65
8/22/2006	71	0.875	0.991	124
8/22/2006	72	1.106	1.145	67
8/22/2006	73	1.046	1.144	71
8/22/2006	74	0.910	0.615	87
8/22/2006	75	0.854	1.020	90
8/22/2006	76	1.100	0.697	75
8/22/2006	77	1.468	1.259	61
8/22/2006	78	1.403	1.083	85
8/22/2006	79	1.266	0.782	67
8/22/2006	80	1.031	0.845	89
8/22/2006	81	1.119	0.788	63
8/22/2006	82	1.046	0.731	67
8/22/2006	83	0.619	0.463	46
8/22/2006	85	1.130	0.702	53
8/22/2006	86	0.348	0.100	18
8/22/2006	87	1.378	0.769	53
8/22/2006	88	0.783	0.597	117
8/22/2006	89	1.155	1.096	56
8/22/2006	90	1.315	1.018	54
8/22/2006	91	1.308	1.171	117
8/22/2006	92	1.242	0.949	57

Date	Event #	Optical Path at 670 nm (Un-		Plume Duration (sec)
		Lower Path	Upper Path	
8/22/2006	93	0.371	0.107	36
8/22/2006	94	1.029	0.774	130
8/22/2006	95	0.952	0.727	54

Table A-2-5 FTIR data

	Optical Path in Lower Path (Unitless)						Optical Path in Upper Path (Unitless)					
Wave number (cm^{-1})	4425	4225	2875	2525	2225	775	4425	4225	2875	2525	2225	775
Wavelength (μm)	2.26	2.37	3.48	3.96	4.49	12.9	2.26	2.37	3.48	3.96	4.49	12.9
Event #:												
1	0.144	0.143	0.139	0.132	0.121	0.092	0.142	0.146	0.140	0.139	0.133	0.100
2	0.276	0.273	0.256	0.238	0.214	0.163	0.271	0.281	0.264	0.252	0.238	0.176
3	0.210	0.208	0.195	0.184	0.165	0.127	0.204	0.206	0.199	0.189	0.178	0.133
4	0.171	0.170	0.156	0.145	0.129	0.094	0.112	0.122	0.117	0.113	0.108	0.078
5	0.142	0.142	0.136	0.128	0.117	0.090	0.097	0.107	0.102	0.099	0.095	0.068
6	0.084	0.087	0.080	0.075	0.067	0.046	0.099	0.099	0.093	0.087	0.081	0.059
7	0.159	0.155	0.146	0.137	0.123	0.090	0.244	0.249	0.237	0.227	0.213	0.158
8	0.087	0.088	0.079	0.073	0.065	0.044	0.093	0.092	0.087	0.084	0.080	0.058
9	0.048	0.049	0.044	0.040	0.035	0.027	0.052	0.055	0.043	0.041	0.039	0.024
10	0.148	0.146	0.137	0.127	0.114	0.082	0.151	0.161	0.153	0.147	0.137	0.099
11	0.569	0.557	0.539	0.493	0.436	0.355	0.610	0.580	0.557	0.526	0.493	0.373

	Optical Path in Lower Path (Unitless)						Optical Path in Upper Path (Unitless)					
Wave number (cm^{-1})	4425	4225	2875	2525	2225	775	4425	4225	2875	2525	2225	775
Wavelength (μm)	2.26	2.37	3.48	3.96	4.49	12.9	2.26	2.37	3.48	3.96	4.49	12.9
Event #:												
12	0.393	0.392	0.366	0.335	0.298	0.229	0.420	0.403	0.381	0.359	0.336	0.247
13	0.171	0.169	0.152	0.139	0.120	0.082	0.216	0.223	0.206	0.194	0.177	0.123
14	0.540	0.517	0.512	0.458	0.401	0.335	0.690	0.680	0.660	0.629	0.607	0.452
15	0.641	0.586	0.559	0.506	0.441	0.355	0.537	0.530	0.510	0.484	0.453	0.333
16	0.206	0.200	0.189	0.175	0.157	0.117	0.253	0.250	0.238	0.225	0.210	0.153
17	0.187	0.185	0.169	0.153	0.133	0.086	0.159	0.157	0.144	0.137	0.127	0.085
18	0.267	0.263	0.229	0.204	0.174	0.101	0.368	0.360	0.314	0.285	0.256	0.368
19	0.629	0.622	0.564	0.508	0.442	0.301	0.814	0.699	0.540	0.502	0.460	0.315
20	0.317	0.308	0.270	0.243	0.210	0.128	0.257	0.267	0.238	0.220	0.200	0.130
22	0.540	0.531	0.478	0.427	0.369	0.243	0.598	0.561	0.528	0.484	0.441	0.293
23	0.754	0.731	0.719	0.643	0.565	0.443	1.110	1.105	1.100	1.050	0.980	0.813
24	0.528	0.521	0.484	0.438	0.383	0.274	0.778	0.768	0.724	0.675	0.621	0.429

	Optical Path in Lower Path (Unitless)						Optical Path in Upper Path (Unitless)					
Wave number (cm^{-1})	4425	4225	2875	2525	2225	775	4425	4225	2875	2525	2225	775
Wavelength (μm)	2.26	2.37	3.48	3.96	4.49	12.9	2.26	2.37	3.48	3.96	4.49	12.9
Event #:												
28	0.535	0.529	0.490	0.454	0.408	0.285	0.451	0.467	0.435	0.413	0.386	0.282
29	0.538	0.535	0.494	0.455	0.408	0.286	0.689	0.558	0.521	0.489	0.457	0.324
30	0.512	0.505	0.470	0.433	0.387	0.269	0.689	0.754	0.810	0.791	0.782	0.573
31	0.320	0.315	0.283	0.261	0.234	0.157	0.339	0.348	0.318	0.298	0.274	0.184
32	0.776	0.768	0.744	0.685	0.610	0.455	0.800	0.860	1.013	0.996	0.895	0.709
33	0.906	0.898	0.862	0.788	0.701	0.519	0.777	0.948	1.114	1.097	0.921	0.815
34	0.679	0.653	0.635	0.595	0.539	0.418	1.555	1.431	1.302	1.260	1.064	0.878
35	0.749	0.735	0.653	0.579	0.500	0.324	0.884	0.776	0.714	0.679	0.637	0.505
36	0.478	0.476	0.436	0.399	0.353	0.236	0.517	0.543	0.582	0.561	0.506	0.380
47	0.405	0.399	0.374	0.346	0.310	0.211	0.987	0.809	0.720	0.687	0.685	0.758
48	0.556	0.552	0.549	0.502	0.444	0.334	1.075	1.047	1.041	1.022	1.022	0.989
49	0.270	0.266	0.250	0.232	0.210	0.143	0.397	0.384	0.327	0.326	0.332	0.406

	Optical Path in Lower Path (Unitless)						Optical Path in Upper Path (Unitless)					
Wave number (cm^{-1})	4425	4225	2875	2525	2225	775	4425	4225	2875	2525	2225	775
Wavelength (μm)	2.26	2.37	3.48	3.96	4.49	12.9	2.26	2.37	3.48	3.96	4.49	12.9
Event #:												
50	0.461	0.451	0.435	0.398	0.352	0.253	0.516	0.506	0.516	0.500	0.493	0.546
62	0.432	0.429	0.419	0.386	0.342	0.248	0.614	0.585	0.597	0.567	0.545	0.491
63	0.285	0.282	0.267	0.248	0.221	0.156	0.397	0.397	0.240	0.239	0.209	0.143
64	0.408	0.405	0.397	0.365	0.321	0.239	0.599	0.573	0.433	0.413	0.393	0.329
65	0.556	0.546	0.509	0.471	0.424	0.297	0.274	0.281	0.267	0.256	0.241	0.184
66	0.613	0.603	0.578	0.539	0.489	0.355	0.267	0.277	0.265	0.255	0.240	0.168
67	0.819	0.798	0.743	0.678	0.601	0.424	0.872	0.812	0.720	0.680	0.677	0.494
69	0.813	0.809	0.737	0.672	0.594	0.406	1.120	1.097	1.005	1.054	0.961	0.779
70	0.824	0.827	0.765	0.694	0.612	0.426	1.029	0.970	0.911	0.837	0.797	0.600
71	0.955	0.936	0.840	0.749	0.647	0.421	1.030	0.865	0.800	0.721	0.700	0.664
72	0.612	0.611	0.575	0.537	0.488	0.362	1.477	1.257	1.489	1.419	1.295	1.079
73	0.671	0.660	0.600	0.542	0.477	0.310	1.140	1.022	0.880	0.898	0.882	0.717

	Optical Path in Lower Path (Unitless)						Optical Path in Upper Path (Unitless)					
Wave number (cm^{-1})	4425	4225	2875	2525	2225	775	4425	4225	2875	2525	2225	775
Wavelength (μm)	2.26	2.37	3.48	3.96	4.49	12.9	2.26	2.37	3.48	3.96	4.49	12.9
Event #:												
74	1.065	1.041	1.010	0.890	0.774	0.543	0.879	1.056	1.045	1.006	0.916	0.815
75	0.515	0.506	0.457	0.412	0.360	0.234	0.926	0.783	0.777	0.787	0.723	0.651
76	0.670	0.670	0.611	0.559	0.494	0.380	0.680	0.763	0.782	0.821	0.764	0.569
77	0.583	0.579	0.549	0.504	0.451	0.342	1.514	1.278	1.289	1.396	1.350	1.014
78	0.837	0.824	0.743	0.655	0.555	0.343	1.350	1.114	1.003	0.905	0.905	0.780
79	0.720	0.693	0.685	0.632	0.566	0.434	0.767	0.716	0.670	0.662	0.634	0.523
80	1.037	1.010	0.953	0.855	0.738	0.493	1.130	1.042	1.014	1.004	0.961	0.733
81	0.818	0.804	0.758	0.691	0.612	0.434	0.848	0.808	0.819	0.805	0.777	0.534
82	0.590	0.581	0.561	0.515	0.459	0.338	0.325	0.288	0.271	0.258	0.241	0.169
83	0.481	0.475	0.442	0.403	0.357	0.229	0.400	0.405	0.386	0.365	0.339	0.225
85	0.779	0.776	0.723	0.650	0.566	0.402	0.771	0.607	0.618	0.602	0.619	0.405
86	0.290	0.284	0.267	0.250	0.229	0.158	0.126	0.132	0.127	0.123	0.116	0.087

	Optical Path in Lower Path (Unitless)						Optical Path in Upper Path (Unitless)					
Wave number (cm^{-1})	4425	4225	2875	2525	2225	775	4425	4225	2875	2525	2225	775
Wavelength (μm)	2.26	2.37	3.48	3.96	4.49	12.9	2.26	2.37	3.48	3.96	4.49	12.9
Event #:												
87	0.940	0.912	0.858	0.771	0.674	0.448	0.751	0.761	0.705	0.656	0.598	0.397
88	1.164	1.109	1.015	0.892	0.760	0.483	0.848	0.913	0.974	0.888	0.800	0.529
89	0.872	0.838	0.776	0.689	0.592	0.380	0.879	1.024	1.108	1.051	0.942	0.642
90	0.903	0.895	0.808	0.718	0.616	0.397	1.077	1.020	1.001	0.958	0.894	0.660
91	1.125	1.095	1.017	0.907	0.783	0.527	1.070	1.010	0.942	0.937	0.870	0.668
92	0.824	0.800	0.758	0.684	0.599	0.448	0.912	0.780	0.770	0.715	0.720	0.550
93	0.322	0.316	0.307	0.291	0.266	0.186	0.120	0.119	0.118	0.114	0.110	0.083
94	1.078	1.050	0.993	0.895	0.783	0.578	1.216	1.184	1.230	1.198	1.144	0.861
95	1.001	0.968	0.922	0.827	0.722	0.531	0.857	0.818	0.753	0.704	0.646	0.453

Table A-2-6 Wind data

Event #	Wind Speed (m/s)	Wind Direction (from North, °)	Wind Direction (from Normal Plane, °)
1	9.1	44	-29
2	7.8	22	-51
3	5.9	31	-42
4	6.7	15	-58
5	6.7	15	-58
6	6.6	5	-68
7	6.4	33	-41
8	6.4	15	-58
9	3.2	33	-41
10	6.8	43	-31
11	5.2	71	-3
12	6.4	43	-31
13	2.9	49	-25
14	7.1	29	-44
15	5.2	59	-14
16	5.8	73	0
17	4.4	60	-13
18	1.6	245	-9
19	2.6	276	23
20	2.1	248	-5
21	5.3	200	-53
22	2.9	221	-32
23	3.9	226	-27
24	3.4	202	-52
25	1.7	175	-78
26	1.6	262	9
27	5.1	281	28

Event #	Wind Speed (m/s)	Wind Direction (from North, º)	Wind Direction (from Normal Plane, º)
28	5.4	279	25
29	5.5	278	24
30	5.8	275	21
31	6.5	291	37
32	7.1	271	18
33	5.4	275	22
34	5.4	284	31
35	4.7	286	32
36	6.0	263	10
37	6.5	279	25
38	8.3	282	29
39	7.3	282	28
40	8.3	284	30
41	9.3	269	16
42	8.5	280	27
43	7.8	282	29
44	7.6	283	29
45	8.4	275	21
46	7.2	297	44
47	9.3	300	47
48	8.7	301	48
49	8.4	316	63
50	7.1	297	43
51	6.9	304	50
52	6.5	292	39
53	8.5	312	59
54	7.3	297	44
55	7.7	312	59

Event #	Wind Speed (m/s)	Wind Direction (from North, º)	Wind Direction (from Normal Plane, º)
56	7.9	304	50
57	7.4	317	64
58	6.5	301	48
59	7.8	309	55
60	7.3	307	54
61	7.9	294	40
62	8.7	308	54
63	6.7	302	49
64	8.2	309	56
65	3.3	321	60
83	2.7	213	-49
85	3.4	271	9
86	4.8	273	11
87	2.6	278	16
88	1.6	234	-28
89	1.6	234	-28
90	2.8	268	6
91	1.7	270	8
92	5.2	269	8
93	4.0	281	19
94	2.0	277	16
95	0.7	115	33
96	3.1	261	-1
97	3.7	247	-15
98	3.3	246	-16
102	2.7	279	18
103	2.2	255	-7

Figure A-2-1 Field map of YTC tracked vehicle field campaign on 8/22/06

August 22 plane map (before moving the equipment to the east)

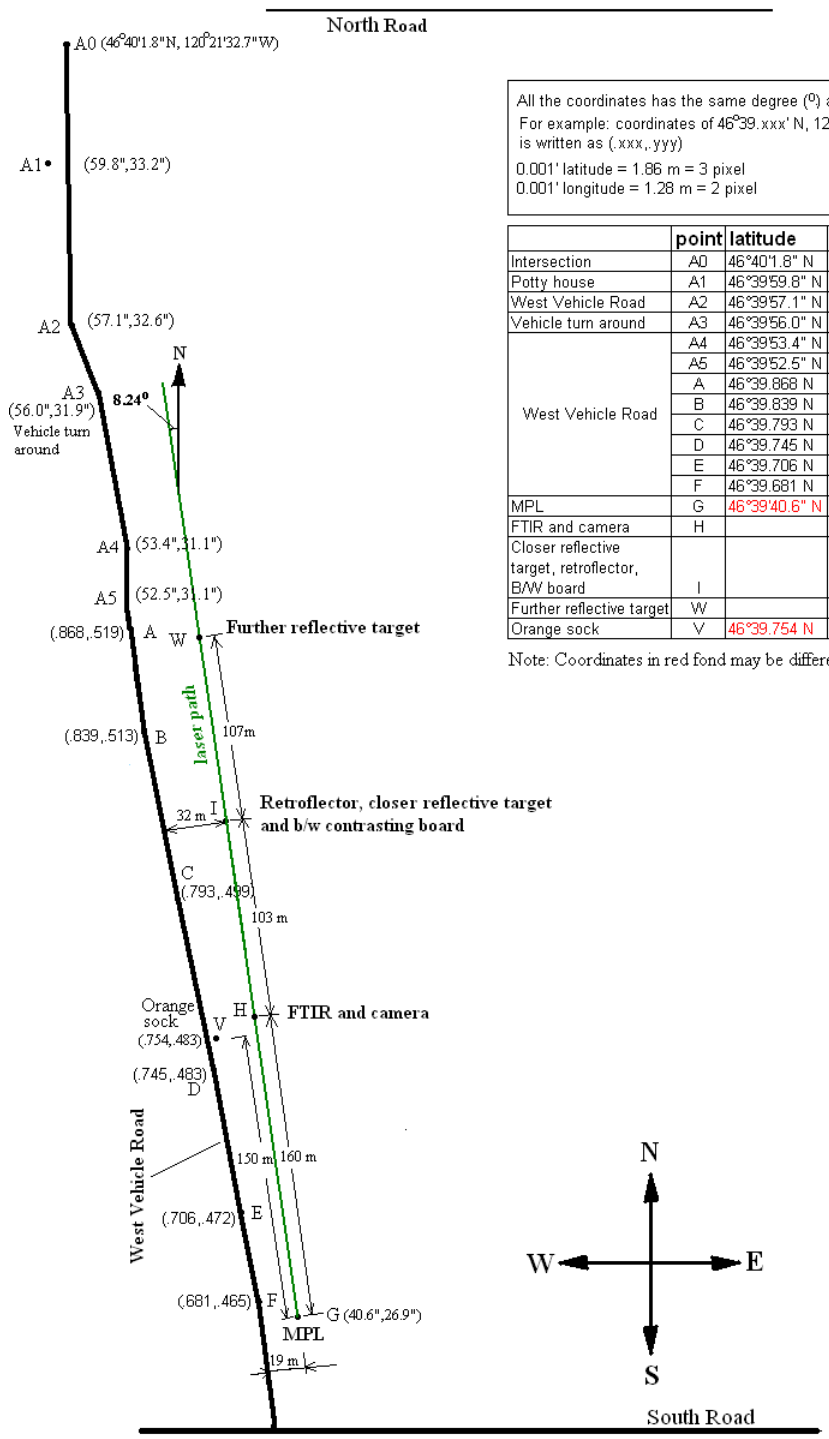

All the coordinates has the same degree (°) and minute (): For example: coordinates of 46°39.xxx' N, 120°21.yyy' W is written as (.xxx,.yyy)

0.001' latitude = 1.86 m = 3 pixel
0.001' longitude = 1.28 m = 2 pixel

	point	latitude	longitude	elevation
Intersection	A0	46°40'1.8" N	120°21'32.7" W	m
Potty house	A1	46°39'59.8" N	120°21'33.2" W	m
West Vehicle Road	A2	46°39'57.1" N	120°21'32.6" W	m
Vehicle turn around	A3	46°39'56.0" N	120°21'31.9" W	m
West Vehicle Road	A4	46°39'53.4" N	120°21'31.1" W	m
	A5	46°39'52.5" N	120°21'31.1" W	m
	A	46°39.868 N	120°21.519 W	m
	B	46°39.839 N	120°21.513 W	m
	C	46°39.793 N	120°21.499 W	m
	D	46°39.745 N	120°21.483 W	m
	E	46°39.706 N	120°21.472 W	m
	F	46°39.681 N	120°21.465 W	m
MPL	G	46°39'40.6" N	120°21'26.9" W	m
FTIR and camera	H			m
Closer reflective target, retroflector, B/W board	I			m
Further reflective target	W			m
Orange sock	V	46°39.754 N	120°21.483 W	m

Note: Coordinates in red fond may be different on different days.

Figure A-2-2 Field map of YTC tracked vehicle field campaign on 8/23/06

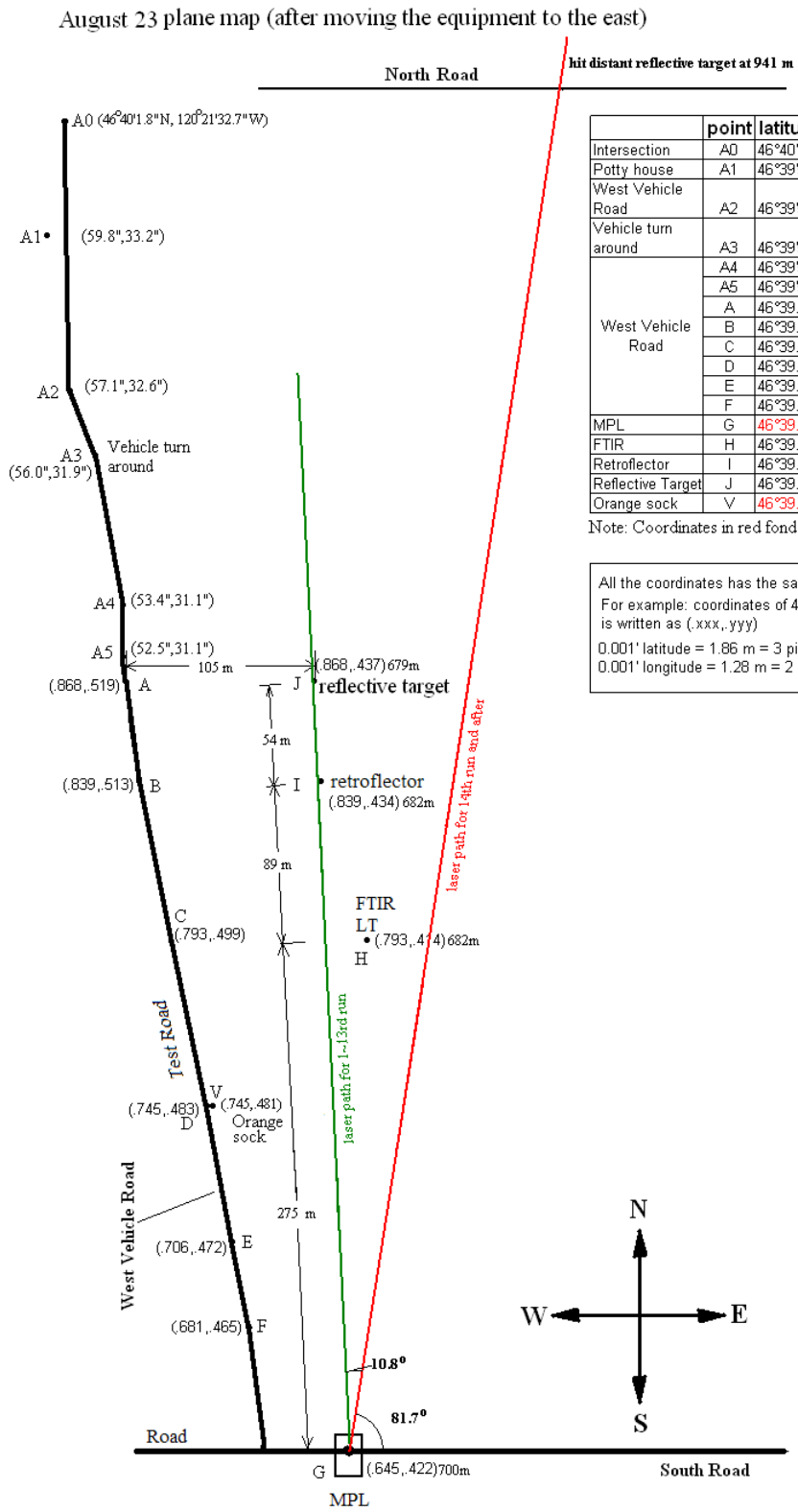

	point	latitude	longitude	elevation	
Intersection	A0	46°40'1.8" N	120°21'32.7" W		m
Potty house	A1	46°39'59.8" N	120°21'33.2" W		m
West Vehicle Road	A2	46°39'57.1" N	120°21'32.6" W		m
Vehicle turn around	A3	46°39'56.0" N	120°21'31.9" W		m
West Vehicle Road	A4	46°39'53.4" N	120°21'31.1" W		m
	A5	46°39'52.5" N	120°21'31.1" W		m
	A	46°39.868 N	120°21.519 W		m
	B	46°39.839 N	120°21.513 W		m
	C	46°39.793 N	120°21.499 W		m
	D	46°39.745 N	120°21.483 W		m
	E	46°39.706 N	120°21.472 W		m
	F	46°39.681 N	120°21.465 W		m
MPL	G	46°39.645 N	120°21.422 W	700	m
FTIR	H	46°39.793 N	120°21.414 W	682	m
Retroflector	I	46°39.839 N	120°21.434 W	682	m
Reflective Target	J	46°39.868 N	120°21.437 W	679	m
Orange sock	V	46°39.745 N	120°21.481 W		m

Note: Coordinates in red fond may be different on different days.

All the coordinates has the same degree (°) and minute (′):
For example: coordinates of 46°39.xxx′ N, 120°21.yyy′ W
is written as (.xxx,.yyy)
0.001′ latitude = 1.86 m = 3 pixel
0.001′ longitude = 1.28 m = 2 pixel

Figure A-2-3 Field map of YTC tracked vehicle field campaign on 8/24/06

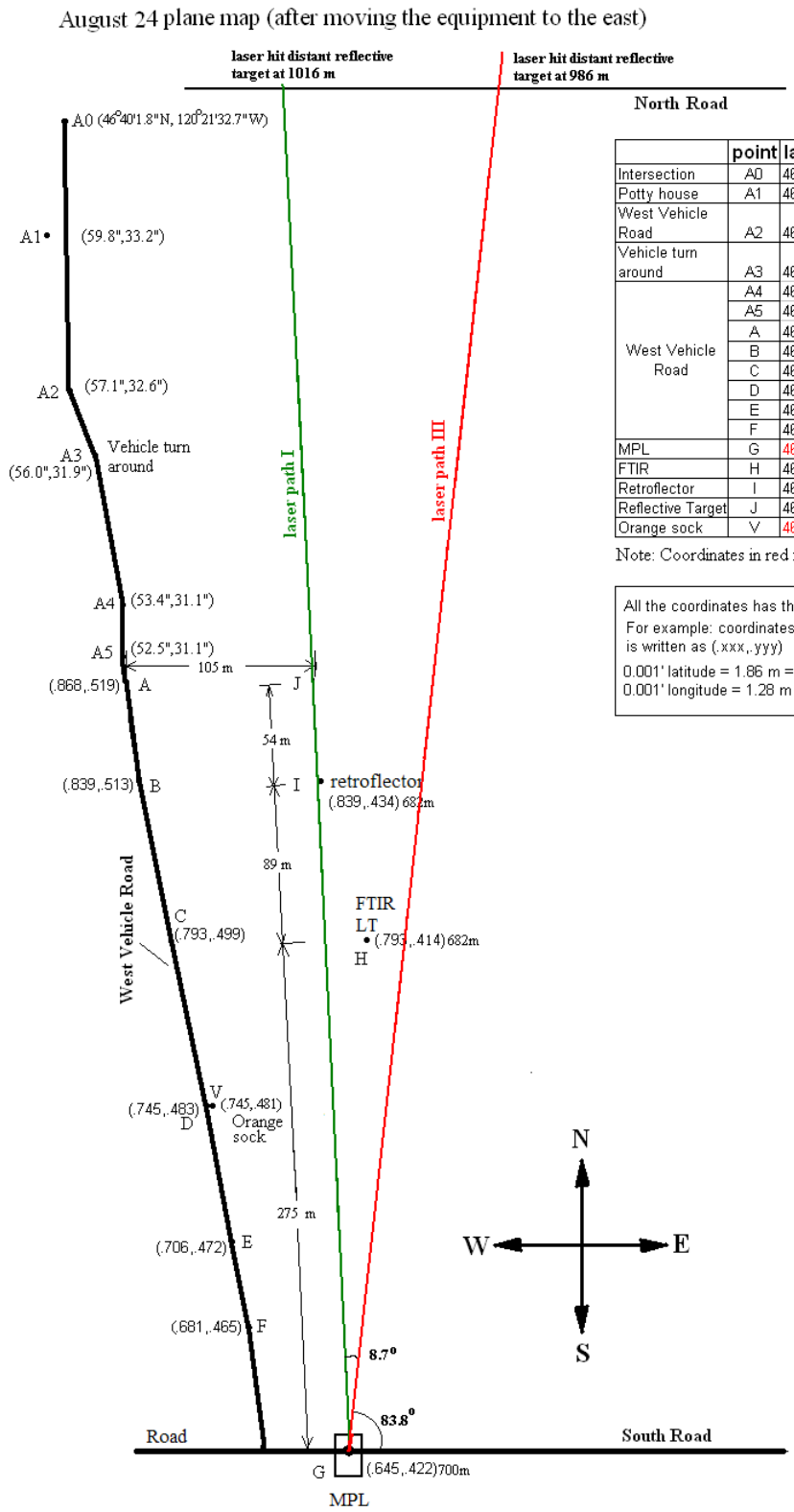

	point	latitude	longitude	elevation	
Intersection	A0	46°40'1.8" N	120°21'32.7" W		m
Potty house	A1	46°39'59.8" N	120°21'33.2" W		m
West Vehicle Road	A2	46°39'57.1" N	120°21'32.6" W		m
Vehicle turn around	A3	46°39'56.0" N	120°21'31.9" W		m
West Vehicle Road	A4	46°39'53.4" N	120°21'31.1" W		m
	A5	46°39'52.5" N	120°21'31.1" W		m
	A	46°39.868 N	120°21.519 W		m
	B	46°39.839 N	120°21.513 W		m
	C	46°39.793 N	120°21.499 W		m
	D	46°39.745 N	120°21.483 W		m
	E	46°39.706 N	120°21.472 W		m
	F	46°39.681 N	120°21.465 W		m
MPL	G	46°39.645 N	120°21.422 W	700	m
FTIR	H	46°39.793 N	120°21.414 W	682	m
Retroflector	I	46°39.839 N	120°21.434 W	682	m
Reflective Target	J	46°39.868 N	120°21.437 W	679	m
Orange sock	V	46°39.745 N	120°21.481 W		m

Note: Coordinates in red fond may be different on different days.

All the coordinates has the same degree (°) and minute (): For example: coordinates of 46°39.xxx' N, 120°21.yyy' W is written as (.xxx,.yyy)

0.001' latitude = 1.86 m = 3 pixel
0.001' longitude = 1.28 m = 2 pixel

Figure A-2-4 Field map of YTC tracked vehicle field campaign on 8/25/06

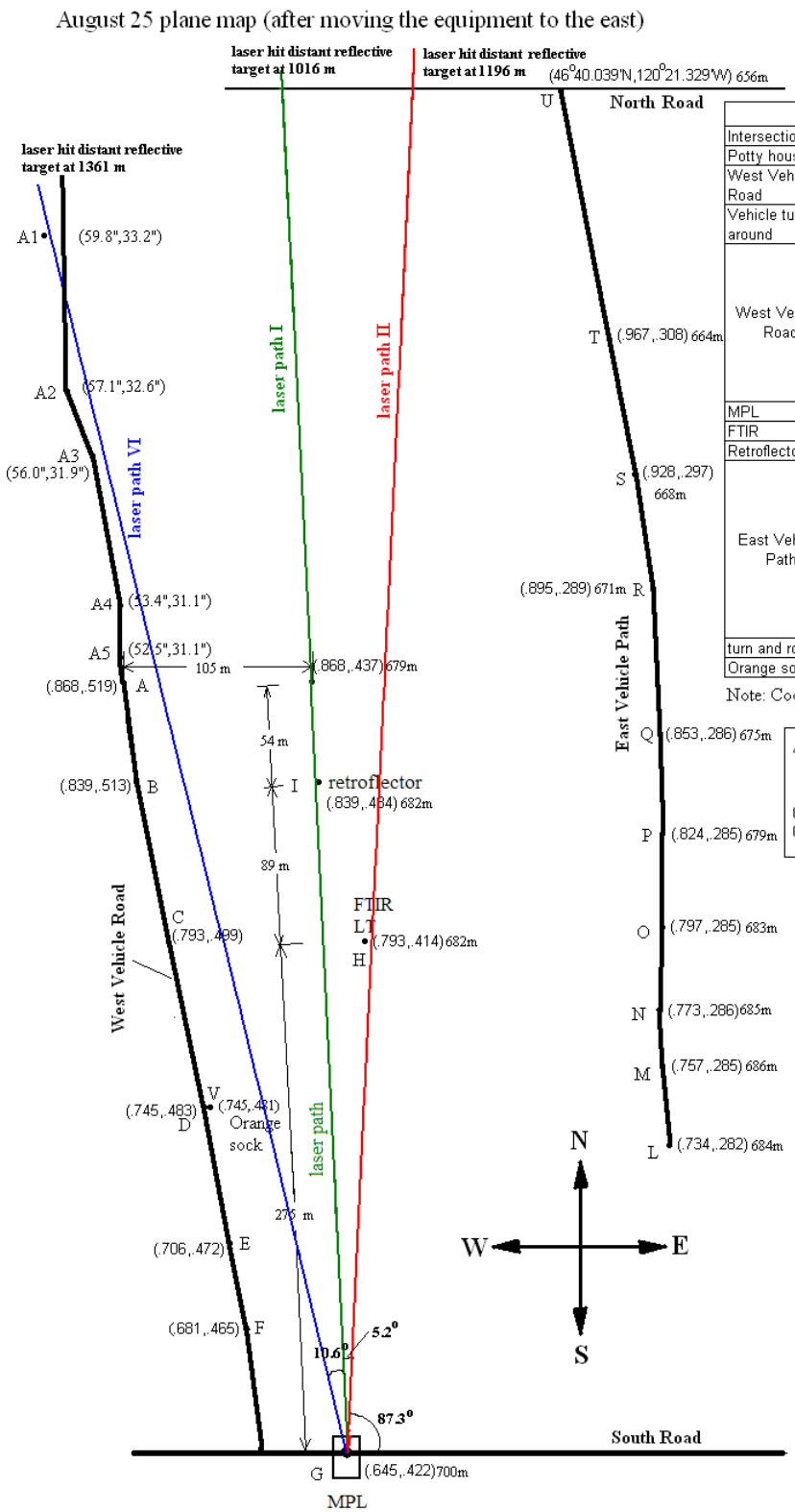

	point	latitude	longitude	elevation	
Intersection	A0	46°40'1.8" N	120°21'32.7" W		m
Potty house	A1	46°39'59.8" N	120°21'33.2" W		m
West Vehicle Road	A2	46°39'57.1" N	120°21'32.6" W		m
Vehicle turn around	A3	46°39'56.0" N	120°21'31.9" W		m
West Vehicle Road	A4	46°39'53.4" N	120°21'31.1" W		m
	A5	46°39'52.5" N	120°21'31.1" W		m
	A	46°39.868 N	120°21.519 W		m
	B	46°39.839 N	120°21.513 W		m
	C	46°39.793 N	120°21.499 W		m
	D	46°39.745 N	120°21.483 W		m
	E	46°39.706 N	120°21.472 W		m
	F	46°39.681 N	120°21.465 W		m
MPL	G	46°39.645 N	120°21.422 W	700	m
FTIR	H	46°39.793 N	120°21.414 W	682	m
Retroflector	I	46°39.839 N	120°21.434 W	682	m
East Vehicle Path	L	46°39.734 N	120°21.282 W	684	m
	M	46°39.757 N	120°21.285 W	686	m
	N	46°39.773 N	120°21.286 W	685	m
	O	46°39.797 N	120°21.285 W	683	m
	P	46°39.824 N	120°21.285 W	679	m
	Q	46°39.853 N	120°21.286 W	675	m
	R	46°39.895 N	120°21.289 W	671	m
	S	46°39.928 N	120°21.297 W	668	m
	T	46°39.967 N	120°21.308 W	664	m
turn and road	U	46°40.039 N	120°21.329 W	656	m
Orange sock	V	46°39.745 N	120°21.481 W		m

Note: Coordinates in red fond may be different on different days.

All the coordinates has the same degree (°) and minute (') :
For example: coordinates of 46°39.xxx' N, 120°21.yyy' W is written as (.xxx,.yyy)
0.001' latitude = 1.86 m = 3 pixel
0.001' longitude = 1.28 m = 2 pixel

Appendix A-3: Supporting Data for Tested Flying Helicopters during the 2007 YPG Field Campaign

Table A-3-1 Specifications of the UH-1 Iroquois (Huey)

Primary function	Utility helicopter
Manufacturer	Bell Helicopter Textron
Power plant	Pratt and Whitney T400-CP-400
Power	Burst: 1290 shaft horsepower (transmission limited) Continuous: 1134 shaft horsepower (transmission limited)
Length	57.3 feet (17.46 meters)
Height	14.9 feet (4.54 meters)
Rotor Diameter	48 feet (14.62 meters)
Speed	121 knots (139.15 miles per hour) at sea level
Ceiling	14,200 feet (4331 meters) (limited to 10,000 feet (3050 meters) by oxygen requirements)
Maximum takeoff weight	10,500 pounds (4,767 kilograms)
Range	172 nautical miles (197.8 miles)
Crew	Officer: 2 Enlisted: 2

Table A-3-2 Summary of emission factors for the Desert Pavement Surface during the 2007 YPG Field Campaign

Pass #	Start Time	End Time	PM_{10} Emission [g-PM/hkf]	Wind Direction (from North) [°]	Wind [m/s]	Wind Direction (from Normal Plane) [°]
1	12:18:49	12:21:25	42,747	140	2.8	-46
2	12:21:24	12:22:40	13,843	168	4.3	-18
3	12:24:01	12:24:52	474	180	3.4	-6
4	12:21:24	12:23:07	5,620	170	4.4	-16
5	12:27:30	12:29:25	6,484	163	3.4	-23
6	12:30:07	12:31:10	2,041	156	3.5	-30
7	12:32:34	12:33:43	598	150	3.9	-36
8	12:34:25	12:36:04	1,752	154	4.1	-32
9	12:36:27	12:39:36	5,739	156	3.1	-30
10	12:40:28	12:42:07	640	156	3.2	-30
11	12:42:39	12:43:18	78	161	4.4	-25
12	12:44:40	12:45:49	193	176	3.8	-10
13	12:46:51	12:48:49	613	174	3.2	-12
14	13:18:03	13:19:12	865	166	3.8	-20
15	13:20:34	13:21:33	220	174	3.8	-12
16	13:22:55	13:23:13	14	173	4.5	-13
17	13:25:04	13:25:54	21	187	2.0	1
18	13:28:07	13:29:46	455	179	2.2	-7
19	13:31:18	13:32:37	138	165	2.7	-21
20	13:33:28	13:34:07	42	164	3.0	-22
21	13:36:00	13:36:39	57	191	3.7	5
23	13:40:01	13:40:19	14	195	3.4	9
24	13:41:42	13:43:10	561	149	4.9	-37
25	13:44:13	13:45:52	578	153	5.4	-33
26_27	13:45:54	13:47:22	111	133	2.7	-53
28_29	13:49:13	13:50:43	192	177	3.2	-9
30_31	13:52:46	13:53:45	37	205	1.8	19
31_33	13:55:37	13:56:36	21	174	1.4	-12

Table A-3-3 Summary of emission factors for the Disturbed Soil Surface on 5/23/07 during the 2007 YPG Field Campaign

Pass #	Start Time	End Time	PM_{10} Emission [g-PM/hkf]	Wind Direction (from North) [°]	Wind [m/s]	Wind Direction (from Normal Plane) [°]
7	11:42:49	11:44:58	76,350	216	1.7	19
8	11:46:51	11:48:07	19,729	196	2.1	-1
9	11:50:36	11:52:31	6,967	162	1.6	-35
12	12:05:28	12:08:16	13,048	195	1.3	-2
13	12:12:43	12:14:49	1,377	238	2.8	41
14	12:16:12	12:19:27	920	192	0.5	-5
16	12:27:43	12:29:34	531	348	1.3	151
17	12:32:54	12:34:58	601	336	2.2	139
18	12:36:52	12:38:43	262	338	1.8	141
19	12:46:00	12:47:51	107	89	1.5	-108
20	12:57:30	12:59:34	2,178	68	2.0	-129

Table A-3-4 Summary of emission factor for the Disturbed Soil Surface on 5/25/07 during the 2007 YPG Field Campaign

Pass #	Start Time	End Time	PM_{10} Emission [g-PM/hkf]	Wind Direction (from North) [°]	Wind [m/s]	Wind Direction (from Normal Plane) [°]
1	13:07:49	13:09:55	51,642	225	3.1	29
2	13:10:52	13:12:58	23,017	208	4.2	12
3	13:13:42	13:15:33	10,764	164	2.1	-32
5	13:26:19	13:27:28	581	212	1.4	16
6	13:28:57	13:30:06	1,133	227	4.6	31
7	13:31:57	13:33:06	831	222	3.1	26
8	13:36:10	13:37:19	2,571	207	4.8	11
9	13:39:27	13:42:00	2,506	203	2.1	7
10	13:43:12	13:44:49	441	227	2.9	31
11	13:46:15	13:47:10	273	210	4.2	14
12	13:48:49	13:49:30	29	227	3.3	31
13	13:51:10	13:51:37	38	180	2.0	-16
15	13:55:51	13:56:46	116	214	2.3	18
16	13:57:58	13:59:07	385	207	5.8	11
17	14:01:01	14:02:24	569	193	3.4	-3
18	14:07:34	14:09:12	6,687	212	4.3	16
19	14:12:30	14:13:03	6	302	0.6	106
20	14:14:07	14:15:58	626	232	4.3	36
21	14:17:25	14:18:34	363	217	4.7	21
22	14:19:46	14:20:55	492	213	3.9	17
23	14:22:21	14:23:16	26	259	4.0	63
24	14:24:40	14:25:49	84	249	3.1	53
25	14:27:01	14:27:57	135	214	3.8	18
26	14:29:51	14:31:55	162	210	0.9	14
27	14:34:04	14:35:13	203	215	5.2	19
28	14:36:52	14:38:30	802	205	2.7	9

Pass #	Start Time	End Time	PM_{10} Emission [g-PM/hkf]	Wind Direction (from North) [°]	Wind [m/s]	Wind Direction (from Normal Plane) [°]
29	14:40:37	14:44:49	1,169	242	4.9	46
30	14:43:12	14:44:21	115	247	5.1	51
31	14:45:46	14:46:42	165	234	4.7	38
32	14:47:54	14:49:03	230	195	3.8	-1
33	14:49:46	14:50:40	109	193	4.1	-3
34	14:51:10	14:52:19	202	207	4.4	11
35	14:53:45	14:55:49	420	212	2.8	16
36	14:56:34	14:57:43	1,163	219	4.4	23
37	14:59:22	15:01:42	182	242	1.4	46

Figure A-3-1 Field map of YPG helicopter field campaign on 5/21/07

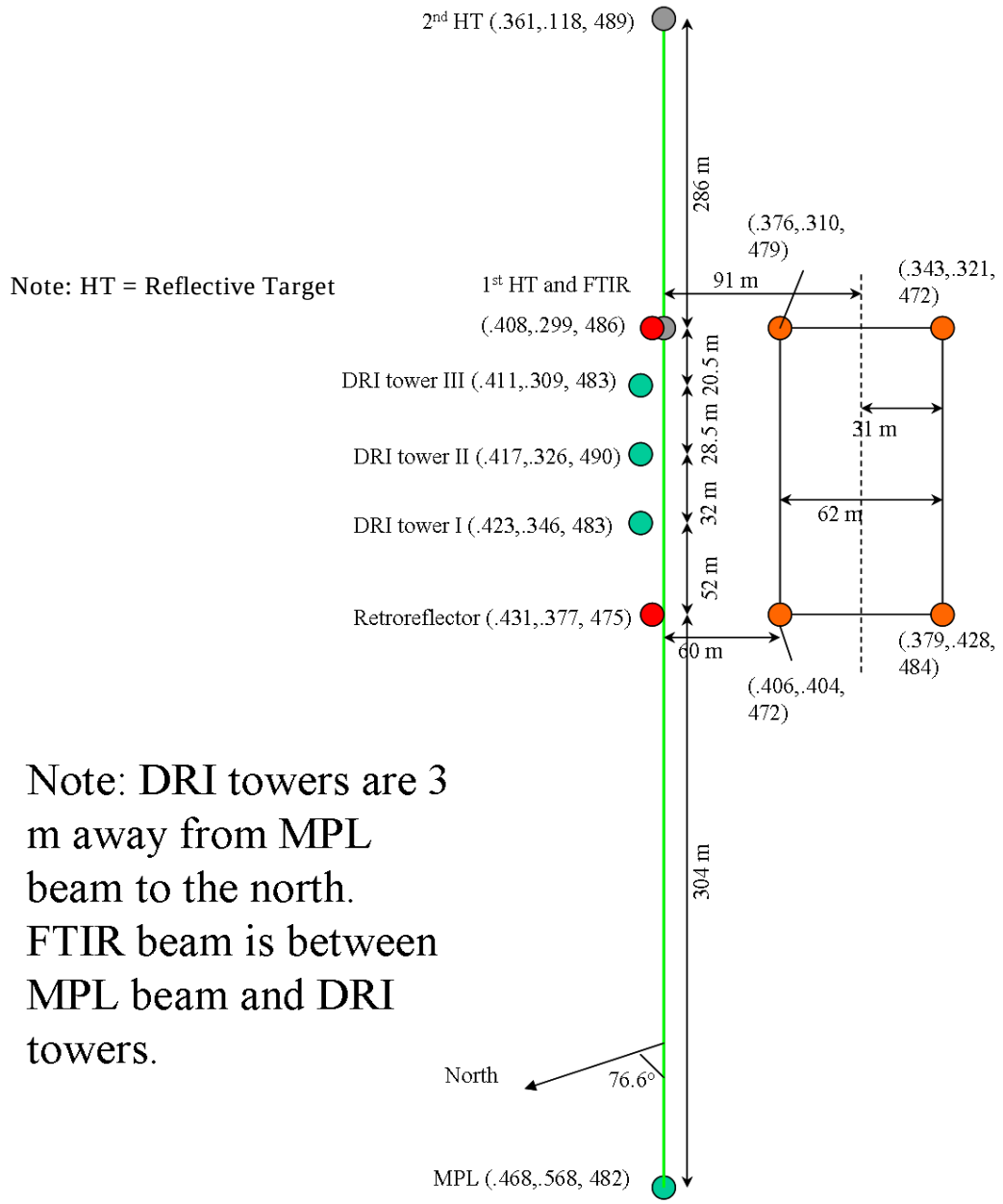

Coordinate of (32°54.361'N, 114°.21.118', 489ft El) is written as (.361,.118, 489)

Figure A-3-2 Field map of YPG helicopter field campaign on 5/23/07

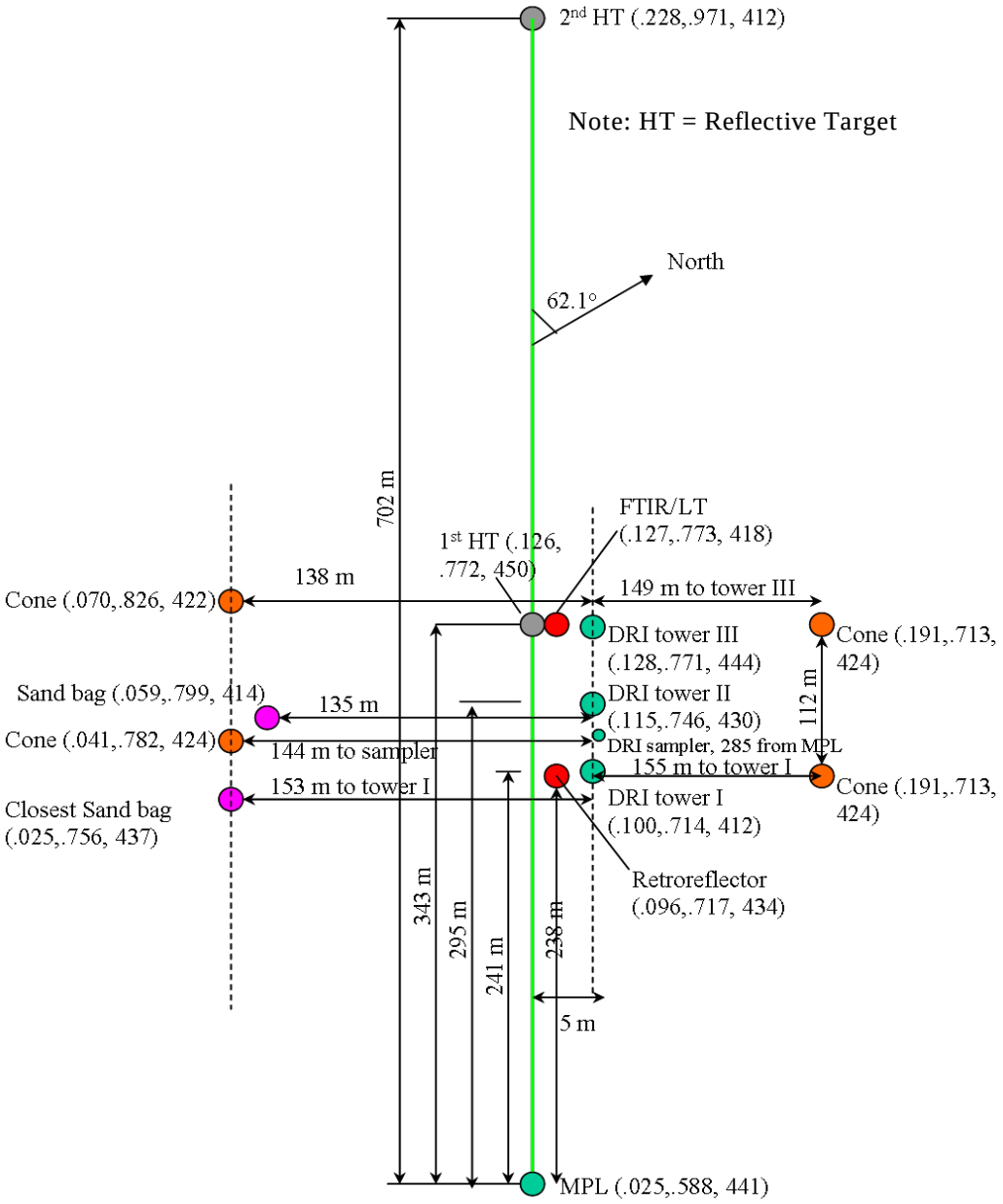

Coordinate of (32°55.025'N, 114°.22.588', 441ft El) is written as (.025,.588, 441)

Appendix A-4: Supporting Data for Tested Military Vehicles during the 2008 Fort Carson Field Campaign

Table A-4-1 Specifications of tested military vehicles

Model	Tracked/Wheeled?	Maximum Speed [MPH]	Weight [USA ton]
M88 HERCULES [1]	Tracked	30	70
M270 MLRS [2]	Tracked	40	27.5
M577 [3]	Tracked	41	13.6
HEMTT [4]	Wheeled	57	19-25

Sources:

1. Global Security. http://www.globalsecurity.org/military/systems/ground/m88-specs.htm (Accessed March 2009).
2. FAS. http://www.fas.org/man/dod-101/sys/land/m270.htm (Accessed March 2009).
3. FAS. http://www.fas.org/man/dod-101/sys/land/m113.htm (Accessed March 2009).
4. Global Security. http://www.globalsecurity.org/military/systems/ground/hmett-specs.htm (Accessed March 2009).

Table A-4-2 Number of tests for select military vehicles

Vehicle	Travel Direction	Vehicle Speed					
		5 MPH	10 MPH	15 MPH	20 MPH	25 MPH	Maxi-mum
M88	Towards MPL	3	3	4	2	1	0
	Away MPL	3	3	4	3	1	0
M270	Towards MPL	4	5	6	5	0	6
	Away MPL	4	5	6	5	0	6
M577	Towards MPL	3	4	5	4	0	5
	Away MPL	3	4	5	4	0	5
HEMTT	Towards MPL	0	4	4	4	0	4
	Away MPL	0	4	4	4	0	4

Table A-4-3 Detailed test data of military vehicles

Date	Vehicle Type	Pass	Site #	Start Time	End Time	Speed (mph)	Speed (km/h)	Mass Emission Factor (g-PM/vkt)	
								PM_{10}	$PM_{2.5}$
9/16/2008	M88	1	1	---	---	---	---	---	---
9/16/2008	M88	2	1	12:45:35	12:46:45	7.6	12.2	---	---
9/16/2008	M88	3	1	12:50:07	12:50:57	11.7	18.7	---	---
9/16/2008	M88	4	1	12:52:49	12:53:39	12.0	19.2	259	458
9/16/2008	M88	5	1	12:55:09	12:55:49	14.6	23.4	---	---
9/16/2008	M88	6	1	12:57:29	12:58:09	17.3	27.7	---	---
9/16/2008	M88	7	1	13:01:43	13:02:23	17.7	28.3	419	937
9/16/2008	M88	8	1	13:07:55	13:08:25	23.7	37.9	---	---
9/16/2008	M88	9	1	13:12:37	13:14:17	5.9	9.4	---	---
9/16/2008	M88	10	1	13:21:31	13:21:51	25.6	41.0	---	---
9/16/2008	M88	11	1	13:23:41	13:24:21	17.8	28.5	455	742
9/16/2008	M88	12	1	13:26:23	13:27:03	17.7	28.3	297	683
9/16/2008	M88	13	1	13:30:37	13:31:17	16.4	26.2	---	---
9/16/2008	M88	14	1	13:36:17	13:37:07	12.4	19.8	546	1,221
9/16/2008	M88	15	1	13:41:21	13:42:11	13.1	21.0	272	427
9/16/2008	M88	16	1	13:44:11	13:45:31	8.5	13.6	554	1,259
9/16/2008	M88	17	1	13:47:43	13:49:03	7.5	12.0	---	---
9/16/2008	M88	18	1	13:51:13	13:52:33	8.2	13.1	280	397
9/16/2008	M88	19	1	13:55:45	13:56:45	11.7	18.7	417	833
9/16/2008	M88	20	1	13:59:07	13:59:57	12.0	19.2	---	---
9/16/2008	M88	21	1	14:06:59	14:07:39	15.8	25.3	634	1,133
9/16/2008	M88	22	1	14:08:51	14:09:31	17.0	27.2	401	894
9/16/2008	M88	23	1	14:12:21	14:13:01	17.1	27.4	---	---
9/16/2008	M88	24	1	14:15:53	14:16:23	22.4	35.8	969	1,538
9/16/2008	M88	25	1	14:27:07	14:27:47	16.1	25.8	503	830
9/16/2008	M88	26	1	14:29:29	14:30:09	17.5	28.0	449	993

Date	Vehicle Type	Pass	Site #	Start Time	End Time	Speed (mph)	Speed (km/h)	Mass Emission Factor (g-PM/vkt)	
								PM_{10}	$PM_{2.5}$
9/16/2008	M88	27	1	14:32:41	14:34:01	8.0	12.8	---	---
9/16/2008	M88	28	1	14:37:21	14:38:31	8.7	13.9	194	296
9/17/2008	M270	1	1	12:14:53	12:16:57	5.4	8.6	---	---
9/17/2008	M270	2	1	12:18:19	12:19:51	5.6	9.0	---	---
9/17/2008	M270	3	1	12:27:01	12:28:07	10.3	16.5	70	231
9/17/2008	M270	4	1	12:30:13	12:31:13	10.9	17.4	381	722
9/17/2008	M270	5	1	12:36:51	12:37:33	15.0	24.0	677	1,105
9/17/2008	M270	6	1	12:39:39	12:40:19	17.0	27.2	224	479
9/17/2008	M270	7	1	12:42:09	12:42:41	20.1	32.2	520	1,147
9/17/2008	M270	8	1	12:44:21	12:44:51	21.3	34.1	567	1,141
9/17/2008	M270	9	1	12:47:03	12:47:23	30.5	48.8	427	1,011
9/17/2008	M270	10	1	12:49:57	12:50:11	20.5	32.8	---	---
9/17/2008	M270	11	1	12:52:05	12:52:25	30.7	49.1	686	1,078
9/17/2008	M270	12	1	12:54:15	12:54:35	35.9	57.4	---	---
9/17/2008	M270	13	1	12:56:55	12:57:25	20.6	33.0	360	994
9/17/2008	M270	14	1	13:00:41	13:01:15	21.4	34.2	---	---
9/17/2008	M270	15	1	13:10:31	13:11:11	17.2	27.5	692	1,502
9/17/2008	M270	16	1	13:13:53	13:14:33	15.7	25.1	154	452
9/17/2008	M270	17	1	13:16:35	13:17:35	11.3	18.1	220	459
9/17/2008	M270	18	1	13:19:55	13:20:45	11.4	18.2	45	134
9/17/2008	M270	19	1	13:23:17	13:25:17	5.3	8.5	---	---
9/17/2008	M270	20	1	13:27:23	13:28:59	7.3	11.7	---	---
9/17/2008	M270	21	1	13:39:53	13:41:13	7.0	11.2	---	---
9/17/2008	M270	22	1	13:42:43	13:44:27	6.4	10.2	---	---
9/17/2008	M270	23	1	13:46:45	13:47:35	15.0	24.0	316	782
9/17/2008	M270	24	1	13:49:05	13:49:45	15.7	25.1	215	475
9/17/2008	M270	25	1	13:52:07	13:52:27	31.1	49.8	607	1,540

Date	Vehicle Type	Pass	Site #	Start Time	End Time	Speed (mph)	Speed (km/h)	Mass Emission Factor (g-PM/vkt)	
								PM_{10}	$PM_{2.5}$
9/17/2008	M270	26	1	13:54:17	13:54:35	37.5	60.0	---	---
9/17/2008	M577	27	1	14:15:36	14:17:16	6.9	11.0	---	---
9/17/2008	M577	28	1	14:22:50	14:24:10	7.8	12.5	---	---
9/17/2008	M577	29	1	14:26:12	14:27:02	11.8	18.9	92	278
9/17/2008	M577	30	1	14:28:22	14:29:12	12.3	19.7	63	134
9/17/2008	M577	31	1	14:31:24	14:32:04	15.9	25.4	86	219
9/17/2008	M577	32	1	14:38:52	14:39:32	16.2	25.9	150	330
9/17/2008	M577	33	1	---	---	---	---	396	931
9/17/2008	M577	34	1	14:44:14	14:44:44	20.6	33.0	422	1,068
9/17/2008	M577	35	1	14:48:26	14:48:56	20.4	32.6	---	---
9/17/2008	M577	36	1	---	---	---	---	163	373
9/17/2008	M577	37	1	14:56:00	14:56:30	20.2	32.3	275	846
9/17/2008	M577	38	1	---	---	---	---	335	855
9/17/2008	M577	39	1	15:01:10	15:01:40	20.0	32.0	705	1,252
9/17/2008	M577	40	1	15:03:12	15:03:42	21.5	34.4	203	452
9/17/2008	M577	41	1	15:08:14	15:08:54	16.2	25.9	113	306
9/17/2008	M577	42	1	15:11:06	15:11:36	16.4	26.2	89	231
9/17/2008	M577	43	1	15:13:38	15:14:38	12.0	19.2	---	---
9/17/2008	M577	44	1	15:15:50	15:16:40	12.9	20.6	59	203
9/17/2008	M577	45	1	15:18:40	15:20:10	7.5	12.0	---	---
9/17/2008	M577	46	1	15:22:02	15:23:22	8.1	13.0	---	---
9/17/2008	M577	47	1	15:26:02	15:27:32	7.7	12.3	---	---
9/17/2008	M577	48	1	15:30:12	15:31:32	8.3	13.3	---	---
9/17/2008	M577	49	1	15:33:24	15:34:04	16.0	25.6	---	---
9/17/2008	M577	50	1	15:37:40	15:38:34	16.5	26.4	141	393
9/17/2008	M577	51	1	15:40:56	15:41:26	20.6	33.0	868	1,616
9/17/2008	M577	52	1	15:43:16	15:43:36	27.2	43.5	629	1,181

Date	Vehicle Type	Pass	Site #	Start Time	End Time	Speed (mph)	Speed (km/h)	Mass Emission Factor (g-PM/vkt)	
								PM_{10}	$PM_{2.5}$
9/19/2008	M270	1	2	12:10:19	12:11:01	10.5	16.8	500	772
9/19/2008	M270	2	2	12:12:53	12:13:35	13.3	21.3	88	237
9/19/2008	M270	3	2	12:14:15	12:14:53	15.2	24.3	---	---
9/19/2008	M270	4	2	12:16:37	12:17:05	16.6	26.6	102	240
9/19/2008	M270	5	2	12:18:07	12:18:33	19.8	31.7	---	---
9/19/2008	M270	6	2	12:21:05	12:21:33	21.5	34.4	---	---
9/19/2008	M270	7	2	12:23:31	12:23:53	28.0	44.8	---	---
9/19/2008	M270	8	2	12:25:19	12:25:33	34.3	54.9	---	---
9/19/2008	M270	9	2	12:27:25	12:27:39	26.8	42.9	188	489
9/19/2008	M270	10	2	12:28:51	12:29:05	34.8	55.7	---	---
9/19/2008	M270	11	2	12:30:51	12:31:15	20.3	32.5	---	---
9/19/2008	M270	12	2	12:34:55	12:35:23	21.6	34.6	---	---
9/19/2008	M270	13	2	12:37:29	12:37:57	16.3	26.1	636	1,045
9/19/2008	M270	14	2	12:40:59	12:41:27	17.1	27.4	---	---
9/19/2008	M270	15	2	12:45:14	12:45:56	11.1	17.8	45	89
9/19/2008	M270	16	2	12:46:39	12:47:21	11.1	17.8	---	---
9/19/2008	M577	17	2	---	---	---	---	373	845
9/19/2008	M577	18	2	---	---	---	---	---	---
9/19/2008	M577	19	2	---	---	---	---	888	2,196
9/19/2008	M577	20	2	13:10:32	13:11:00	15.5	24.8	69	227
9/19/2008	M577	21	2	13:11:56	13:12:24	19.2	30.7	808	1,461
9/19/2008	M577	22	2	13:13:48	13:14:16	21.1	33.8	---	---
9/19/2008	M577	23	2	13:15:56	13:16:24	18.9	30.2	1,229	3,617
9/19/2008	M577	24	2	13:17:32	13:17:46	28.5	45.6	684	1,738
9/19/2008	M577	25	2	13:18:44	13:19:12	20.3	32.5	325	690
9/19/2008	M577	26	2	13:20:22	13:20:36	26.6	42.6	536	1,566
9/19/2008	M577	27	2	13:22:16	13:22:44	15.8	25.3	806	2,392

Date	Vehicle Type	Pass	Site #	Start Time	End Time	Speed (mph)	Speed (km/h)	Mass Emission Factor (g-PM/vkt)	
								PM_{10}	$PM_{2.5}$
9/19/2008	M577	28	2	13:24:22	13:24:50	20.0	32.0	484	1,611
9/19/2008	M577	29	2	13:26:00	13:26:28	16.3	26.1	166	537
9/19/2008	M577	30	2	13:27:38	13:28:06	15.9	25.4	---	---
9/19/2008	M577	31	2	13:29:16	13:29:38	11.6	18.6	157	752
9/19/2008	M577	32	2	13:30:54	13:31:36	12.0	19.2	49	385
9/19/2008	HEMTT	39	2	15:17:49	15:18:31	9.9	15.8	---	---
9/19/2008	HEMTT	40	2	15:20:37	15:21:19	12.2	19.5	---	---
9/19/2008	HEMTT	41	2	15:23:27	15:23:55	14.3	22.9	320	972
9/19/2008	HEMTT	42	2	15:25:19	15:25:47	15.1	24.2	893	3,808
9/19/2008	HEMTT	43	2	15:28:07	15:28:35	19.8	31.7	1,665	6,707
9/19/2008	HEMTT	44	2	15:31:25	15:31:53	21.2	33.9	648	2,561
9/19/2008	HEMTT	45	2	15:33:03	15:33:17	36.2	57.9	911	3,007
9/19/2008	HEMTT	46	2	15:35:51	15:36:05	37.5	60.0	1,874	5,839
9/19/2008	HEMTT	47	2	15:37:29	15:37:43	37.2	59.5	---	---
9/19/2008	HEMTT	48	2	15:41:01	15:41:15	38.2	61.1	1,568	3,360
9/19/2008	HEMTT	49	2	15:42:13	15:42:41	19.0	30.4	2,610	10,652
9/19/2008	HEMTT	50	2	15:44:31	15:44:59	19.9	31.8	755	2,224
9/19/2008	HEMTT	51	2	15:45:57	15:46:25	14.8	23.7	---	---
9/19/2008	HEMTT	52	2	15:48:17	15:48:45	16.6	26.6	442	1,561
9/19/2008	HEMTT	53	2	15:51:07	15:51:49	9.6	15.4	---	---
9/19/2008	HEMTT	54	2	15:56:31	15:57:13	12.2	19.5	79	327
9/19/2008	HEMTT	55	2	16:02:21	16:03:03	11.8	18.9	64	337
9/19/2008	HEMTT	56	2	16:05:09	16:05:51	11.1	17.8	28	234
9/19/2008	HEMTT	57	2	16:07:59	16:08:27	14.7	23.5	161	907
9/19/2008	HEMTT	58	2	16:10:05	16:10:33	17.1	27.4	96	371
9/19/2008	HEMTT	59	2	16:13:07	16:13:35	20.2	32.3	501	2,745
9/19/2008	HEMTT	60	2	16:15:29	16:15:57	20.0	32.0	267	967

Date	Vehicle Type	Pass	Site #	Start Time	End Time	Speed (mph)	Speed (km/h)	Mass Emission Factor (g-PM/vkt)	
								PM_{10}	$PM_{2.5}$
9/19/2008	HEMTT	61	2	16:19:57	16:20:11	37.5	60.0	1,154	3,513
9/19/2008	HEMTT	62	2	16:22:03	16:22:17	42.2	67.5	1,437	3,817
9/19/2008	HEMTT	63	2	16:23:55	16:24:09	35.0	56.0	724	2,412
9/19/2008	HEMTT	64	2	16:25:47	16:26:01	43.0	68.8	---	---
9/19/2008	HEMTT	65	2	16:27:13	16:27:41	20.5	32.8	---	---
9/19/2008	HEMTT	66	2	16:29:33	16:30:01	19.1	30.6	224	1,226
9/19/2008	HEMTT	67	2	16:30:57	16:31:25	15.2	24.3	662	3,793
9/19/2008	HEMTT	68	2	16:33:31	16:33:59	15.7	25.1	28	179
9/19/2008	HEMTT	69	2	16:36:07	16:36:49	10.0	16.0	247	1,435
9/19/2008	HEMTT	70	2	16:38:55	16:39:37	11.6	18.6	25	108

Figure A-4-1 Field map of Fort Carson military vehicle field campaign on 9/16/08 and 9/17/08

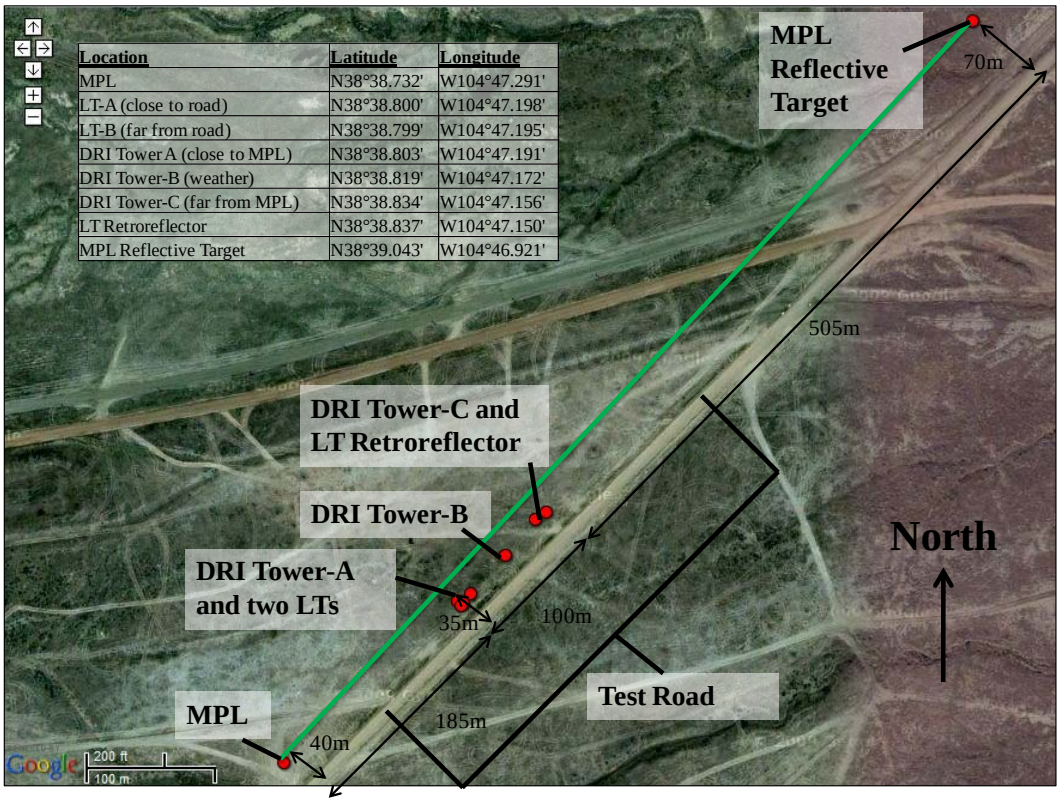

Location	Latitude	Longitude
MPL	N38°38.732'	W104°47.291'
LT-A (close to road)	N38°38.800'	W104°47.198'
LT-B (far from road)	N38°38.799'	W104°47.195'
DRI Tower A (close to MPL)	N38°38.803'	W104°47.191'
DRI Tower-B (weather)	N38°38.819'	W104°47.172'
DRI Tower-C (far from MPL)	N38°38.834'	W104°47.156'
LT Retroreflector	N38°38.837'	W104°47.150'
MPL Reflective Target	N38°39.043'	W104°46.921'

Figure A-4-2 Field map of Fort Carson military vehicle field campaign on 9/19/08

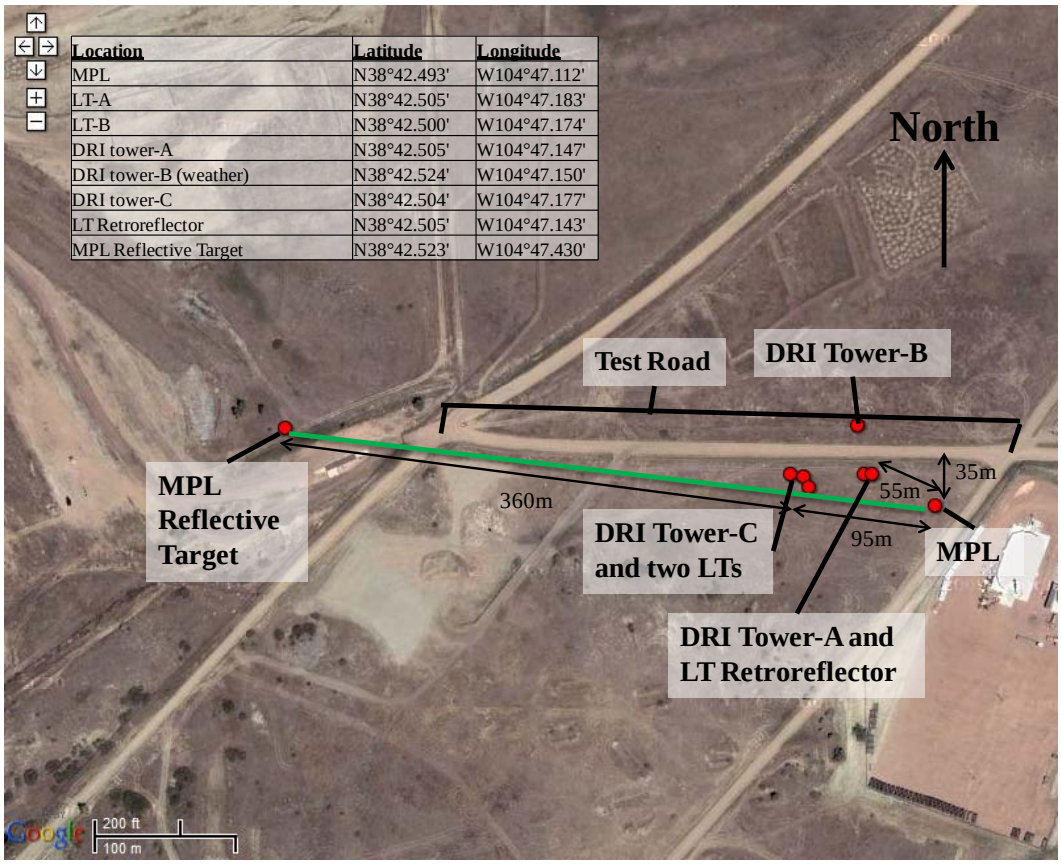

Location	Latitude	Longitude
MPL	N38°42.493'	W104°47.112'
LT-A	N38°42.505'	W104°47.183'
LT-B	N38°42.500'	W104°47.174'
DRI tower-A	N38°42.505'	W104°47.147'
DRI tower-B (weather)	N38°42.524'	W104°47.150'
DRI tower-C	N38°42.504'	W104°47.177'
LT Retroreflector	N38°42.505'	W104°47.143'
MPL Reflective Target	N38°42.523'	W104°47.430'

Appendix B – List of Scientific/Technical Publications

Du, K., Rood, M. J., Kim, B. J., Kemme, M., Hashmonay, R., Varma, R., Optical Remote Sensing of Dust Plumes Using Micropulse Lidar. in 99th Annual Meeting of the Air & Waste Management Association. 2006. New Orleans, LA.

Du, K., Rood, M. J., Kim, B. J., Kemme, M., Hashmonay, R., Varma, R., Ground-based Lidar Measurements of Dust Plumes Generated from Unique Military Activities. in 100th Annual Meeting of the Air & Waste Management Association. 2007. Pittsburgh, PA.

Du, K., Rood, M. J., Kim, B. J., Kemme, M., Hashmonay, R., Use of Vertical Scanning Lidar to Quantify and Characterize Dust Plumes Generated from Flying Helicopters. in 101st Annual Meeting of the Air & Waste Management Association. 2008. Portland, OR.

Hashmonay, R.A., Kagann, R. H., Rood, M. J., Kim, B. J., Kemme, M. R., Gillies, J., An Advanced Test Method for Measuring Fugitive Dust Emissions Using a Hybrid System of Optical Remote Sensing and Point Monitor Techniques, in Atmospheric and Biological Environmental Monitoring, U.P. Y. J. Kim, M. B. Gu, H. Iwahashi, Editor. 2009, Springer Netherlands. p. 73-81.

Varma, R.M., Hashmonay, R. A., Du, K., Rood, M. J., Kim, B. J., Kemme, M. R., A Novel Methodology for Fugitive Dust Emission Estimation using Optical Remote Sensing, in Advanced Environmental Monitoring, Y.J. Kim, Platt, U., Editor. 2007, Springer-Verlag GmbH.

Yuen, W., Du, K., Rood, M. J., Kim, B. J., Kemme, M., Hashmonay, R., Measurement of Dust Emissions Generated by Military Vehicles Using Optical Remote Sensing Method at Ford Carson, Colarado. in 102nd Annual Meeting of the Air & Waste Management Association. 2009. Detroit, MI.

Appendix C – Other Supporting Materials

Justification for the Assumption That K = 0

The imaginary part of the refractive index (k) was assumed to be zero when calculating the extinction efficiency factor, K^*. However, k was reported to range from 0.003 to 0.009[33] in the visible spectrum for desert dust. Mie-Lorenz model calculations describing K^* for n′ ranging from 1.35 to 1.60, k ranging from 0 to 0.01, and the particle size distributions determined by the OP-FTIR and OP-LT measurements as reported by Varma *et al.*[34] for desert dust are presented in Table C-1. The small dependence of K^* (standard deviation/mean < 1%) over the reasonable range of k values justifies the use of k = 0 when calculating K^*.

Table C-1 Sensitivity analysis of K^*, [g/m²] *§

	K^*				
n′ \ k	0	0.001	0.003	0.005	0.01
1.60	2.929	2.929	2.931	2.933	2.939
1.55	2.899	2.908	2.912	2.915	2.921
1.50	2.896	2.896	2.897	2.900	2.906
1.45	2.896	2.897	2.900	2.903	2.911
1.40	2.895	2.899	2.904	2.910	2.923
1.35	2.971	2.973	2.976	2.980	2.990

§ Refractive index = n′

REPORT DOCUMENTATION PAGE

Form Approved
OMB No. 0704-0188

Public reporting burden for this collection of information is estimated to average 1 hour per response, including the time for reviewing instructions, searching existing data sources, gathering and maintaining the data needed, and completing and reviewing this collection of information. Send comments regarding this burden estimate or any other aspect of this collection of information, including suggestions for reducing this burden to Department of Defense, Washington Headquarters Services, Directorate for Information Operations and Reports (0704-0188), 1215 Jefferson Davis Highway, Suite 1204, Arlington, VA 22202-4302. Respondents should be aware that notwithstanding any other provision of law, no person shall be subject to any penalty for failing to comply with a collection of information if it does not display a currently valid OMB control number. PLEASE DO NOT RETURN YOUR FORM TO THE ABOVE ADDRESS.

1. REPORT DATE (DD-MM-YYYY)
09-16-2010

2. REPORT TYPE
Final Report

3. DATES COVERED (From - To)

4. TITLE AND SUBTITLE
Development of Emission Factors for Dust Generated by Unique Military Activities

5a. CONTRACT NUMBER

5b. GRANT NUMBER

5c. PROGRAM ELEMENT

6. AUTHOR(S)
Byung J. Kim Michael R. Kemme, Mark J. Rood, Ke Du, Wangki Yuen, Wei Wang, Ram Hashmonay and Ravi Varma

5d. PROJECT NUMBER
SERDP SI-1400

5e. TASK NUMBER

5f. WORK UNIT NUMBER

7. PERFORMING ORGANIZATION NAME(S) AND ADDRESS(ES)
U.S. Army Engineer Research and Development Center (ERDC)
Construction Engineering Research Laboratory (CERL)
PO Box 9005,
Champaign, IL 61826-9005

8. PERFORMING ORGANIZATION REPORT NUMBER
ERDC/CERL TR-10-DRAFT

9. SPONSORING / MONITORING AGENCY NAME(S) AND ADDRESS(ES)
Strategic Environmental Research and Development Program Office
901 North Stuart Street
Suite 303
Arlington, VA 22203

10. SPONSOR/MONITOR'S ACRONYM(S)
SERDP

11. SPONSOR/MONITOR'S REPORT NUMBER(S)

12. DISTRIBUTION / AVAILABILITY STATEMENT
Approved for public release; distribution is unlimited.

13. SUPPLEMENTARY NOTES

14. ABSTRACT

The SERDP SI-1400 research team has successfully developed a novel optical remote sensing method to characterize and quantify fugitive particulate matter dust emissions generated by unique military activities. This research team provided Department of Defense installations with results that can be used to estimate the generation of fugitive dust from military activities. Unique military activities that were studied with this project include: 1) artillery back blast, 2) rotary wing aircraft and, 3) tracked vehicles.

The optical remote sensing method includes a Micro-Pulse Light detection and ranging device (MPL), an Open Path-Fourier Transform Infrared Spectrometer (OP-FTIR), and an Open Path-Laser Transmissometer (OP-LT). The new analytical technique developed as part of this project quantifies the extinction of light caused by dust plumes passing through the measurement plane of the MPL. The path-integrated OP-FTIR and OP-LT measures the dusts' ability to attenuate light as a function of the dusts' particle size distribution. During the fourth year, the OP-FTIR measurements were replaced with a hybrid system using OP-LT and DustTraks™ to measure the dusts' light extinction efficiencies in a simpler and cost effective manner.

The novel optical remote sensing method was used to quantify PM dust mass emission factors with aerodynamic diameter < 2.5 μm and < 10 μm for artillery back blast, military vehicles, and for a flying helicopter. Regressions were developed to determine PM-mass emission factors based on type of fugitive source, speed of the mobile sources, and momentum of the mobile sources

15. SUBJECT TERMS
optical remote sensing, Lidar, particulate matter, fugitive emission, dust, extinction, emission factor, artillery firing, tracked vehicle, wheeled vehicle, helicopter

16. SECURITY CLASSIFICATION OF:			17. LIMITATION OF ABSTRACT	18. NUMBER OF PAGES	19a. NAME OF RESPONSIBLE PERSON
a. REPORT	b. ABSTRACT	c. THIS PAGE			19b. TELEPHONE NUMBER (include area code)
Unclassified	Unclassified	Unclassified	SAR	127	